Stability Analysis of Composites and Structures Having Negative Stiffness Components

By

Tuan M. Hoang

A dissertation submitted in partial fulfillment of

the requirements for the degree of

Doctor of Philosophy

(Engineering Mechanics)

at the

UNIVERSITY OF WISCONSIN-MADISON

2014

Date of final oral examination: 05/05/2014

The dissertation is approved by the following members of the Final Oral Committee:

Walter J. Drugan Professor, Engineering mechanics

Roderic S. Lakes Professor, Engineering mechanics

Michael E. Plesha Profesor, Engineering mechanics

Fabian Waleffe Professor, Math

Donald S. Stone Professor, Materials Science

ACKNOWLEDGMENTS

I would like to thank all those who have supported and assisted me during the process of pursuing my Ph.D. degree. First of all, I would like to thank Professor Robert E. Rowlands for helping me when I was in the Mechanical Engineering Department at the University of Wisconsin-Madison. Secondly, I would like to thank Professor Walter J. Drugan for his support, guidance and patience during my Ph.D. period in the Engineering Physics Department. Lastly, I would like to thank Professor Roderic S. Lakes for his collaborations and for giving me the chance to carry out the interesting research in his advanced materials group.

Let me thank H. Kalathur for showing me his beautiful experiments and for many fruitful discussions. Furthermore, I would like to express my appreciation to the J. Gordon Baker fellowship prize, the American Nuclear Society William R. and Mila Kimel Memorial Scholarship Award and the Vietnamese government fellowship, which made this research possible.

Finally, I am grateful to my parents and my lovely family, who are always with me, encourage and motivate me during this interesting journey of my life.

CONTENTS

List of figures **vi**

Abstract **ix**

Chapter 1. Buckling Mode Jump at Very Close Load Values in Unattached Flat-End Columns **1**

1.1 Introduction 1

1.2 Experiments of Kalathur and Lakes 2

1.3 Theoretical Modeling and Analysis 4

1.3.1 Timoshenko analysis of initial buckling of a column having rounded ends . . 7

1.3.2 Analysis of secondary buckling via the Timoshenko formulation 8

1.3.3 Alternative analysis of secondary buckling load 14

1.4 Discussion and Conclusions 17

Chapter 2. Tailored Heterogeneity Increases Overall Stability Regime of Composites Having a Negative-Stiffness Inclusion: Piecewise Homogeneity **19**

2.1 Introduction 19

2.2 Complete representation of equilibrium displacement field in a homogeneous, isotropic, linear elastic annular domain 21

2.3 Stability condition for a composite solid with zero traction on the outside boundary 26

2.3.1 Nontrivial equilibrium solution for the m = 0 mode 26

2.3.2 No nontrivial equilibrium solution for the m = 1 mode 28

2.3.3 Nontrivial equilibrium solutions for the remaining m modes (m≥2) 31

2.4 Stability requirements for a traction-free composite having a two-layer coating 37

2.4.1 Demonstration that coating heterogeneity can change the critical instability mode 37

2.4.2 Determination of optimal two-layer coating composites 40

2.4.2.1 Constant shear modulus in the two-layer coating 43

2.4.2.2 Constant bulk modulus in the two-layer coating 45

2.4.2.3 Both moduli varying in the two-layer coating 48

2.5 Conclusions 52

Chapter 3. Tailored Heterogeneity Increases Overall Stability Regime of Composites Having a Negative-Stiffness Inclusion: Continuously Varying Heterogeneity 53

3.1 Introduction 53

3.2 Derivation of the optimal composite with a smoothly–varying shear modulus in the coating 54

3.2.1 Stability condition for a composite with a smoothly–varying shear modulus in the coating 54

3.2.1.1 Determination of composite stability domain–multiple homogeneous layer approach 55

3.2.1.2 Determination of composite stability domain–continuum approach 60

3.2.2 Determination of optimal composite with smoothly–varying coating shear modulus 63

3.2.3 Confirmation of m = 0 mode criticality for optimal composite with smoothly–varying coating shear modulus 68

3.3 Determination of the optimal coating 70

3.4 Conclusions 76

Chapter 4. Viscoelastic composite solids **77**

4.1 Introduction 77

4.2 Linear viscoelastic solids 78

4.2.1 Constitutive model 78

4.2.2 Harmonic viscoelastic response. 79

4.3 Spring-dashpot system. 80

4.3.1 Inertia effects neglected 83

4.3.2 Inertia effects retained 85

4.4 Viscoelastic composite solids 88

4.4.1 Viscoelastic composite solids with a homogeneous coating 89

4.4.1.1 Inertial effects neglected 89

4.4.1.2 Inertial effects retained 92

4.4.2 Viscoelastic composite solids with a heterogeneous coating. 96

4.4.2.1 Inertial effects neglected 96

4.4.2.2 Inertial effects retained 98

4.5 Conclusions 101

Chapter 5. Future work **102**

Appendix A. Structure of equilibrium solutions in the isotropic, circular domain for the optimal composite with a radially–varying coating shear modulus **104**

Appendix B. The optimal composite with a smoothly–varying bulk modulus in the coating **115**

References **119**

FIGURES

1.1 Polymer column. (a) Column secured between flat platens solely by contact under compression. (b) Column deflection at first buckling, identical to that of a clamped-ended column. (c) Column deflection at second buckling, exhibiting end tilt. (d) Column end tilt in close-up 2

1.2 The force-displacement relationship of a PMMA column with d=6.453 mm and ℓ =197.6mm from zero load through both buckling events. 3

1.3 (a) Curved end of column, modeled as a portion of a circle having radius R; (b) Displacement of forces action line due to rotation of curved column ends. 5

1.4 The two columns with different end conditions analyzed to predict the second buckling load. 16

2.1 The coated-cylinder composite. 22

2.2 Restrictions on the elastic moduli in the plane $\kappa_1/\mu_1 - \kappa_2/\mu_2$ for a composite solid with (a) thin and (b) thick homogeneous coatings. 33

2.3 Geometry of a composite solid having (a) a heterogeneous coating comprised of two homogeneous layers with different shear moduli and (b) a homogeneous coating 38

2.4 Restrictions on the elastic moduli in the plane $\kappa_1/\mu_1 - \kappa_2/\mu_2$ for a three fixed volume ratios a/b= 0.9, b/c =0.8. 40

2.5 Restrictions on the elastic moduli in the plane $\kappa_1/\mu_1 - \kappa/\mu$ for a composite solid with (a) thin and (b) thick homogeneous coatings 48

3.1 (a) A composite solid with a heterogeneous coating (b) the coating divided into n discrete layers. 55

3.2 Restrictions on the elastic moduli in the plane $\kappa_0/\mu_0 - \kappa/\mu$ for the optimal composite with a smoothly-varying shear modulus in the coating with (a) thin and (b) thick coatings. 70

3.3 Composite stability regimes (above and to the right of the curves) in the plane $\kappa_0/\mu_0 - \overline{\kappa}/\overline{\mu}$ for (a) a fixed shear ratio and (b) a fixed volume ratio. 75

4.1 Spring-dashpot system 81

4.2 The effective damping of the spring-dashpot system of negligible masses versus $x > -2/3$ for different frequencies $\overline{\Omega}$ with parameters $y = 2,\ u = v = 0.1$ 84

4.3 The effective damping of the spring-dashpot system versus $x > -2/3$ for different frequencies $\overline{\Omega}$ with masses included and parameters $y = 2,\ u = v = 0.1$ 86

4.4 The effective damping of the spring-dashpot system near resonance versus $x > -2/3$ with parameters $y = 2,\ u = v = 0.1$ 87

4.5 The coated-cylinder composite. 88

4.6 The effective loss tangent of the viscoelastic composite for different frequencies versus the normalized inclusion bulk modulus $x = \kappa_1/\mu_1$ for parameter values $y = 7/26,\ s = 26/50 > 0,\ \alpha = 0.142$. 91

4.7 Moduli combinations leading to infinite static and infinite dynamic effective composite bulk modulus for a homogeneous coating for parameter values $a/b = 0.5,\ \mu_2/\mu_1 = 0.5,\ \rho_1 = \rho_2 = \rho,\ \Omega = \overline{\Omega}\sqrt{\mu_2/(\rho b^2)}$ 95

4.8 The effective loss tangent at the stability boundary of the viscoelastic composite for homogeneous and heterogeneous coatings versus excitation frequency with parameters $y = 7/26,\ s = 26/50 > 0,\ \alpha = 0.142$. 98

4.9 Moduli combinations leading to infinite static and infinite dynamic effective composite bulk modulus for a heterogeneous coating for parameter values $a/b = 0.5,\ \mu_2/\mu_1 = 0.5,\ \rho_1 = \rho_2 = \rho,\ \Omega = \overline{\Omega}\sqrt{\mu_2/(\rho b^2)}$. 100

ABSTRACT

Stability theory plays a key role in structural and materials engineering. When examining the stability of a system, one examines whether an arbitrary infinitesimal perturbation of the system's displacement field that satisfies the system's displacement boundary conditions will remain infinitesimal for the expected practical life of the system. If it will, the system is stable; if not, it is unstable.

The most broadly-valid approach for stability analysis is the fully dynamic one, in which an arbitrary infinitesimal displacement perturbation is applied to the structure under analysis, and a full dynamic analysis of the ensuing behavior of the structure is determined, to assess whether the displacement perturbation will grow in time (unstable) or not (stable). However, to assess stability of an equilibrium state when only conservative loading is applied, the so-called adjacent-equilibrium-position method or static stability method is valid – that is, it gives the same results as the fully dynamic approach. In this method, a state of equilibrium is stable so long as no other adjacent equilibrium state exists. Stability analysis in solid mechanics began with Euler's invention and application of this method to the solution of buckling of an elastic compressed column. Mathematically, in this approach, the problem is reduced to an eigen-boundary-value problem and adjacent equilibrium states are "eigen" states, e.g., Simitses (2005).

In Chapter 1, buckling of compressed flat-end columns loaded by unattached flat platens is shown, theoretically and experimentally (experiments performed by UW colleagues Kalathur and Lakes), to occur first at the critical load and associated mode shape of a built-in column,

followed extremely closely by a second critical load and different mode shape characterized by column end-tilt. The theoretical critical load for secondary or end tilt buckling is shown to be only 0.13% greater than the critical load for primary buckling for the column geometries examined, in which the ends are in full contact with the compression platens. The experimental value is consistent with this theoretical one. Interestingly, under displacement control, the first buckling instability is characterized by a smoothly-increasing applied load, whereas the closely-following second instability causes an abrupt and large load drop (and hence exhibits incremental negative stiffness). The end tilt buckling gives rise to large hysteresis that can be useful in structural damping but that is non-conservative and potentially catastrophic in the context of design of structural support columns. The theoretical research described in this chapter, together with the experimental work of UW colleagues Kalathur and Lakes, has been published in a joint paper in the *Journal of Applied Mechanics* (Kalathur et al., 2013).

In the context of deformable bodies subject to conservative or non-conservative loads, a body is stable if for an arbitrary kinematically-admissible (i.e., continuous, single-valued and compatible with all displacement boundary conditions) infinitesimal displacement field, the work done by the surface and body forces does not exceed that absorbed as an increase in internal energy, Pearson (1956). This criterion also ensures that there are no adjacent equilibrium states satisfying both Cauchy's equilibrium equations inside the body and the boundary conditions on the surface of the body. Hence, a stable equilibrium solution is unique (the converse is not true) and non-uniqueness means instability, Hill (1957). In other words, a necessary condition for stability is the uniqueness of the equilibrium solution. The sufficient condition for stability is the positivity of the total strain energy for arbitrary kinematically-admissible infinitesimal displacement fields (Pearson, 1956; Hill, 1957).

For a *homogeneous* linear elastic body with boundary conditions of pure traction or mixed traction/displacement, this sufficient condition for stability requires positive-definiteness of the elastic modulus tensor, which for the isotropic material case means, for plane strain deformations

$$\lambda + \mu > 0, \quad \mu > 0 \quad \text{which imply} \quad \kappa = \lambda + \mu > 0,$$

where λ, μ are Lamé's moduli (μ being the shear modulus) and κ is the bulk modulus.

For a *homogeneous* linear elastic body subject to pure displacement boundary conditions, however, Kelvin (1888) showed that the sufficient stability condition is weaker, requiring merely strong ellipticity of the elastic modulus tensor, which for the isotropic material case means, for plane strain deformations

$$\lambda + 2\mu > 0, \quad \mu > 0 \quad \text{which imply} \quad \kappa = \lambda + \mu > -\mu.$$

Observe that these latter conditions permit a substantial range of negative bulk modulus. Thus a homogeneous, isotropic, linear elastic solid with negative bulk modulus (negative stiffness) is unstable by itself but is stable if it is constrained at all boundary points and its bulk modulus is larger than minus its shear modulus.

Recent theoretical and experimental results have shown the possibility of enormous increases in composite material overall elastic stiffnesses (and other overall properties such as damping, thermal expansion, piezoelectricity, etc.) when the composite contains a tuned non-positive-definite (i.e., negative stiffness) constituent. For such composite materials to have practical value, they must be stable. Very recent research has shown for the first time that if a homogeneous, isotropic linear elastic inclusion is completely encapsulated by a different, sufficiently stiff positive-definite homogeneous, isotropic linear elastic material, the resulting

composite material will be stable even under pure traction boundary conditions when the inclusion has a negative bulk modulus lying within a permissible but limited range determined by the composite geometry and coating properties (Drugan, 2007; Kochmann & Drugan, 2009, 2012). This research has treated linear elastic composite materials having homogeneous phases, and has done so via the energy method and full dynamic stability analyses.

In Chapters 2 and 3, we first show how to analyze the composites previously analyzed dynamically by the comprehensive but simpler static stability approach. We then employ this approach to show that permitting heterogeneity of the positive-definite phase can substantially increase the range of constituent negative stiffness while maintaining overall composite stability. In Chapter 2, we treat the positive-definite phase heterogeneity as piecewise homogeneous, while in Chapter 3 we treat it as continuously-varying. In both cases, we determine the heterogeneity type that permits the greatest range of constituent negative stiffness while maintaining overall composite stability. Such an increased range of constituent negative stiffness provides an enlarged tuning parameter range for the development of novel, high-performance composite materials. Chapters 2 and 3 were combined into a single manuscript which has been accepted for publication in the *Journal of the Mechanics and Physics of Solids* (Hoang and Drugan, 2014).

In Chapter 4, we expand results obtained for elastic composite solids to viscoelastic ones in which both phases are comprised of linear, isotropic, viscoelastic materials by employing the correspondence principle. We demonstrate that the specific heterogeneity of the positive-definite phase that was shown in Chapter 3 to permit the largest inclusion negative stiffness while maintaining overall composite stability, can increase the effective loss tangent of the composites

near the stability boundary and decrease the critical exciting frequency at which the dynamic effective composite bulk modulus becomes infinite.

Chapter 1. Buckling Mode Jump at Very Close Load Values in Unattached Flat-End Columns

1.1. Introduction

Post-buckling theory plays an important role in the context of design and assessment of structures and in hysteresis damping that can occur in post-buckled structures. As for damping, buckling occurs when the structural stiffness is negative and hence gives high damping. For example, structures containing buckled flexible tubes exhibited negative stiffness and consequent giant increases in damping under small deformation oscillatory load (Lakes (2001)).

For structural damping, column buckling offers the advantage of much greater stiffness in comparison with buckling of tubes (which must be flexible owing to large local strain) or snap-through of discrete spring structures. Column post-buckling and snap back via end tilt has been used to demonstrate extremely high values of hysteresis damping in polymer based modules (Dong and Lakes (2012)), in stiff modules based on steel (Dong and Lakes (2013)), and in small amplitude oscillations (Kalathur and Lakes (2013)).

This chapter is devoted to developing a clearer understanding of the process of post-buckling for columns, in particular, the interesting case in which the column ends are flat and not attached to the flat loading device.

1.2. Experiments of Kalathur and Lakes

A PMMA column with length of 197.6 mm and diameter of 6.453 mm was compressed between flat platens, to which it was not attached, under displacement control. As compressive deformation increases, the initially straight column (Fig. 1.1(a)) buckles when a critical imposed displacement is reached into a shape with the ends remaining horizontal (zero slopes at both ends) and in full contact with the platens, just like a column having built-in ends (Fig. 1.1(b)). When a very slight additional displacement is imposed, the buckled shape jumps to an end tilt buckling one, with nonzero slopes at both ends (Fig. 1.1(c)). This happens approximately when the lateral deflection in Fig. 1.1(b) exceeds the column diameter. A zoom-in image of the end tilt is shown in Fig. 1.1(d).

(a) (b) (c) (d)

Figure 1.1: Polymer column. (a) Column secured between flat platens solely by contact under compression. (b) Column deflection at first buckling, identical to that of a clamped-ended column. (c) Column deflection at second buckling, exhibiting end tilt. (d) Column end tilt in close-up. (Kalathur and Lakes, 2013)

The critical loads are determined from the experiments as in Fig. 1.1; the first critical load is determined when there is a sufficient change in slope of the load-displacement curve, while the second one is where an abrupt drop in load magnitude occurs, (Kalathur and Lakes, 2013). The experiments show that the critical load for tilt buckling exceeds that for initial buckling by about 0.2%. This agrees with theory (below) which predicts a 0.13% difference in buckling loads. The deviation of experiment from theory is likely due at least in part to the local deformation at the column edge (Fig. 1.1(d)) which is not included in the theory.

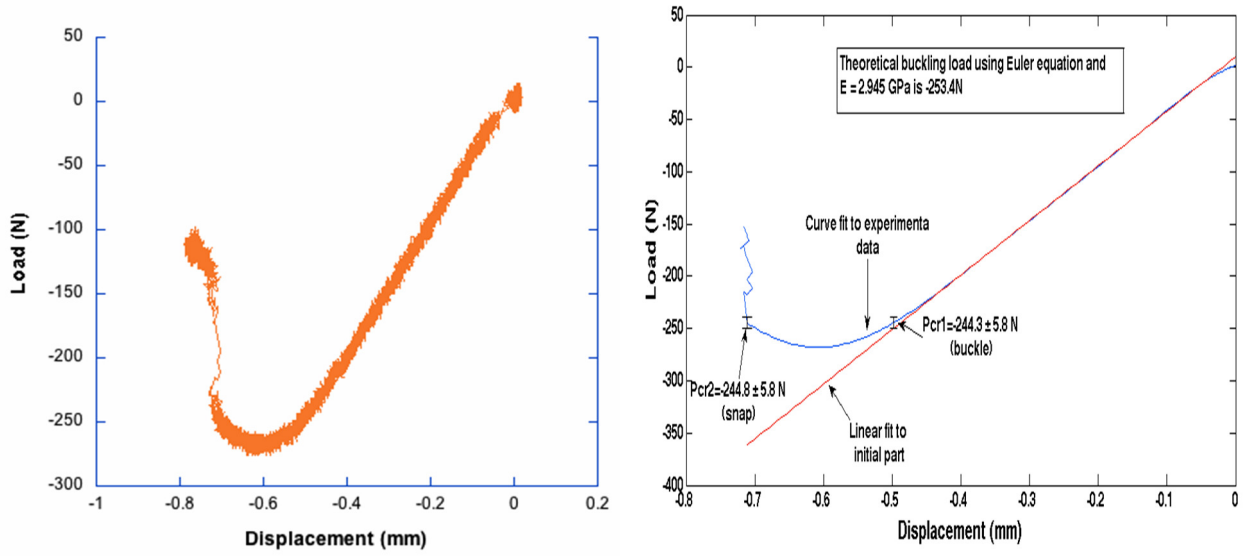

(a) (b)

Figure 1.2: (a) The force-displacement relationship of a PMMA column with d = 6.453 mm and ℓ =197.6mm from zero load through both buckling events. (b) Curve fit of experimental data prior to snap (second buckling) instability used to determine the thresholds for initial buckling and end tilt buckling. On the left, a portion of the raw experimental data for snap-through associated with tilt of column ends is shown. (Kalathur and Lakes, 2013)

1.3. Theoretical Modeling and Analysis

We have successfully modeled theoretically the initial and secondary (end-tilt) buckling events observed in the experiments on compressed columns having flat, unattached ends. The initial buckling can be predicted by direct application of an analysis first done by Timoshenko and Gere (1963) of buckling of a column having rounded ends; this is summarized in Section 1.3.1. The subsequent secondary buckling event can be analyzed in two different ways, leading to identical results; these analyses are presented in Sections 1.3.2 and 1.3.3.

1.3.1. Timoshenko analysis of initial buckling of a column having rounded ends

To facilitate theoretical treatment of the problem of initial buckling of a column with unattached flat ends resting against flat "rigid" platens which load it in compression, to explore the effect of end shape on buckling, and to provide the framework for one approach for analyzing the experimentally-observed secondary buckling event, we model the column ends as being curved. We follow Timoshenko and Gere (1963) and in two dimensions treat the ends as portions of a circle with radius R, as illustrated in Figure 1.3(a). When a column with rounded ends buckles laterally due to compressive loading by contact with rigid flat platens, the line of action of the compressive forces P will displace a distance b as shown Figure 1.3(a, b). Since the angle of rotation of the ends of the bar is small, the displacement is $b = R\theta$.

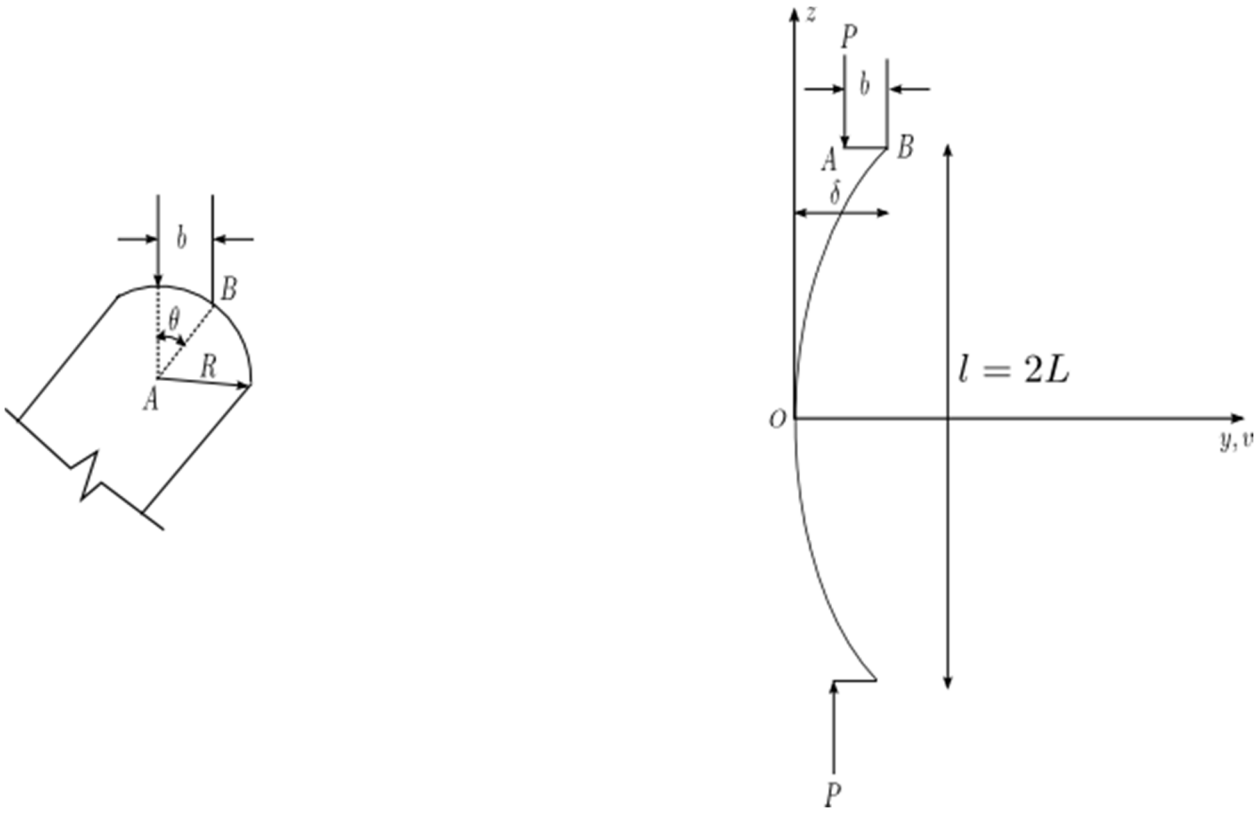

(a) **(b)**

Figure 1.3. (a) Curved end of column, modeled as a portion of a circle having radius *R*; (b) Displacement of forces action line due to rotation of curved column ends.

To analyze the round-ended column, we treat half of a column since it first buckles into a symmetrical shape. We take the origin of the *y*, *z* Cartesian coordinate system at the center O of the column as shown in Figure 1.6(b). We employ the slender beam moment-curvature relation:

$$E I v''(z) = M(z) \tag{1.1}$$

where E, I, $M(z)$ and $v(z)$ are Young's modulus, moment of inertial of the cross-section, moment and deflection at arbitrary cross-section location *z*, respectively. The moment is

$$M(z) = P\left[\delta - v(z) - b\right] \tag{1.2}$$

where $\delta = v(L)$ is the beam end deflection with respect to its center with L = ℓ/2.

Substituting (1.2) into (1.1) and differentiating the result twice with respect to z gives:

$$EI\frac{d^4v}{dz^4} + P\frac{d^2v}{dz^2} = 0. \tag{1.3}$$

To solve (1.3) one needs four boundary conditions on the half-column; these are:

At $z = 0$: displacement and slope are zero:

$$v(0) = v'(0) = 0. \tag{1.4}$$

At $z = L$: shear force and moment are, respectively:

$$EIv'''(L) = -Pv'(L), \qquad EIv''(L) = -Pb = -PRv'(L). \tag{1.5}$$

In the second of (1.5) we have employed the relation between deflection and slope $v' = \tan\theta \approx \theta$: $b = R\theta = Rv'(L)$. Nondimensionalizing (1.3), with dimensionless position $\xi = z/L$, we have

$$\frac{d^4v}{d\xi^4} + k^2\frac{d^2v}{d\xi^2} = 0 \tag{1.6}$$

where

$$k^2 = \frac{PL^2}{EI}. \tag{1.7}$$

The boundary conditions then transform to:

$$v(0) = v'(0) = 0, \quad v'''(1) = -k^2 v'(1), \quad \varepsilon v''(1) = -k^2 v'(1) \tag{1.8}$$

where we have defined $\varepsilon = L/R$.

Equation (1.6) has the general solution

$$v(\xi) = C_1 \sin(k\xi) + C_2 \cos(k\xi) + C_3 \xi + C_4, \tag{1.9}$$

and application of (1.8) to (1.9) requires

$$C_1 = C_3 = 0, \;\; C_2 = -C_4, \;\; C_2 k^2 (k \sin k + \varepsilon \cos k) = 0, \tag{1.10}$$

showing that the system has nontrivial solutions only if

$$k \sin k + \varepsilon \cos k = 0. \tag{1.11}$$

Equation (1.11), recalling the definition (1.7), summarizes the influence of end-roundedness on the initial buckling load. The case of interest here, to predict first buckling of the unattached flat-ended column, is the extreme one in which the column ends are perfectly flat: this occurs when $R \to \infty$, so that $\varepsilon = L/R \to 0$, showing that (1.11) reduces to, for the lowest buckling load and by use of (1.7):

$$\sin k = 0 \quad \Rightarrow \quad k^2 = \frac{PL^2}{EI} = \pi^2 \quad \Rightarrow \quad P_{cr1} = \frac{\pi^2 EI}{L^2}. \tag{1.12}$$

Thus, the initial buckling load for an unattached flat-ended column is the same as for a clamped-ended one. These results were obtained by Timoshenko and Gere (1963).

We conclude that as the compressive load increases from zero to the (first) buckling load $P_{cr1} = \frac{\pi^2 EI}{L^2}$, the straight column buckles to the curved shape, from (1.9) with (1.10)

$$v(\xi) = C_4 \left[1 - \cos(\pi\xi)\right] = f \left[1 - \cos(\pi\xi)\right], \tag{1.13}$$

having renamed C_4 as f. The results (1.12) and (1.13) clearly agree with the experimental results for the initial buckling load and column shape at first buckling described in Section 1.2.

1.3.2. Analysis of secondary buckling via the Timoshenko formulation

The static (or adjacent-equilibrium) method of stability analysis employed by Timoshenko and Gere (1963) only gives the initial buckling load, not the behavior of the column after the load exceeds the critical value. In other words, it does not give the relation between the load P and the maximum lateral column deflection f ($v_{\max} = 2f$) from (1.13); the value of f is not determined. Post-buckling theory for elastic structures deals with this situation and does give this information, e.g., Budiansky (1974). For a truly clamped ended column, the post-buckling curve

(1.13) is always stable and the relation between the coefficient f and the applied load level exceeding the initial buckling load is

$$\frac{P}{P_{cr1}} = 1 + \frac{1}{8}\frac{\pi^2 f^2}{L^2} \tag{1.14}$$

where P_{cr1} is that given in (1.12).

Here we show how (1.14) is derived in a simple, transparent way, applied to a column using the large deflection theory of a beam, Bolotin (1964); we show this because we shall employ this approach in our derivation of the second buckling load below.

The full moment-curvature relation for large deflections is:

$$\frac{1}{\rho} = \frac{\dfrac{d^2 v}{dz^2}}{\sqrt{1 - \left(\dfrac{dv}{dz}\right)^2}} = \frac{M}{EI}. \tag{1.15}$$

When deflections are small, this of course reduces to (1.1) to leading order. For a more accurate result, we employ the following expansion, valid for small $\dfrac{dv}{dz}$:

$$\left[1 - \left(\frac{dv}{dz}\right)^2\right]^{-1/2} = 1 + \frac{1}{2}\left(\frac{dv}{dz}\right)^2 + \frac{3}{8}\left(\frac{dv}{dz}\right)^4 + \ldots \cdot \tag{1.16}$$

Substitution of this and (1.2) into (1.15) gives

$$\frac{d^2v}{dz^2}\left[1+\frac{1}{2}\left(\frac{dv}{dz}\right)^2+\frac{3}{8}\left(\frac{dv}{dz}\right)^4+\ldots\right]+\frac{Pv}{EI}+\frac{P(b-\delta)}{EI}=0. \tag{1.17}$$

Following Galerkin's method, we substitute (1.13) into the left-hand side of (1.17) and require the resulting equation to be orthogonal to the selected function $\cos(\pi\xi)=\cos\left(\frac{\pi z}{L}\right)$, Bolotin (1964):

$$\int_0^L\left\{\frac{d^2v}{dz^2}\left[1+\frac{1}{2}\left(\frac{dv}{dz}\right)^2+\frac{3}{8}\left(\frac{dv}{dz}\right)^4+\ldots\right]+\frac{Pv}{EI}+\frac{P(b-\delta)}{EI}\right\}\cos\left(\frac{\pi z}{L}\right)dz=0 \quad . \tag{1.18}$$

After integration, (1.18) reduces to

$$\frac{P}{P_{cr1}}=1+\frac{1}{8}\frac{\pi^2 f^2}{L^2}+\frac{3}{64}\frac{\pi^4 f^4}{L^4}+\ldots \tag{1.19}$$

where P_{cr1} is that given in (1.12). Comparison with the exact solution of the same problem (elastica problem) using elliptic integrals shows that approximation (1.14) is accurate if $P<1.045\,P_{cr1}$ (Bolotin (1964)).

Although the unattached flat-ended column undergoes initial buckling at the same critical load as the clamped-ended one, their post-buckling behaviors are entirely different. While the post-buckling shape (1.13) of the clamped ended column is stable, Budiansky (1974), that of the unattached flat-ended column is not, as shown by the experiments described in Section 1.2 above. As described there, as the load is increased beyond the initial buckling load (1.12) for the unattached flat-ended column to a second, slightly higher critical load, the shape (1.13) having zero slopes at both column ends buckles into an entirely different shape having nonzero column end slopes, in which the column ends have rocked up onto their corners; this transition is illustrated in Figures 1.1 (b, c).

We model theoretically this change from the first buckled shape to the different second one by now treating the column ends as deviating very slightly from perfect flatness, i.e., as having a very small curvature. This means $\varepsilon = L/R$ is not identically zero but is extremely small.

To determine the critical load for the second buckling event, we interpret the experimental observations in the context of a column whose ends have very small curvature: in this case, the column ends rocking onto their corners corresponds to the load application point moving from the center of the column end all the way to its corner, i.e., b of Figure 1.3 going from zero to $b = d/2$. The second critical buckling load is thus the applied load value needed for $b = d/2$.

Assuming small ε, we expand k in ε through first order:

$$k = k_0 + k_1\varepsilon. \tag{1.20}$$

Substituting (1.20) into (1.11) [which, recall, is valid for any end curvature] and retaining terms through first order of ε gives

$$k_0 \sin(k_0) + \left[cos(k_0) + k_1 sin(k_0) + k_0 k_1 cos(k_0) \right] \varepsilon = 0. \tag{1.21}$$

Enforcing this for each of the two ε powers appearing shows that

$$k_0 = \pi, \quad k_1 = -\frac{1}{\pi}. \tag{1.22}$$

Similarly to (1.20), we expand the other needed variables in ε through first order:

$$f = f_0 + f_1 \varepsilon \tag{1.23}$$

$$P = P_0 + P_1 \varepsilon. \tag{1.24}$$

Employing (1.20) and (1.23) in (1.13) and writing the result through first order in ε gives:

$$v(\xi) = f_0 (1 - cos[k_0 \xi]) + (f_1 - f_1 cos[k_0 \xi] + f_0 k_1 \xi sin[k_0 \xi]) \varepsilon. \tag{1.25}$$

Similarly to (1.18), we impose the condition

$$\int_0^L \left\{ \frac{d^2 v}{dz^2} \left[1 + \frac{1}{2} \left(\frac{dv}{dz} \right)^2 + \frac{3}{8} \left(\frac{dv}{dz} \right)^4 + \ldots \right] + \frac{Pv}{EI} + \frac{P(b-\delta)}{EI} \right\} \cos\left[(k_0 + k_1 \varepsilon) \frac{z}{L} \right] dz = 0. \tag{1.26}$$

We obtain from this after integration and simplification the relation between load and deflection amplitude

$$\frac{P_0}{P_{cr1}} = 1 + \frac{1}{8}\frac{\pi^2 f_0^2}{L^2}. \tag{1.27}$$

The displacement of the force is, from $b = R\theta = Rv'(L)$:

$$b = \frac{R}{L}v'(1) = \frac{1}{\varepsilon}v'(1) = f_0 k_0 k_1 \cos[k_0] = f_0. \tag{1.28}$$

Hence when $b = d/2$

$$v_{\max} = \delta = v(1) = 2f_0 + 2f_1\varepsilon \approx 2f_0 = 2b = d. \tag{1.29}$$

Thus, the second critical load – the load at which the load application point has just reached the corner of the column – is:

$$\frac{P_{cr2}}{P_{cr1}} \approx \frac{P_0}{P_{cr1}} = 1 + \frac{\pi^2}{8}\left(\frac{d}{2L}\right)^2. \tag{1.30}$$

Employing the experimental data from Section 1.2:

$d = 6.453\,mm$, $\ell = 2L = 197.6\,mm$, we calculate from (1.30): $\dfrac{P_{cr2} - P_{cr1}}{P_{cr1}} = 0.13\%$.

That is, the second critical load is predicted to be 0.13% higher than the first critical load. Equation (1.29) provides a useful result for comparing with the experiments: it shows that when the maximum lateral deflection of the column reaches approximately the column diameter, the change in buckled patterns occurs. As noted in Section 1.2, the experiments were in accord with this prediction.

1.3.3. Alternative analysis of secondary buckling load

We now present a completely different analysis of the secondary buckling load which leads to exactly the same result derived in the previous section. The approach here is to consider two identical columns under unchanging end conditions: one column has built-in ends and is loaded above its initial buckling load, and the other has flat ends and is loaded by compressive loads acting at one corner of each end and is deformed such that the end has rotated onto the corner, both as shown in Figure 1.4. The secondary buckling load is the load value at which the vertical deflections of the two columns first becomes identical.

When $P > P_{cr1}$, the post-buckled shape of the clamped-ended column is that obtained in (1.13) and the vertical deflection Δ in Figure 7(a) is obtained as in, e.g. Budiansky (1974):

$$\Delta = \int_0^L \frac{1}{2}\left[v'(z)\right]^2 dz = \frac{1}{2L}\int_0^1 \left[v'(\xi)\right]^2 d\xi = \frac{\pi^2 f^2}{4L}. \tag{1.31}$$

Thus, combining (1.14) and (1.31) gives the relation between the applied load and the vertical deflection:

$$\frac{P}{P_{cr1}} = 1 + \frac{\Delta}{2L}. \tag{1.32}$$

Next consider a column compressed by forces applied at the corners in the manner illustrated in Figure 1.7(b). The boundary conditions in (1.8) do not change except for the moment, which becomes $M = -P\,d/2$, so these conditions become:

$$v(0) = v'(0) = 0, \quad v'''(1) = -k^2 v'(1), \quad v''(1) = -k^2\, d/2. \tag{1.33}$$

Differential equation (1.6) with boundary conditions (1.33) has solution:

$$v(\xi) = \frac{d}{2\cos(k)}\left[\cos(k\xi) - 1\right]. \tag{1.34}$$

The vertical deflection corresponding to the curve (1.34) as illustrated in Figure 1.7(b) is obtained by substitution of (1.34) into (1.31):

$$\frac{\Delta}{L} = \frac{d^2}{16L^2}\frac{k}{\cos^2(k)}\left[k - \sin(k)\cos(k)\right]. \tag{1.35}$$

The second critical load, P_{cr2}, producing the transition shown in Figure 1.1(b) to 1.1(c) is the applied load level at which the vertical deflection in the column of Figure 1.4(a) just equals that of the column of Figure 1.4(b); this means that the Δ in (1.35) just equals that in (1.32).

Thus, substitution of (1.35) into (1.32) and using (1.12) to express P/P_{cr1} in terms of k gives the following equation for k:

$$\frac{k^2}{\pi^2} = 1 + \frac{d^2}{32L^2}\frac{k}{\cos^2(k)}\left[k - \sin(k)\cos(k)\right]. \tag{1.36}$$

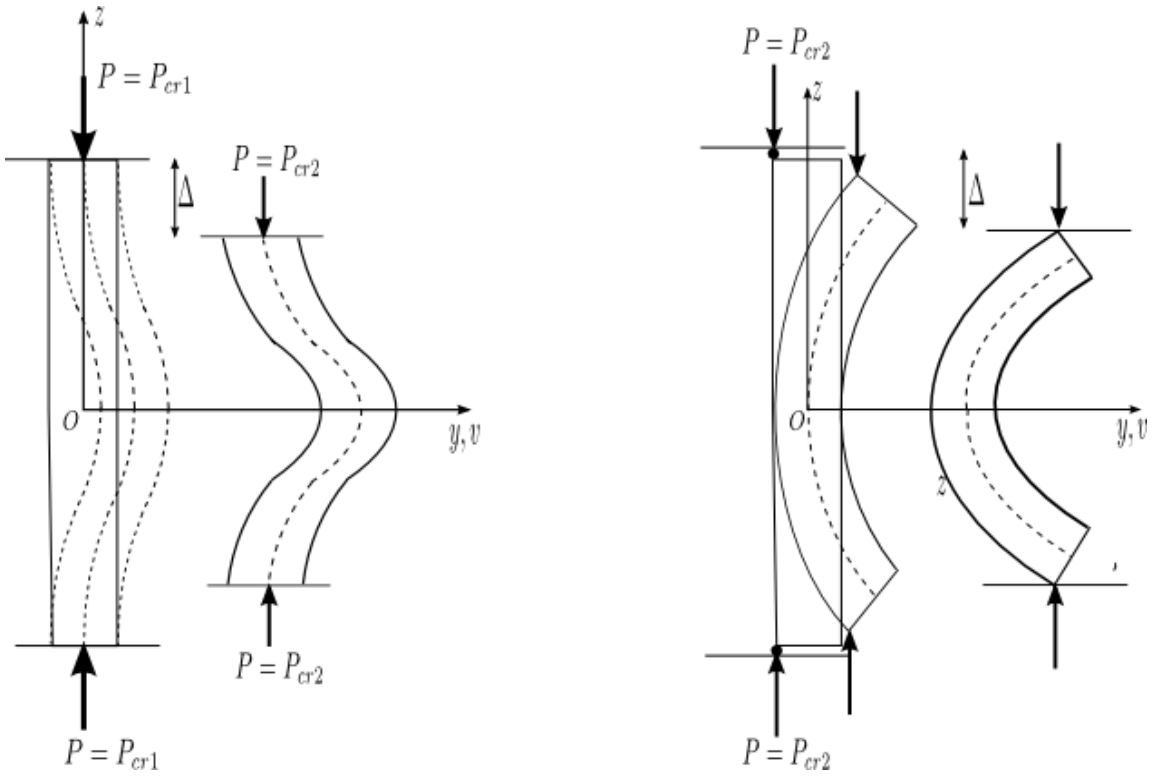

(a) **(b)**

Figure 1.4. The two columns with different end conditions analyzed to predict the second buckling load.

If we call the smallest positive k solution to (1.36) k_{cr}, then the second critical buckling load P_{cr2} is given by:

$$\frac{P_{cr2}}{P_{cr1}} = \frac{k_{cr}^2}{\pi^2}. \tag{1.37}$$

It is easy to verify numerically that (1.37) agrees with (1.30). Alternatively, if we assume $\left(\frac{d}{2L}\right)^2 << 1$, solution of (1.36) for $\frac{k_{cr}^2}{\pi^2}$ through order $\left(\frac{d}{2L}\right)^2$ gives exactly the right side of (1.30).

1.4. Discussion and Conclusions

Buckling mode jump from built in mode to end tilt mode, under an extremely small increase in applied load, was observed experimentally by Kalathur and Lakes for compressed unattached flat-ended columns. This behavior is consistent with our theory, which predicts that secondary or end tilt buckling is only 0.13% greater, for the column geometry tested, than the threshold for primary buckling in which the ends are in full contact with the compression platens.

As for designed dampers, end tilt buckling gives rise to large hysteresis that can be useful in structural damping. In that context, the change in contact condition is critical in achieving high damping and consequently a high stiffness-damping product (Dong and Lakes (2012), Kalathur and Lakes (2013)). Dampers of this type are stabilized by incorporating press-fit columns

designed to buckle in an assemblage of thicker built-in columns that remain straight under a range of intended loads (Dong and Lakes (2012)).

Chapter 2. Tailored Heterogeneity Increases Overall Stability Regime of Composites Having a Negative-Stiffness Inclusion: Piecewise Homogeneity

2.1. Introduction

In contrast to traditional composite materials whose constituents all have positive stiffnesses (i.e., positive-definite elastic modulus tensors), the novel composite solids having a negative-stiffness phase (non-positive-definite elastic modulus tensor) introduced by Lakes (Lakes, 2001; Lakes and Drugan, 2002) can exhibit extreme properties such as extremely high damping, stiffness, thermal expansion and piezoelectric coefficient. Jaglinski et al. (2007) have shown that such a negative-stiffness phase can be implemented in practice, e.g. via phase-transforming particles whose phase transformation is held in limbo by an encapsulating sufficiently stiff matrix phase.

A key issue regarding the practical implementation of these concepts is that the composite material containing the negative-stiffness phase must be stable overall. Investigations of the stability of composite materials containing a negative-stiffness phase were begun only recently (Drugan, 2007; Kochmann and Drugan, 2009, 2012). These have shown that a limited range of negative stiffness of one phase is permissible while retaining overall composite stability under traction boundary conditions provided the negative-stiffness phase is completely encapsulated by

a sufficiently stiff and thick positive-stiffness phase. To date, these investigations have all assumed homogeneous composite phases.

Here, for the first time, we investigate the effects of heterogeneity of the stable phase, and show analytically that if this heterogeneity is appropriately tailored, a larger range of inclusion negative stiffness is permitted while retaining overall composite stability. In the interests of completeness, clarity and practical implementation, we investigate two types of heterogeneity: piecewise homogeneity and continuously-varying heterogeneity.

In the present chapter, we employ the static stability method to investigate for the first time how heterogeneity of the coating material affects the permissible stability regime of a composite material having a negative-stiffness inclusion. We analyze the two-dimensional plane strain isotropic linear elastic composite consisting of a circular cylindrical inclusion with a concentric coating. The inclusion material is homogeneous, but the coating material is permitted to be radially heterogeneous. First, we employ the static stability method to rederive analytical stability conditions derived via a full dynamic analysis by Kochmann & Drugan (2009, 2012) for such a composite with a homogeneous coating of arbitrary thickness to illustrate the validity, relative simplicity and utility of the static stability method. Next, we consider the case in which the material is heterogeneous in the coating.

For homogeneous, isotropic linear elastic materials, of course any set of two constant elastic moduli can be examined: these can be Poisson's ratio and Young's modulus; or the Lamé moduli; or an arbitrary combination these resulting in two independent parameters. In the context

of isotropic, non-homogeneous media, much work has been done but most of it assumes one constant elastic modulus (Poisson's ratio) and one variable one (Young's modulus) but varying in a restricted, not general, way; see, e.g., the works of L.N. Ter-mkrtich'ian (1961), S.G. Lekhnitskii (1962), V.P. Plevako (1971).

Here we work with bulk and shear moduli and in this chapter consider the simplest heterogeneous coating model – a coating comprised of two different homogeneous layers. We show via this simple model that if the coating is sufficiently heterogeneous – that is, if the two layers have sufficiently different moduli – the stability domain of the entire composite can be significantly increased, meaning that a greater range of inclusion negative stiffness is permitted while retaining overall composite stability. We also show that this heterogeneity can change the type of deformation mode that causes first instability of the composite.

The chapter is organized as follows: In Section 2.2, we derive a complete representation for equilibrium solutions in a homogeneous, isotropic, annular cylindrical domain. Section 2.3 shows how these are employed to perform static stability analysis of the composite cylinder with homogeneous phases. Section 2.4 shows application of the static stability approach to the simple two-homogeneous-layer heterogeneous coating.

2.2. Complete representation of equilibrium displacement field in a homogeneous, isotropic, linear elastic annular domain

In the next section we will analyze the stability of a circular cylindrical composite solid consisting of an inclusion of radius a, Lamé moduli λ_1, μ_1, bulk modulus $\kappa_1 = \lambda_1 + \mu_1$ and a coating of outer radius b, Lamé moduli λ_2, μ_2, bulk modulus $\kappa_2 = \lambda_2 + \mu_2$, as illustrated in Fig. 2.1. Here we derive the form of the complete equilibrium displacement field in an annulus for use in the upcoming stability analyses.

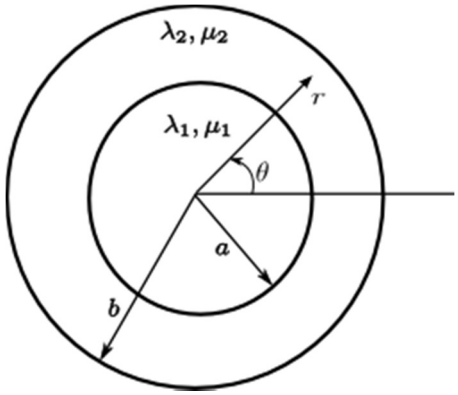

Figure 2.1. The coated-cylinder composite.

Assume the cylinder is infinitely long so plane strain conditions are guaranteed. A polar coordinate system is employed with the origin at the center of the cylinder. Equilibrium when no body forces act requires

$$\nabla \bullet \boldsymbol{\sigma} = \mathbf{0}. \tag{2.1}$$

Applying the isotropic stress-strain relations and the strain-displacement relations, (2.1) becomes the Navier equation

$$(\lambda + \mu)\nabla(\nabla \bullet \mathbf{u}) + \mu\nabla^2\mathbf{u} = \mathbf{0}, \tag{2.2}$$

where $\boldsymbol{\sigma}, \mathbf{u}$ are the stress tensor and the displacement vector, respectively.

Express (2.2) in polar coordinates r, θ with $\mathbf{u} = u_r \mathbf{e}_r + u_\theta \mathbf{e}_\theta$ to obtain, where a subscript comma denotes partial differentiation with respect to ensuing variables

$$(\lambda+\mu)(r^2 u_{r,rr} + r u_{r,r} - u_r + r u_{\theta,r\theta} - u_{\theta,\theta}) + \mu(r^2 u_{r,rr} + r u_{r,r} - u_r + u_{r,\theta\theta} - 2u_{\theta,\theta}) = 0 \qquad (2.3a)$$

$$(\lambda+\mu)(r u_{r,r\theta} + u_{r,\theta} + u_{\theta,\theta\theta}) + \mu(r^2 u_{\theta,rr} + r u_{\theta,r} + 2u_{r,\theta} + u_{\theta,\theta\theta} - u_\theta) = 0. \qquad (2.3b)$$

Following Kochmann and Drugan (2009), we assume solutions can be written in the following separable forms without loss of generality:

$$u_r = f(r)e^{im\theta}, \qquad u_\theta = g(r)e^{im\theta}. \qquad (2.4)$$

Since u_r, u_θ are 2π-periodic functions of θ, m must be an integer. Substituting (2.4) into (2.3) and assuming $\lambda + 2\mu \neq 0$ and $\mu \neq 0$, system (2.3) is equivalent to, where primes denote r-differentiation

$$f'' + \frac{f'}{r} - \left(1 + \frac{m^2\mu}{\lambda+2\mu}\right)\frac{f}{r^2} = \frac{im}{\lambda+2\mu}\left[(\lambda+3\mu)\frac{g}{r^2} - (\lambda+\mu)\frac{g'}{r}\right] \qquad (2.5a)$$

$$g'' + \frac{g'}{r} - \left(1 + \frac{(\lambda+2\mu)m^2}{\mu}\right)\frac{g}{r^2} = -\frac{im}{\mu}\left[(\lambda+3\mu)\frac{f}{r^2} + (\lambda+\mu)\frac{f'}{r}\right]. \qquad (2.5b)$$

For each integer m, (2.5) has a solution $\{f_m(r),\ g_m(r)\}$, and the general solution of (2.3) is a summation of (2.4) over all possible integer values of m:

$$u_r = \sum_{m=-\infty}^{\infty} f_m(r)e^{im\theta},\quad u_\theta = \sum_{m=-\infty}^{\infty} g_m(r)e^{im\theta}. \tag{2.6}$$

Since u_r, u_θ are displacements, they are real and hence we must have (overbar denotes complex-conjugate)

$$f_m(r) = \overline{f_{-m}(r)} \quad \text{and} \quad g_m(r) = \overline{g_{-m}(r)}. \tag{2.7}$$

Use (2.7) to rewrite (2.6) as

$$u_r = 2\Re\left(\sum_{m=0}^{\infty} f_m(r)e^{im\theta}\right), \qquad u_\theta = 2\Re\left(\sum_{m=0}^{\infty} g_m(r)e^{im\theta}\right) \tag{2.8}$$

where $\Re$ denotes the real part. Henceforth we will omit operator $\Re$ for conciseness.

For each mode m, a particular solution is sought in the form, with A, B constants

$$f(r) = Ar^k,\quad g(r) = Br^k. \tag{2.9}$$

Substituting (2.9) into (2.5) gives the following system for the two unknowns A, B:

$$\begin{cases} \left[k^2-\left(1+\dfrac{m^2\mu}{\lambda+2\mu}\right)\right]A+\dfrac{im}{\lambda+2\mu}\left[(\lambda+\mu)k-(\lambda+3\mu)\right]B=0 \\ \dfrac{im}{\mu}\left[(\lambda+\mu)k+(\lambda+3\mu)\right]A+\left[k^2-\left(1+\dfrac{m^2(\lambda+2\mu)}{\mu}\right)\right]B=0. \end{cases} \tag{2.10}$$

A nontrivial solution exists only if the determinant of the coefficient matrix is zero:

$$k^4-2(m^2+1)k^2+(m^2-1)^2=0, \tag{2.11}$$

which has the solutions

$$k=\pm m\pm 1. \tag{2.12}$$

Substitution of (2.9) with (2.12) into (2.8) gives the general solution of (2.3):

$$u_r=Ar+\frac{B}{r}+\left(A_1^1r^2+A_1^2+A_1^3 lnr+A_1^4r^{-2}\right)e^{i\theta}+\sum_{m=2}^{\infty}\left(A_m^1r^{m+1}+A_m^2r^{m-1}+A_m^3r^{-m+1}+A_m^4r^{-m-1}\right)e^{im\theta} \tag{2.13a}$$

$$u_\theta=Cr+\frac{D}{r}+\left(B_1^1r^2+B_1^2+B_1^3 lnr+B_1^4r^{-2}\right)e^{i\theta}+\sum_{m=2}^{\infty}\left(B_m^1r^{m+1}+B_m^2r^{m-1}+B_m^3r^{-m+1}+B_m^4r^{-m-1}\right)e^{im\theta}, \tag{2.13b}$$

where the constants are constrained by (2.10) with (2.12) as follows: A, B, C, D are arbitrary [unconstrained by (2.10) with (2.12) for $m = 0$], while the others must satisfy

$$B_1^1=\frac{i(3\lambda+5\mu)}{\lambda-\mu}A_1^1,\quad B_1^2=iA_1^2+i\frac{(\lambda+\mu)}{\lambda+3\mu}A_1^3,\quad B_1^3=iA_1^3,\quad B_1^4=-iA_1^4 \tag{2.14}$$

$$B_m^1 = \frac{i\left[m(\lambda+\mu)+2(\lambda+2\mu)\right]}{m(\lambda+\mu)-2\mu} A_m^1,\ B_m^2 = iA_m^2,\ B_m^3 = -\frac{i\left[m(\lambda+\mu)-2(\lambda+2\mu)\right]}{m(\lambda+\mu)+2\mu} A_m^3,\ B_m^4 = -iA_m^4. \quad (2.15)$$

2.3. Stability condition for a composite solid with zero traction on the outside boundary

Let us consider the stability of the equilibrium solution $\mathbf{u} = \mathbf{0}, \boldsymbol{\varepsilon} = \mathbf{0}, \boldsymbol{\sigma} = \mathbf{0}$ of the composite solid illustrated in Fig. 2.1 with zero traction on the outside boundary. We do so by seeking nontrivial equilibrium solutions using (2.13). Since the governing equations are linear, and each m contribution in (2.13) is linearly independent of all the others, we may treat each independently.

2.3.1. Nontrivial equilibrium solution for the m = 0 mode

We employ (2.13) to write only the $m = 0$ mode of the solution. [We use the terminology "mode" in analogy to the directly-related dynamic modes in the Kochmann and Drugan (2009) full dynamic analysis.] In the inclusion: $0 \le r \le a$, displacement is finite at $r = 0$, so the $1/r$ term must be removed by setting $B = D = 0$. Hence, renaming constants, the $m = 0$ contribution to the solution in the inclusion is

$$u_r^I = Ar,\ u_\theta^I = Br, \quad (2.16a)$$

while in the coating $a \le r \le b$ it is

$$u_r^{II} = Cr + \frac{D}{r},\ u_\theta^{II} = Er + \frac{F}{r}. \tag{2.16b}$$

The resulting $m = 0$ solution contribution is, in inclusion and coating, respectively, employing Hooke's law and the strain-displacement relations:

$$\begin{cases} \sigma_{rr}^{I} = (\lambda_1 + 2\mu_1)\varepsilon_{rr}^{I} + \lambda_1\varepsilon_{\theta\theta}^{I} = (\lambda_1 + 2\mu_1)u_{r,r}^{I} + \lambda_1\dfrac{u_r^{I}}{r} = 2(\lambda_1 + \mu_1)A = 2\kappa_1 A \\ \sigma_{r\theta}^{I} = 2\mu_1\varepsilon_{r\theta}^{I} = \mu_1(u_{\theta,r}^{I} + \dfrac{u_{r,\theta}^{I} - u_\theta^{I}}{r}) = 0 \end{cases} \tag{2.17a}$$

$$\begin{cases} \sigma_{rr}^{II} = (\lambda_2 + 2\mu_2)\varepsilon_{rr}^{II} + \lambda_2\varepsilon_{\theta\theta}^{II} = (\lambda_2 + 2\mu_2)u_{r,r}^{II} + \lambda_2\dfrac{u_r^{II}}{r} = 2\kappa_2 C - 2\mu_2\dfrac{D}{r^2} \\ \sigma_{r\theta}^{II} = 2\mu_2\varepsilon_{r\theta}^{II} = \mu_2(u_{\theta,r}^{II} + \dfrac{u_{r,\theta}^{II} - u_\theta^{II}}{r}) = -2\mu_2\dfrac{F}{r^2}. \end{cases} \tag{2.17b}$$

Continuity of the displacement and traction vectors across the interface at $r = a$ requires:

$$u_r^{I}(a) = u_r^{II}(a),\quad u_\theta^{I}(a) = u_\theta^{II}(a),\quad \sigma_{rr}^{I}(a) = \sigma_{rr}^{II}(a),\quad \sigma_{r\theta}^{I}(a) = \sigma_{r\theta}^{II}(a), \tag{2.18a}$$

and zero traction on the outside boundary requires

$$\sigma_{rr}^{II}(b) = \sigma_{r\theta}^{II}(b) = 0. \tag{2.18b}$$

Together, (2.18) require

$$F = 0, B = E \tag{2.19a}$$

and

$$\begin{bmatrix} a & -a & -\dfrac{1}{a} \\ 2\kappa_1 & -2\kappa_2 & \dfrac{2\mu_2}{a^2} \\ 0 & 2\kappa_2 & -\dfrac{2\mu_2}{b^2} \end{bmatrix} \begin{Bmatrix} A \\ C \\ D \end{Bmatrix} = \begin{Bmatrix} 0 \\ 0 \\ 0 \end{Bmatrix}. \tag{2.19b}$$

Condition (2.19a) means that if rigid-body rotation is excluded in either phase (it seems physically sensible to exclude it in the outer phase), it will be zero in both phases ($B = E = 0$). Equation (2.19b) has a nontrivial solution only if the determinant of the coefficient matrix is zero:

$$\frac{a^2}{b^2}\mu_2(\kappa_2 - \kappa_1) = \kappa_2(\kappa_1 + \mu_2). \tag{2.20}$$

Relation (2.20) implies $\kappa_1 = -\dfrac{(1 - a^2/b^2)\kappa_2\mu_2}{\kappa_2 + a^2/b^2\,\mu_2}$, meaning that the trivial equilibrium solution is unstable when this condition is satisfied, and that it is stable when κ_1 exceeds this value.

2.3.2. Nontrivial equilibrium solution for the m = 1 mode

The $m = 1$ mode analysis is similar to that for the $m = 0$ case: one writes from (2.13) the displacement field in each domain, retaining only the $m = 1$ contribution to the solution:

For the inclusion:

$$u_r^I = (A_1 r^2 + A_2)e^{i\theta}, \quad u_\theta^I = (B_1 r^2 + B_2)e^{i\theta}. \tag{2.21a}$$

For the coating:

$$u_r^{II} = (C_1 r^2 + \frac{C_2}{r^2} + C_3 lnr + C_4)e^{i\theta}, \quad u_\theta^{II} = (D_1 r^2 + \frac{D_2}{r^2} + D_3 lnr + D_4)e^{i\theta}. \tag{2.21b}$$

The constants in (2.21) are related by (2.14),

$$B_1 = \frac{i(3\lambda_1 + 5\mu_1)}{\lambda_1 - \mu_1} A_1, \; B_2 = iA_2, \; D_1 = \frac{i(3\lambda_2 + 5\mu_2)}{\lambda_2 - \mu_2} C_1, \; D_2 = -iC_2, \; D_3 = iC_3, \; D_4 = iC_4 + \frac{i(\lambda_2 + \mu_2)}{\lambda_2 + 3\mu_2} C_3.$$

Substituting the above relations into (2.21), the resulting $m = 1$ solution contribution is, in inclusion and coating, respectively, employing Hooke's law and the strain-displacement relations:

$$\begin{cases} u_r^I = \left(A_1 r^2 + A_2\right)e^{i\theta}, \quad u_\theta^I = i\left(\dfrac{3\lambda_1 + 5\mu_1}{\lambda_1 - \mu_1} A_1 r^2 + A_2\right)e^{i\theta} \\ \sigma_{rr}^I = (\lambda_1 + 2\mu_1)\varepsilon_{rr}^I + \lambda_1 \varepsilon_{\theta\theta}^I = (\lambda_1 + 2\mu_1)u_{r,r}^I + \lambda_1\left(\dfrac{u_r^I}{r} + \dfrac{u_{\theta,\theta}^I}{r}\right) = -\dfrac{4\mu_1(\lambda_1 + \mu_1)}{\lambda_1 - \mu_1} A_1 r e^{i\theta} \\ \sigma_{r\theta}^I = 2\mu_1 \varepsilon_{r\theta}^I = \mu_1\left(u_{\theta,r}^I + \dfrac{u_{r,\theta}^I - u_\theta^I}{r}\right) = i\dfrac{4\mu_1(\lambda_1 + \mu_1)}{\lambda_1 - \mu_1} A_1 r e^{i\theta} e^{i\theta}. \end{cases} \tag{2.22a}$$

$$
\begin{cases}
u_r^{II} = (C_1 r^2 + \dfrac{C_2}{r^2} + C_3 \ln r + C_4) e^{i\theta}, \\
u_\theta^{II} = i\left(\dfrac{3\lambda_2 + 5\mu_2}{\lambda_2 - \mu_2} C_1 r^2 - \dfrac{C_2}{r^2} + C_3 \ln r + \dfrac{\lambda_2 + \mu_2}{\lambda_2 + 3\mu_2} C_3 + C_4\right) e^{i\theta} \\
\sigma_{rr}^{II} = (\lambda_2 + 2\mu_2)\varepsilon_{rr}^{II} + \lambda_2 \varepsilon_{\theta\theta}^{II} = (\lambda_2 + 2\mu_2) u_{r,r}^{II} + \lambda_2 \left(\dfrac{u_r^{II}}{r} + \dfrac{u_{\theta,\theta}^{II}}{r}\right) \\
\quad = -2\mu_2 \left\{ 2\dfrac{\lambda_2 + \mu_2}{\lambda_2 - \mu_2} C_1 r + \dfrac{2C_2}{r^3} - \dfrac{2\lambda_2 + 3\mu_2}{\lambda_2 + 3\mu_2} \dfrac{C_3}{r} \right\} e^{i\theta} \\
\sigma_{r\theta}^{II} = 2\mu_2 \varepsilon_{r\theta}^{II} = \mu_2 \left(u_{\theta,r}^{I} + \dfrac{u_{r,\theta}^{I} - u_\theta^{I}}{r} \right) = 2i\mu_2 \left\{ 2\dfrac{\lambda_2 + \mu_2}{\lambda_2 - \mu_2} C_1 r + \dfrac{2C_2}{r^3} + \dfrac{\mu_2}{\lambda_2 + 3\mu_2} \dfrac{C_3}{r} \right\} e^{i\theta}.
\end{cases}
\tag{2.22b}
$$

Using (2.22) and applying the conditions of continuous tractions and displacements across the interface, and zero traction boundary conditions on the outside, i.e. conditions (2.18), the original system of 6 equations reduces to $C_3 = 0$ and:

$$
\begin{bmatrix}
a^2 & 1 & -a^2 & -\dfrac{1}{a^2} & -1 \\
a^2 \dfrac{3\lambda_1 + 5\mu_1}{\lambda_1 - \mu_1} & 1 & -a^2 \dfrac{3\lambda_2 + 5\mu_2}{\lambda_2 - \mu_2} & \dfrac{1}{a^2} & -1 \\
a^2 \dfrac{\mu_1(\lambda_1 + \mu_1)}{\lambda_1 - \mu_1} & 0 & -a^2 \dfrac{\mu_2(\lambda_2 + \mu_2)}{\lambda_2 - \mu_2} & -\dfrac{\mu_2}{a^2} & 0 \\
0 & 0 & \dfrac{b^2(\lambda_2 + \mu_2)}{\lambda_2 - \mu_2} & \dfrac{1}{b^2} & 0
\end{bmatrix}
\begin{Bmatrix} A_1 \\ A_2 \\ C_1 \\ C_2 \\ C_4 \end{Bmatrix}
= \begin{Bmatrix} 0 \\ 0 \\ 0 \\ 0 \end{Bmatrix}.
\tag{2.23a}
$$

If rigid-body motion (translation) is removed simultaneously in both phases (setting $A_2 = C_4 = 0$), the above system is over-determined (four independent equations constraining three unknowns), so in general it has only a trivial solution.

However, if rigid-body motion (translation) is retained either one of the two phases and $(A_2 - C_4) \neq 0,$ the above system reduces to

$$\begin{bmatrix} a^2 & -a^2 & -\frac{1}{a^2} & 1 \\ a^2\frac{3\lambda_1+5\mu_1}{\lambda_1-\mu_1} & -a^2\frac{3\lambda_2+5\mu_2}{\lambda_2-\mu_2} & \frac{1}{a^2} & 1 \\ a^2\frac{\mu_1(\lambda_1+\mu_1)}{\lambda_1-\mu_1} & -a^2\frac{\mu_2(\lambda_2+\mu_2)}{\lambda_2-\mu_2} & -\frac{\mu_2}{a^2} & 0 \\ 0 & \frac{b^2(\lambda_2+\mu_2)}{\lambda_2-\mu_2} & \frac{1}{b^2} & 0 \end{bmatrix} \begin{Bmatrix} A_1 \\ C_1 \\ C_2 \\ A_2 - C_4 \end{Bmatrix} = \begin{Bmatrix} 0 \\ 0 \\ 0 \\ 0 \end{Bmatrix} \tag{2.23b}$$

and a nontrivial solution contribution corresponding to the m = 1 mode does exist provided that the determinant of the matrix of coefficients of (2.23b) is zero, namely:

$$\frac{\mu_2}{\mu_1}\left(-1+\frac{a^4}{b^4}\right)\left(2+\frac{\kappa_1}{\mu_1}\right)\frac{\kappa_2}{\mu_2} - \left[\frac{\kappa_2}{\mu_2}+\left(2+\frac{\kappa_2}{\mu_2}\right)\frac{a^4}{b^4}\right]\frac{\kappa_1}{\mu_1} = 0\,.$$

Although the m = 1 mode can exist, throughout the manuscript we focus on mode m = 0 which is assumed to be critical. We later prove this to be the case for all optimal solutions found.

2.3.3. Nontrivial equilibrium solutions for the remaining *m* modes ($m \geq 2$)

Following the same procedures as above, we express the displacement field for each $m \geq 2$ contribution as:

In the inclusion:

$$u_r = \left(A_1 r^{m+1} + A_2 r^{m-1}\right) e^{im\theta} \tag{2.24a}$$

$$u_\theta = \left(B_1 r^{m+1} + B_2 r^{m-1}\right) e^{im\theta}. \tag{2.24b}$$

In the coating:

$$u_r = \left(C_1 r^{m+1} + C_2 r^{m-1} + C_3 r^{-m+1} + C_4 r^{-m-1}\right) e^{im\theta} \tag{2.25a}$$

$$u_\theta = \left(D_1 r^{m+1} + D_2 r^{m-1} + D_3 r^{-m+1} + D_4 r^{-m-1}\right) e^{im\theta}. \tag{2.25b}$$

The constants in (2.25) are related by (2.15)

$$\begin{aligned} B_1 &= \frac{i\left[m\kappa_1 + 2(\kappa_1+\mu_1)\right]}{m\kappa_1 - 2\mu_1} A_1, \quad B_2 = iA_2, \\ D_1 &= \frac{i\left[m\kappa_2 + 2(\kappa_2+\mu_2)\right]}{m\kappa_2 - 2\mu_2} C_1, \quad D_2 = iC_2, \quad D_3 = -\frac{i\left[m\kappa_2 - 2(\kappa_2+\mu_2)\right]}{m\kappa_2 + 2\mu_2} C_3, \quad D_4 = -iA_4. \end{aligned} \tag{2.26}$$

Applying the six conditions (2.18) with the six relations (2.26), one obtains a system of twelve equations for twelve unknowns. A nontrivial solution corresponding to the mode m contribution exists only if the determinant of the coefficient matrix is zero. This determinant reduces to:

$$\frac{\kappa_2}{\mu_2}\left[\frac{\kappa_1}{\mu_1} + \frac{\mu_2}{\mu_1}\left(2 + \frac{\kappa_1}{\mu_1}\right)\right]\left(2 + \frac{\kappa_1}{\mu_1} + \frac{\mu_2}{\mu_1}\frac{\kappa_1}{\mu_1}\right)\left(\frac{a}{b}\right)^2 + \frac{\kappa_2}{\mu_2}\left(\frac{\mu_2}{\mu_1} - 1\right)\left\{2\frac{\mu_2}{\mu_1}\frac{\kappa_2}{\mu_2} + \frac{\kappa_1}{\mu_1}\left[-2 + \left(\frac{\mu_2}{\mu_1} - 1\right)\frac{\kappa_2}{\mu_2}\right]\right\}\left(\frac{a}{b}\right)^{2+4m}$$

$$+\left(\frac{a}{b}\right)^{2m}\left\{\begin{array}{l}-2\left(\frac{\mu_2}{\mu_1}-1\right)\left[\frac{\kappa_1}{\mu_1}+\frac{\mu_2}{\mu_1}\left(2+\frac{\kappa_1}{\mu_1}\right)\right]\left(\frac{\kappa_2}{\mu_2}\right)^2\left(\frac{a}{b}\right)^2+4\left(1+\frac{\kappa_2}{\mu_2}\right)\left(\frac{\kappa_1}{\mu_1}-\frac{\mu_2}{\mu_1}\frac{\kappa_2}{\mu_2}\right)\left(\frac{a}{b}\right)^4 \\ -m^2\left(\frac{\mu_2}{\mu_1}-1\right)\left[\frac{\kappa_1}{\mu_1}+\frac{\mu_2}{\mu_1}\left(2+\frac{\kappa_1}{\mu_1}\right)\right]\left(\frac{\kappa_2}{\mu_2}\right)^2\left[\left(\frac{a}{b}\right)^2-1\right]^2\end{array}\right\}=0 \qquad (2.27)$$

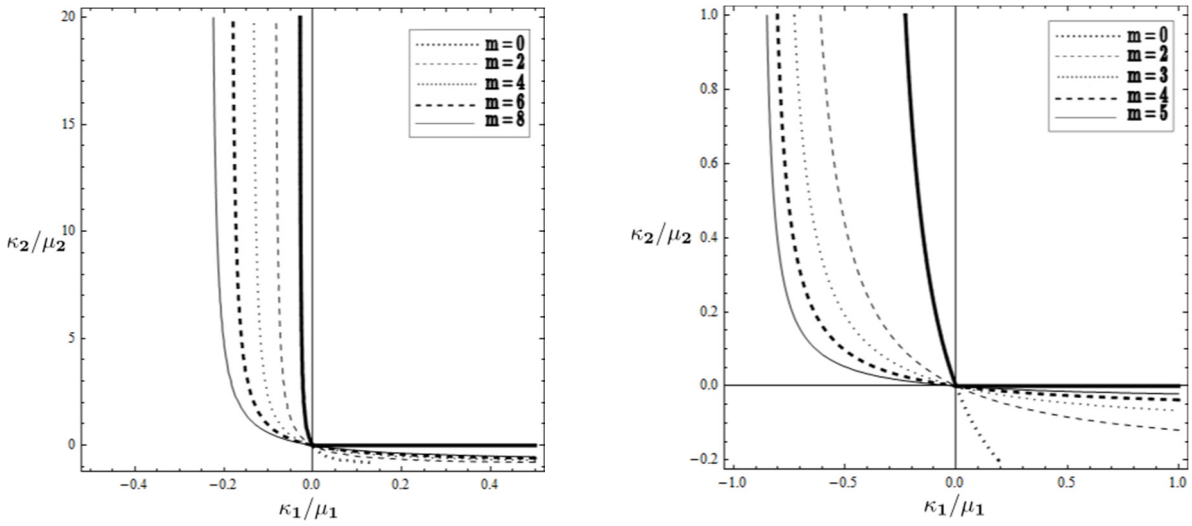

a) $\mu_2/\mu_1 = 1.5,\ a/b = 0.99$ b) $\mu_2/\mu_1 = 0.85,\ a/b = 0.76$

Figure 2.2 Restrictions on the elastic moduli in the plane $\kappa_1/\mu_1 - \kappa_2/\mu_2$ for a composite solid with (a) thin and (b) thick homogeneous coatings.

Figure 2.2 shows the stability maps using (20) with (27) for two illustrative cases: a very thin coating and a thicker coating. As the composite must satisfy pointwise necessary conditions for stability, its moduli must be strongly-elliptic: $\mu > 0,\ \kappa/\mu > -1$. It is worth mentioning that outside of the strongly elliptic conditions (i.e. $\kappa_1/\mu_1 < -1$), a second branch of the derived solution (27) can appear to the left of the solution shown in Fig. 2 but this second branch is

irrelevant for the stability limit. The stability-instability boundary is the bold and thicker curve in both figures. Each curve separates the stable and unstable regimes for the mode it presents; above and to the right of the curve is the stable regime. This is because one begins in the strongly positive-definite upper-right portion of the figure, where stability is assured; the composite remains stable until the first curve is encountered, indicating that an adjacent equilibrium solution exists.

Another way to prove this mathematically is via the energy approach. The equilibrium solution $\mathbf{u} = \mathbf{0}, \boldsymbol{\varepsilon} = \mathbf{0}, \boldsymbol{\sigma} = \mathbf{0}$ is stable if

$$\int_V \mathbf{e}:\mathbf{C}:\mathbf{e}\, dV = \int_V \left[\lambda (tr\mathbf{e})^2 + 2\mu \mathbf{e}:\mathbf{e} \right] dV > 0 \tag{2.28}$$

where $\mathbf{e} = sym(\nabla \mathbf{u})$, $\mathbf{u}$ is any kinematically-admissible infinitesimal displacement field, $\mathbf{C}$ is the fourth order elastic modulus tensor and V is the domain of the composite solid. Since (2.28) must be true for all kinematically admissible infinitesimal displacement fields in general, it is true for any axisymmetric infinitesimal displacement field in particular. Hence, let us use the following trial axisymmetric displacement field:

$$\begin{cases} u_r^I = Ar, \;\; u_\theta^I = 0 \\ \varepsilon_{rr}^I = u_{r,r}^I = A, \varepsilon_{\theta\theta}^I = \dfrac{u_r^I}{r} = A. \end{cases} \tag{2.29a}$$

$$\begin{cases} u_r^{II} = Br + \dfrac{C}{r}, \quad u_\theta^{II} = 0 \\ \varepsilon_{rr}^{II} = u_{r,r}^{II} = B - \dfrac{C}{r^2}, \quad \varepsilon_{\theta\theta}^{II} = \dfrac{u_r^{II}}{r} = B + \dfrac{C}{r^2}. \end{cases} \tag{2.29b}$$

where A, B, C are arbitrary constants. The only requirement is that the trial displacement field is continuous across the inclusion-coating interface (kinematic admissibility), which requires:

$$u_r^I(a) = u_r^{II}(a) \qquad \text{or} \qquad Aa = Ba + \frac{C}{a}. \tag{2.30}$$

Substituting (2.29) into (2.28) with condition (2.30), one must satisfy

$$\left[a^2\kappa_1 + \left(b^2 - a^2\right)\kappa_2\right]B^2 + 2\kappa_1 BC + \left[\frac{\kappa_1}{a^2} + \mu_2\left(\frac{1}{a^2} - \frac{1}{b^2}\right)\right]C^2 > 0 \tag{2.31}$$

for all constants B, C which are not zero simultaneously. (2.31) is a quadratic form of B, C and positive if

$$a^2\kappa_1 + \left(b^2 - a^2\right)\kappa_2 > 0, \qquad Det\begin{bmatrix} a^2\kappa_1 + \left(b^2 - a^2\right)\kappa_2 & \kappa_1 \\ \kappa_1 & \dfrac{\kappa_1}{a^2} + \mu_2\left(\dfrac{1}{a^2} - \dfrac{1}{b^2}\right) \end{bmatrix} > 0$$

which imply

$$\frac{a^2}{b^2}\mu_2\left(\kappa_2-\kappa_1\right)<\kappa_2\left(\kappa_1+\mu_2\right) \quad \Rightarrow \quad \kappa_1>-\frac{\left(1-a^2/b^2\right)\kappa_2\mu_2}{\kappa_2+a^2/b^2\,\mu_2}. \tag{2.32}$$

Also from (27), taking limit as $m\to\infty$ one obtains $\kappa_2/\mu_2\to 0$. By plotting all solution contribution requirements in the plane $\kappa_1/\mu_1-\kappa_2/\mu_2$, we reconfirm analytically what Kochmann & Drugan (2009) showed analytically for a thin coating and numerically for a thick one via a full dynamic analysis. We also show that for all coating thicknesses the stability-instability boundary is composed of two parts: the $m = 0$ mode, which defines the left side of the boundary, and the $m=\infty$ mode, which defines the lower part of the boundary. So the dynamic $m = 0$ mode (axisymmetric mode) is the most restrictive, hence critical, mode for a composite solid comprised of homogeneous constituents, having a positive stiffness coating ($\kappa_2,\mu_2>0$) and a traction-free outer boundary. Hence, condition (20) is the boundary between overall composite stability and instability, written as inequality (32) for the sufficient stability condition. It has a clear physical meaning if one determines the overall bulk composite modulus $\overline{\kappa}$ of the present composite (Lakes & Drugan, 2002):

$$\overline{\kappa}=\frac{\kappa_2\left(\kappa_1+\mu_2\right)+a^2/b^2\,\mu_2\left(\kappa_1-\kappa_2\right)}{\kappa_1+\mu_2+a^2/b^2\left(\kappa_2-\kappa_1\right)}. \tag{2.33}$$

Thus, (2.32) is the statement that the overall composite bulk modulus must be positive for composite stability, exactly the condition determined by Kochmann & Drugan (2012). We further find that each of the modes determined in the Kochmann and Drugan (2012) dynamic

solution is identically given by those determined here, with the added benefit of the present analysis being that we have determined a reasonably compact analytical expression for all modes in Eq. (2.27). We have thus demonstrated how the static stability approach is employed, illustrated its great simplicity compared to the full dynamic approach (see Kochmann and Drugan, 2009) and confirmed that it gives the correct results, in the nontrivial problem analyzed by Kochmann and Drugan (2009, 2012). This inspires confidence in its use in the inhomogeneous coating cases to be analyzed next.

2.4. Stability requirements for a traction-free composite having a two-layer coating

2.4.1. Demonstration that coating heterogeneity can change the critical instability mode

In this section, we demonstrate that the conclusion obtained above, that the $m = 0$ mode is the critical one, is not always true if the coating is heterogeneous. Let us first consider the simplest version of coating heterogeneity: two different homogeneous layers comprising the coating, as shown in Figure 2.3a.

The focus here is to demonstrate that the $m = 0$ mode is not always the critical one; we shall later employ this coating model to increase the composite stability regime. In the cases when the mode $m = 0$ ceases to be the stability limit, the reason is coating heterogeneity. Specifically, this is only caused by shear modulus heterogeneity, not bulk modulus heterogeneity. For example, in

the simple three-layer-composite model, mode $m = 0$ is always critical if the shear modulus is constant in the coating and it is not critical if the coating bulk modulus is constant (it does not have to be incompressible) and if the torsional stiffness of the middle layer is the least of the three layers and the variance of the torsion stiffness in the coating is sufficiently large (See Fig. 2.4 below.)

For simplicity, we consider the special case in which only the shear modulus differs in the two coating layers, i.e. $\mu_2 \neq \mu_3$, $\kappa_2 = \kappa_3 = \kappa$. Applying exactly the same procedure of the static stability analysis illustrated in Section 2.3 to the 3-layer composite (with the attendant additional layer interface across which we enforce continuous traction and displacement vectors), we have determined the complete stability map for some interesting cases, illustrated in Fig. 2.4.

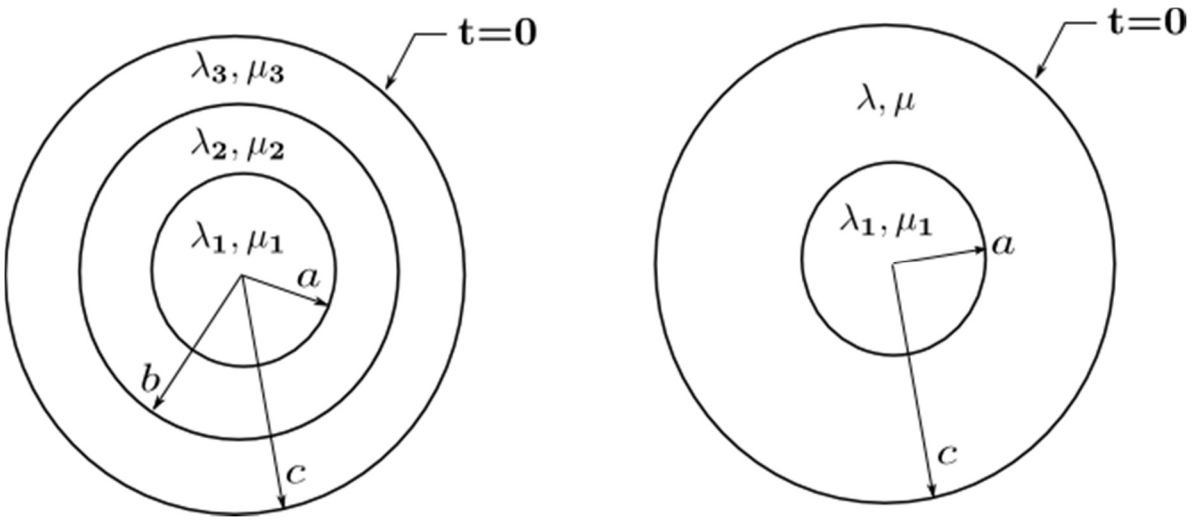

(a) (b)

Figure 2.3. Geometry of a composite solid having (a) a heterogeneous coating comprised of two homogeneous layers with different shear moduli and (b) a homogeneous coating.

When the heterogeneity is small, Fig. 2.4(a), $\mu_2 \approx \mu_3$, the $m = 0$ mode is still the critical one. This remains true for the case in Fig. 2.4(b) when the heterogeneity is large but $\mu_2 > \mu_3$. Criticality of the $m = 0$ mode also applies to the case in Fig. 2.4(c); however, unlike the cases in Figs. 2.4(a) and 2.4(b) in which no modes overlap, in the case of Fig. 2.4(c) all modes except the $m = 0$ one begin to overlap. In Fig. 2.4(d), all modes overlap and hence the $m = 0$ mode is not always critical: in particular, as Fig. 2.4(d) shows, for $\kappa/\mu_2 > 13$, the $m = 8$ mode becomes critical prior to the $m = 0$ one (but note that not all modes are illustrated – actually the $m = \infty$ mode is the critical one for $\kappa/\mu_2 > 13$). Thus making the coating heterogeneous can in general change the distribution order of the modes and can tune a mode of interest into a critical mode.

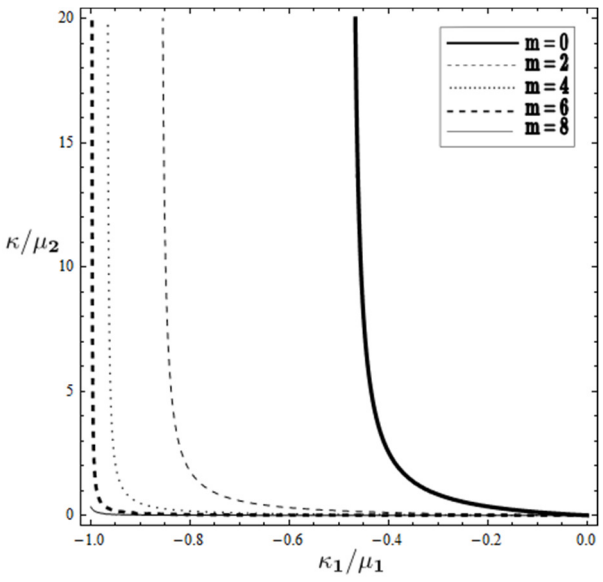

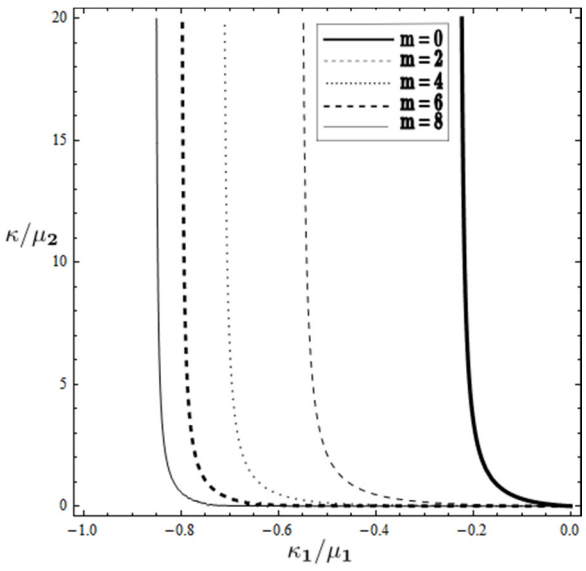

a) $\mu_2 = 1.03\mu_1 > \mu_1 > \mu_3 = 0.97\mu_1$ b) $\mu_1 > \mu_2 = 0.9\mu_1 > \mu_3 = 0.2\mu_1$

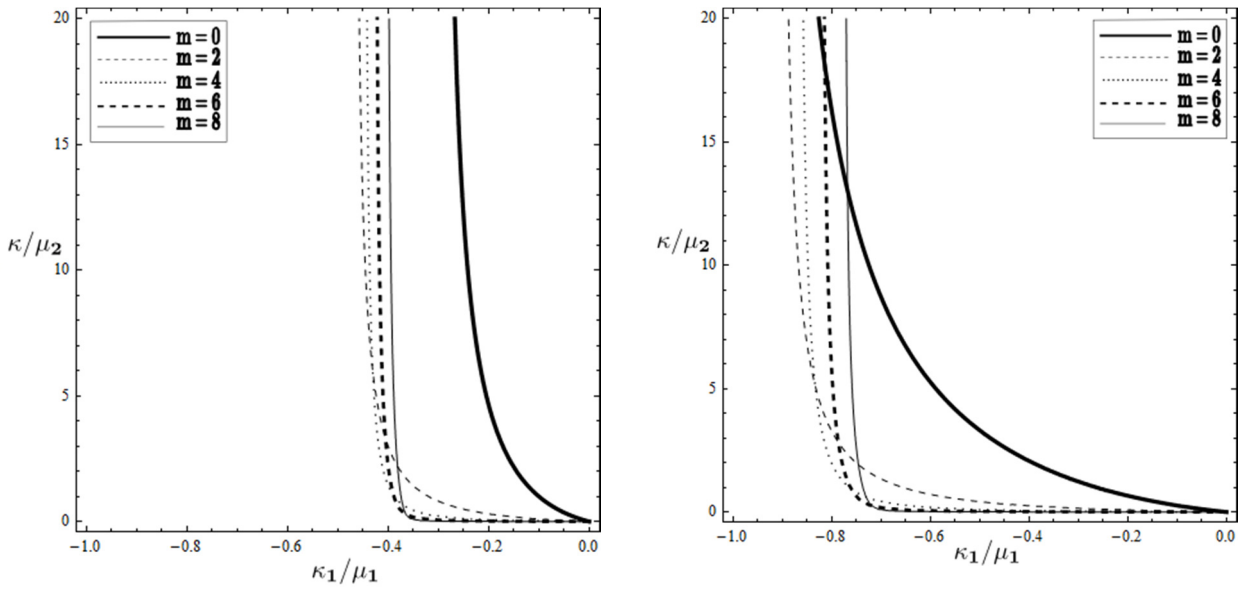

c) $\mu_2 = 0.2\mu_1 < \mu_3 = 0.9\mu_1 < \mu_1$ d) $\mu_2 = 0.5\mu_1 < \mu_1 < \mu_3 = 3\mu_1$

Figure 2.4. Restrictions on the elastic moduli in the plane $\kappa_1/\mu_1 - \kappa/\mu_2$ for a three-layer composite of fixed volume ratios $a/b = 0.9,\ \ b/c = 0.8$.

2.4.2. Determination of optimal two-layer coating composites

Next, we employ this simplest model of coating heterogeneity, the two-homogeneous-layer coating, to determine the optimal stability domain, i.e. to enable the inclusion to have the most negative stiffness possible while keeping the composite stable overall. We do this by considering a particular case in which the most restrictive mode leading to instability for the three-layer composite is the m = 0 one. We compare this composite solid with a two-layer composite solid having the same geometry (see Figure 2.3b) and the same volume averages of elastic moduli in both coatings, which requires:

$$\left(c^2-b^2\right)\mu_3+\left(b^2-a^2\right)\mu_2=\left(c^2-a^2\right)\mu \text{ or } (1-\beta)u+\beta(1-\alpha)v=(1-\alpha\beta) \tag{2.34a}$$

$$\left(c^2-b^2\right)\kappa_3+\left(b^2-a^2\right)\kappa_2=\left(c^2-a^2\right)\kappa \text{ or } (1-\beta)x+\beta(1-\alpha)y=(1-\alpha\beta) \tag{2.34b}$$

where

$$\alpha=\frac{a^2}{b^2},\quad \beta=\frac{b^2}{c^2},\quad x=\frac{\kappa_3}{\kappa},\quad y=\frac{\kappa_2}{\kappa},\quad u=\frac{\mu_3}{\mu},\quad v=\frac{\mu_2}{\mu}. \tag{2.35}$$

The instability domain boundary for the two-layer composite whose coating is homogeneous is, from (2.20)

$$\frac{a^2}{c^2}\mu(\kappa-\kappa_1)=\kappa(\kappa_1+\mu). \tag{2.36}$$

The instability domain boundary for the three-layer composite is sought by determining the conditions to have a nontrivial $m = 0$ solution since we assume (confirmed later) this mode is critical. This solution must satisfy continuity of the displacement and traction vectors across the interfaces $r=a$ and $r=b$ together with zero traction on the outside boundary $r=c$. Following a similar procedure to that above, the stability boundary is determined to be

$$\kappa_1=-\frac{(1-\alpha)\kappa_2\mu_2(\kappa_3+\beta\mu_3)+(1-\beta)\kappa_3\mu_3(\mu_2+\alpha\kappa_2)}{(\kappa_2+\alpha\mu_2)(\kappa_3+\beta\mu_3)+(1-\alpha)(1-\beta)\kappa_3\mu_3} \tag{2.37}$$

which has a similar meaning to (2.20) or (2.36) as it makes the overall 3-layer bulk composite modulus zero. Nondimensionalizing (2.37) gives

$$\frac{\kappa_1}{\mu_1} = sz\frac{-vx(u+yz)+(-u+v)xyz\alpha+u\beta\left[v(x-y)+y(v+xz)\alpha\right]}{xz(u+yz-u\alpha+v\alpha)+u\beta\left[yz+v\alpha+xz(-1+\alpha)\right]} \tag{2.38}$$

where $\alpha, \beta, x, y, u, v$ are as given in (2.35) and

$$s = \frac{\mu}{\mu_1} > 0, \quad z = \frac{\kappa}{\mu} > 0.$$

Now we need to seek the minimum of (2.38) depending on variables *x*, *y*, *u*, *v*, α, β and parameters *s*, *z*. Here the thickness ratio of the two layers in the coating is allowed to vary but the total thickness of those layers is kept constant, i.e. *a* and *c* are constants but *b* is variable, with of course $a \le b \le c$. This implies that α, β are not independent variables but $\beta = \frac{a^2/c^2}{\alpha} = \frac{t}{\alpha}, t \le \alpha \le 1; t = \frac{a^2}{c^2} = \text{const} \in (0,1)$ is the volume ratio of the 3-layer composite. As (2.38) depends linearly on *s*, we will omit this parameter and the problem of constrained optimization is restated as follows:

Minimize the function

$$F(x, y, u, v, \alpha, \beta) = z\frac{-vx(u+yz)+(-u+v)xyz\alpha+u\beta\left[v(x-y)+y(v+xz)\alpha\right]}{xz(u+yz-u\alpha+v\alpha)+u\beta\left[yz+v\alpha+xz(-1+\alpha)\right]} \tag{2.39a}$$

subject to the constraints

$$\begin{aligned}&(1-\beta)x+\beta(1-\alpha)y=(1-\alpha\beta),\ \ (1-\beta)u+\beta(1-\alpha)v=(1-\alpha\beta),\\&x\ge 0,\ \ y\ge 0,\ \ u\ge 0,\ \ v\ge 0,\ \ t\le\alpha\le 1,\ \ \beta=\frac{t}{\alpha}.\end{aligned}\tag{2.39b}$$

For mathematical simplicity but also because the individual results will prove to be interesting and revealing, let us divide (2.39) into the following cases: constant shear modulus $\mu_3=\mu_2=\mu$, constant bulk modulus $\kappa_3=\kappa_2=\kappa$ and both moduli varying $\kappa_3\neq\kappa_2, \mu_3\neq\mu_2$ in the coating.

2.4.2.1. Constant shear modulus in the two-layer coating: $\mu_3=\mu_2=\mu$

This means $u=v=1$ [see (2.35)]. Then (2.39) becomes

Minimize the function:

$$G(x,y,\alpha)=F\left(x,y,1,1,\alpha,\frac{t}{\alpha}\right)=z\frac{-x(1+yz)\alpha+t\left[x-y+y(1+xz)\alpha\right]}{xz(1+yz)\alpha+t\left[yz+\alpha+xz(-1+\alpha)\right]}\tag{2.40a}$$

subject to the constraints

$$\begin{aligned}&\left(1-\frac{t}{\alpha}\right)x+\frac{t}{\alpha}(1-\alpha)y=(1-t),\\&x\ge 0,\ \ y\ge 0,\ \ t\le\alpha\le 1.\end{aligned}\tag{2.40b}$$

The Lagrangian function for the constrained optimization problem (2.40) is:

$$L_1(x,y,\alpha)=G(x,y,\alpha)+l_1\left[\left(1-\frac{t}{\alpha}\right)x+\frac{t(1-\alpha)}{\alpha}y-(1-t)\right]+l_2x+l_3y+l_4(\alpha-t)+l_5(1-\alpha) \qquad (2.41)$$

where Lagrange multipliers l_2, l_3, l_4, l_5 are all nonnegative.

The extreme points satisfy the Karush-Kuhn-Tucker condition which requires:

$$\begin{cases} \dfrac{\partial L_1}{\partial x}=0,\ \dfrac{\partial L_1}{\partial y}=0,\ \dfrac{\partial L_1}{\partial \alpha}=0 \\ \left(1-\dfrac{t}{\alpha}\right)x+\dfrac{t(1-\alpha)}{\alpha}y=1-t,\ \ l_2x=0,\ \ l_3y=0,\ \ l_4(\alpha-t)=0,\ \ l_5(1-\alpha)=0 \\ x\ge 0,\ \ y\ge 0,\ \ t\le\alpha\le 1,\ \ l_2\ge 0,\ \ l_3\ge 0,\ \ l_4\ge 0,\ \ l_5\ge 0. \end{cases} \qquad (2.42)$$

Solutions of (2.42), called extreme points are

$$l_1=\frac{tz}{(t+z)^2},\ \ l_2=l_3=l_4=l_5=0,\ (x,y,\alpha)=\{(1,1,1),(1,1,\mathrm{t}),(1,1,\text{arbitrary})\}.$$

The smallest value among the values of $G(x,y,\alpha)$ at these points is the global minimum whose the extreme point is the optimal one, $\left(x^*,y^*,\alpha^*\right)$. The values of $G(x,y,\alpha)$ at the three extreme points above are the same:

$$G(1,1,1)=G(1,1,\mathrm{t})=G(1,1,\text{arbitrary})=-\frac{(1-t)z}{t+z}.$$

So the optimal point and the global minimum value are:

$$x^* = 1,\ \ y^* = 1,\ \ t \le \alpha^* \le 1,\ \ \ G\left(x^*, y^*, \alpha^*\right) = -\frac{(1-t)z}{t+z} \tag{2.43}$$

(α^* can have any value in its specified range)

In summary, (2.43) means that among all piecewise homogeneous isotropic two layers in the coating whose shear modulus is a constant, the case in which both layers are identical gives the inclusion the most negative stiffness possible while maintaining composite overall stable. This conclusion for piecewise varying bulk modulus in two layers is exactly the same as that for the continuously-varying bulk modulus in the coating, which is shown in Chapter 3.

2.4.2.2 Constant bulk modulus in the two-layer coating: $\kappa_3 = \kappa_2 = \kappa$

This means $x = y = 1$ [see (2.35)]. Then (2.39) becomes:

Minimize the function:

$$H(u, v, \alpha) = F\left(1, 1, u, v, \alpha, \frac{t}{\alpha}\right) = z\frac{-v(u+z)\alpha + tu(v+z)\alpha + (-u+v)z\alpha^2}{tu\alpha(z+v) + z\alpha(u+z-u\alpha+v\alpha)} \tag{2.44a}$$

subject to the constraints

$$\left(1-\frac{t}{\alpha}\right)u+\frac{t}{\alpha}(1-\alpha)v=(1-t),$$
$$u\ge 0,\ \ v\ge 0,\ \ t\le\alpha\le 1. \tag{2.44b}$$

The Lagrangian function for the constrained optimization problem (2.44) is:

$$L_2(u,v,\alpha)=H(u,v,\alpha)+l_1\left[\left(1-\frac{t}{\alpha}\right)u+\frac{t(1-\alpha)}{\alpha}v-(1-t)\right]+l_2u+l_3v+l_4(\alpha-t)+l_5(1-\alpha) \tag{2.45}$$

where Lagrange multipliers l_2, l_3, l_4, l_5 are all nonnegative.

The extreme points satisfy the Karush-Kuhn-Tucker condition which requires:

$$\begin{cases}\dfrac{\partial L_2}{\partial u}=0,\ \ \dfrac{\partial L_2}{\partial v}=0,\ \ \dfrac{\partial L_2}{\partial\alpha}=0\\ \left(1-\dfrac{t}{\alpha}\right)u+\dfrac{t(1-\alpha)}{\alpha}v=1-t,\ \ l_2u=0,\ \ l_3v=0,\ \ l_4(\alpha-t)=0,\ \ l_5(1-\alpha)=0\\ u\ge 0,\ \ v\ge 0,\ \ \ t\le\alpha\le 1,\ \ l_2\ge 0,\ \ l_3\ge 0,\ \ l_4\ge 0,\ \ l_5\ge 0.\end{cases} \tag{2.46}$$

Eq. (2.46) has only one optimal point $\left(u^*,v^*,\alpha^*\right)$:

$$\begin{cases}u^*=\dfrac{1-z+(1+z)\sqrt{t}}{2},\quad v^*=\dfrac{(1-z)+(1+z)/\sqrt{t}}{2},\quad \alpha^*=\sqrt{t}\\ H\left(u^*,v^*,\alpha^*\right)=-\dfrac{(1-t)z\left[(1+z)\sqrt{t}+2t(1-z)+(1+z)t\sqrt{t}\right]}{t\left[4z+(1+z)\sqrt{t}+2t(1-z)+(1+z)t\sqrt{t}\right]}.\end{cases} \tag{2.47}$$

This point lies inside the domain $u \geq 0,\ v \geq 0,\ t \leq \alpha \leq 1$ if and only if

$$0 < z < \frac{1+\sqrt{t}}{1-\sqrt{t}}. \tag{2.48}$$

Last but not least, we must confirm the criticality of the $m = 0$ mode of this optimal 2-layer coating composite. Following the procedures described in detail in Section 2.4.1 above, we determine the complete stability map for very thin and thicker optimal coatings, illustrated in Fig. 2.5. When the coating is very thin, the effects of piecewise homogeneity of the shear modulus become negligible, meaning that the results for the cases of homogeneous and optimal coatings should converge. Our numerical results below demonstrate this, i.e. Fig. 2.2(a) and Fig. 2.5(a) are exactly the same.

For a thicker optimal coating, the stability map indeed confirms the critical property of the $m = 0$ mode as shown in Fig. 2.5(b). This has been drawn for the same parameter values as that for the homogeneous coating shown in Fig. 2.2(b). Comparing Figs. 2.2(b) and 2.5(b), we observe that all stability curves for the "optimal" coating composite lie to the left of those for the homogeneous one, meaning the overall stability regime for the piecewise homogeneous-coating composite is indeed larger than that of the homogeneous-coating one.

So we conclude that among all piecewise homogeneous isotropic materials in the coating whose bulk modulus is a constant and satisfying (2.48), the one defined by (2.47) permits the inclusion to have the most negative stiffness possible while maintaining overall composite

stability. This result for the piecewise-varying shear modulus is also used to interpret that for the continuously-varying shear modulus in the coating, which is analyzed in Chapter 3.

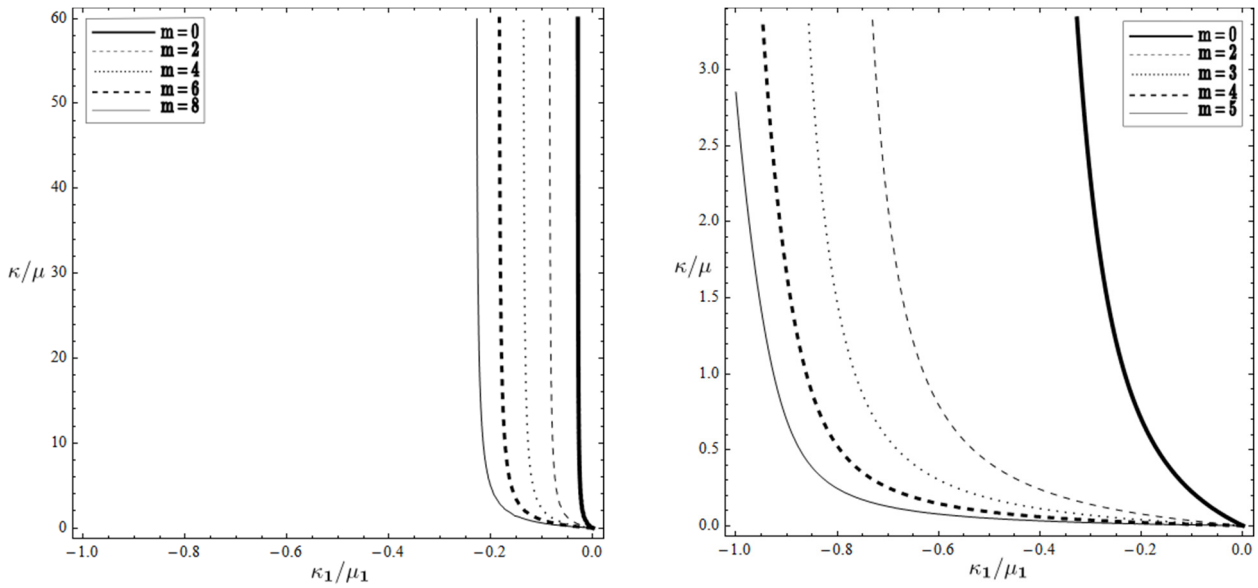

a) $z=\mu/\mu_1=1.5,\ a/c=0.99$ b) $z=\mu/\mu_1=0.85,\ a/c=0.76$

Figure 2.5. Restrictions on the elastic moduli in the plane $\kappa_1/\mu_1-\kappa/\mu$ for a composite solid with (a) thin and (b) thick piece-wise homogeneous coatings.

2.4.2.3. Both moduli varying in the two-layer coating: $\kappa_3\neq\kappa_2,\mu_3\neq\mu_2$

In this case, we must solve the general constrained optimization problem (2.39). Unlike the first two cases above, where one of the moduli in the coating is constant, to reduce mathematical difficulties but also to have the answers in those cases, here we first keep the thickness ratio the

two layers in the coating unchanged, i.e. $\alpha, \beta = \text{const}$. Then the constrained optimization problem is:

Minimize the function

$$F(x, y, u, v) = z\frac{-vx(u+yz)+(-u+v)xyz\alpha+u\beta\left[v(x-y)+y(v+xz)\alpha\right]}{xz(u+yz-u\alpha+v\alpha)+u\beta\left[yz+v\alpha+xz(-1+\alpha)\right]} \tag{2.49a}$$

subject to the constraints

$$\begin{aligned}&(1-\beta)x+\beta(1-\alpha)y=(1-\alpha\beta),\ \ (1-\beta)u+\beta(1-\alpha)v=(1-\alpha\beta),\\ &x\geq 0,\ \ y\geq 0,\ \ u\geq 0,\ \ v\geq 0.\end{aligned} \tag{2.49b}$$

The Lagrangian function for the constrained optimization problem (2.49) is:

$$\begin{aligned}L_3(x, y, u, v) = F(x, y, u, v) &+ l_1\left[(1-\beta)x+\beta(1-\alpha)y-(1-\alpha\beta)\right]\\ &+ l_2\left[(1-\beta)u+\beta(1-\alpha)v-(1-\alpha\beta)\right]+l_3x+l_4y+l_5u+l_6v\end{aligned} \tag{2.50}$$

where Lagrange multipliers l_3, l_4, l_5, l_6 are all nonnegative.

The extreme points satisfy the Karush-Kuhn-Tucker condition which requires:

$$\begin{cases}\dfrac{\partial L_3}{\partial x}=0,\ \ \dfrac{\partial L_3}{\partial y}=0,\ \ \dfrac{\partial L_3}{\partial u}=0,\ \ \dfrac{\partial L_3}{\partial v}=0,\\ (1-\beta)x+\beta(1-\alpha)y=1-\alpha\beta,\ \ (1-\beta)u+\beta(1-\alpha)v=1-\alpha\beta,\\ l_3u=0,\ \ l_4v=0,\ \ l_5(\alpha-t)=0,\ \ l_6(1-\alpha)=0,\\ u\geq 0,\ \ v\geq 0,\ \ l_3\geq 0,\ \ l_4\geq 0,\ \ l_5\geq 0,\ \ l_6\geq 0.\end{cases} \tag{2.51}$$

(2.51) has only one optimal point, $\left(x^*, y^*, u^*, v^*\right)$:

$$\begin{cases} x^* = u^* = 0,\ v^* = y^* = \dfrac{1-\alpha\beta}{\beta(1-\alpha)} \\ F\left(x^*, y^*, u^*, v^*\right) = -\dfrac{(1-\alpha\beta)z}{(z+\alpha)\beta}. \end{cases} \tag{2.52}$$

So the optimal coating has the property:

$$\kappa_3 = \mu_3 = 0,\ \kappa_2 = (1-\alpha\beta)/(\beta-\alpha\beta)\kappa > \kappa, \mu_2 = (1-\alpha\beta)/(\beta-\alpha\beta)\mu > \mu$$

which means no material $\left(\kappa_3 = \mu_3 = 0\right)$ is distributed in the outer layer of the 2-layer coating; all material is concentrated into the inner layer of that coating and hence the piecewise homogeneous 2-layer coating becomes a homogeneous single layer one. This result makes sense physically as it says that instead of having a certain amount of material $\left(\kappa, \mu\right)$ distributed regularly in a larger space from distance $r = a$ to $r = c$, to have more negative stiffness for the inclusion, we should divide equally that amount of material into a smaller but stiffer space $\left(\kappa_2 > \kappa,\ \mu_2 > \mu\right)$ from distance $r = a$ to $r = b$.

Now if one allows the thickness ratio the two layers in the coating to be variable but the total thickness of the coating remains constant $\left(\alpha\beta = t = \text{const}\right)$, from (2.52):

$$F\left(x^*, y^*, u^*, v^*\right) = -\frac{(1-\alpha\beta)z}{(z+\alpha)\beta} = -\frac{(1-t)z}{\beta z + t} \to \min \text{ if } \beta = t\ (t \le \beta \le 1) \text{ or } \alpha = 1 \tag{2.53}$$

When (2.53) is satisfied, one has

$$\begin{cases} x^* = u^* = 0, \;\; v^* = y^* = \infty \\ F\left(x^*, y^*, u^*, v^*\right) = -\dfrac{(1-t)z}{(z+1)t}. \end{cases} \tag{2.54}$$

Eq. (2.54) is a satisfying, expected mathematical result, though it is not obviously practically useful. It says that a single infinitely-thin coating with infinite moduli stabilizes the negative-stiffness inclusion most, i.e. allows it the most negative stiffness possible. This negative stiffness does not in general correspond to strong ellipticity of the inclusion elastic modulus tensor since the ratio $\kappa_2/\mu_2 = \kappa/\mu = \text{const}$, even though both moduli κ_2, μ_2 go to infinity. However, any parameter choices satisfying $\dfrac{s(1-t)z}{(z+1)t} > 1$ will ensure that a strongly-elliptic inclusion is stabilized. More generally, result (2.54) says that the optimal situation for a two-layer coating restricted to have given overall elastic moduli is to have the outer layer vacuous, and the inner layer comprised of material with the highest moduli attainable, with the thickness of this layer then determined by the required overall moduli of the coating. In this case also, the $m = 0$ mode is the critical one, since the resulting composite has a single homogeneous coating – which we had already proved always has $m = 0$ critical.

2.5. Conclusions

We have employed a static stability analysis for a composite solid consisting of a homogeneous circular cylinder with a heterogeneous concentric coating for arbitrary volume ratios. We have considered the simplest heterogeneous coating model – a coating comprised of two different homogeneous layers. The results reveal that by adding appropriate heterogeneity to the composite coating, one can make the axisymmetric mode critical and simultaneously allow the inclusion to have the most negative stiffness while maintaining overall composite stability.

Chapter 3. Tailored Heterogeneity Increases Overall Stability Regime of Composites Having a Negative-Stiffness Inclusion: Continuously Varying Heterogeneity

3.1. Introduction

After thoroughly analyzing in Chapter 2 the piecewise-constant heterogeneous coating model, in which both elastic moduli are permitted to be arbitrary in both coating layers, we here analyze the more difficult continuously-radially-varying heterogeneous coating model. We analyze three cases: the case of constant bulk modulus with arbitrary radial variation of the shear modulus; constant shear modulus with arbitrary radial variation of the bulk modulus; and arbitrary radial variation of both moduli. For the first (constant bulk modulus), we determine the optimal radial distribution of the shear modulus for maximum negative stiffness inclusion range, and also determine the deformation mode leading to first instability for this optimally tailored coating. For the case of constant shear modulus, we show that the optimal distribution of bulk modulus is the uniform one. For the case of both moduli radially-varying, although a direct mathematical derivation of the optimal solution is prohibitively difficult, we nevertheless do obtain the radially optimal distribution of moduli and justify it both heuristically and mathematically by an application of the analysis of the piecewise-varying heterogeneous coating model in Chapter 2.

3.2. Derivation of the optimal composite with a smoothly-varying shear modulus in the coating

3.2.1. Stability condition for a composite with a smoothly-varying shear modulus in the coating

Let us consider a circular cylindrical composite solid having a homogeneous inclusion of radius a, Lamé moduli λ_0, μ_0, bulk modulus $\kappa_0 = \lambda_0 + \mu_0$ and a non-homogeneous coating of radius b, Lamé moduli $\lambda(r), \mu(r)$ continuously varying with radial position, subject to zero traction boundary conditions, as illustrated in Figure 3.1(a).

As in the three-layer case, we still require the volume averages of the elastic moduli in the coating to equal the moduli in the homogeneous coating case:

$$\frac{2}{b^2-a^2}\int_a^b \mu(r) r\,dr = \bar{\mu}, \quad \frac{2}{b^2-a^2}\int_a^b \lambda(r) r\,dr = \bar{\lambda}. \tag{3.1}$$

We will now determine the stability domain for a composite with a coating whose shear modulus heterogeneity is smoothly-varying. We will do this two different ways: the first is a generalization of our previous two-homogeneous-layer coating analysis presented in Chapter 2 to the limit of an infinite-homogeneous-layer coating; the second is a direct continuum analysis.

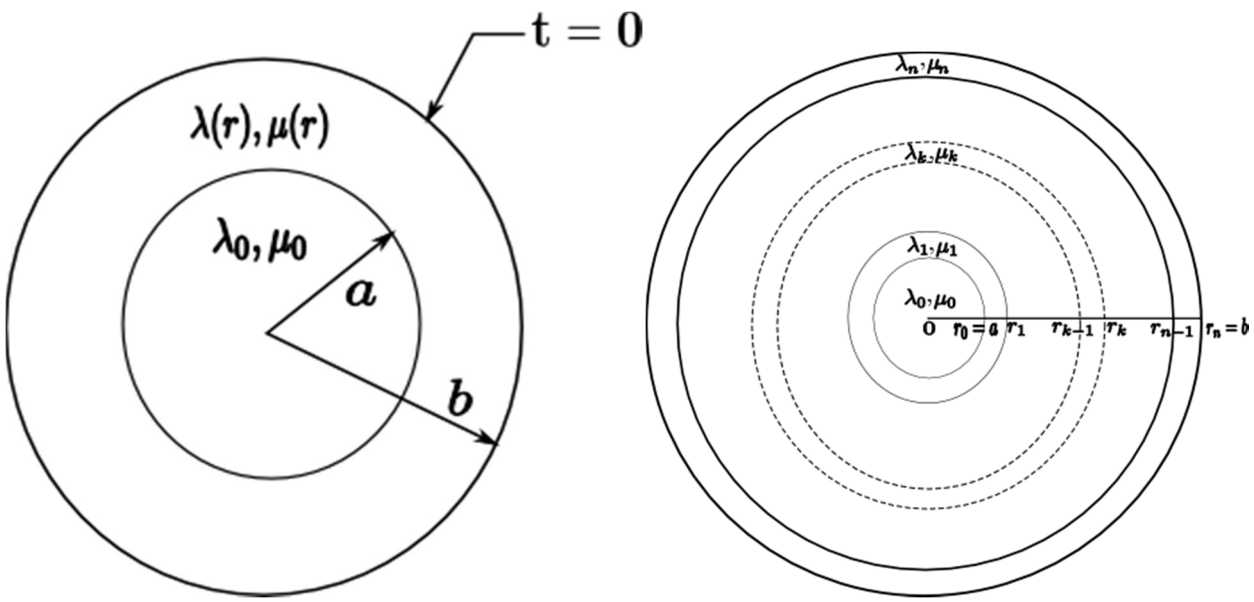

(a) (b)

Figure 3.1. (a) A composite solid with a heterogeneous coating;
(b) The coating divided into *n* discrete layers.

3.2.1.1. Determination of composite stability domain – multiple homogeneous layer approach

For the multiple-layer approach, we mentally cut the continuous coating into *n* discrete layers by equidistant cylindrical cuts as illustrated in Fig. 3.1(b), where

$$a = r_0,\ r_1 = r_0 + \Delta r,\ \ldots r_k = r_0 + k\Delta r,\ \ldots, r_n = b,\ \Delta r = \frac{b-a}{n},\ k = 0,\ldots,n. \tag{3.2}$$

The *k*th layer lies in the domain $r_{k-1} \le r \le r_k$ and has Lamé moduli $\mu_k = \mu(r_k),\ \lambda_k = \lambda(r_k)$ and bulk modulus $\kappa_k = \mu_k + \lambda_k$.

Following the same procedure employed in Chapter 2, we first write the displacement and stress fields for $m = 0$, assumed to be critical (confirmed later), in each layer.

In the inclusion $0 \le r \le r_0$:

$$u_r^{(0)} = C_0 r, \quad \sigma_{rr}^{(0)} = (\lambda_0 + 2\mu_0)\varepsilon_{rr}^{(0)} + \lambda_0 \varepsilon_{\theta\theta}^{(0)} = (\lambda_0 + 2\mu_0) u_{r,r}^{(0)} + \lambda_0 \frac{u_r^{(0)}}{r} = 2(\lambda_0 + \mu_0) C_0 = 2\kappa_0 C_0$$

In layer k of the coating $r_{k-1} \le r \le r_k$: $(k = 1, \ldots, n)$

$$u_r^{(k)} = C_{2k-1} r + \frac{C_{2k}}{r}, \quad \sigma_{rr}^{(k)} = (\lambda_k + 2\mu_k)\varepsilon_{rr}^{(k)} + \lambda_k \varepsilon_{\theta\theta}^{(k)} = (\lambda_k + 2\mu_k) u_{r,r}^{(k)} + \lambda_k \frac{u_r^{(k)}}{r} = 2\kappa_k C_{2k-1} - 2\mu_k \frac{C_{2k}}{r^2}$$

We then impose the conditions of continuous displacement and traction vectors across the n interfaces and the zero traction boundary condition on the external surface, giving a system of $(2n+1)$ equations for $(2n+1)$ unknowns:

$$\begin{bmatrix}
1 & -1 & -1 & 0 & 0 & 0 & & \vdots & \vdots & 0 \\
\kappa_0 & -\kappa_1 & \mu_1 & 0 & 0 & 0 & & \vdots & \vdots & 0 \\
0 & 1 & \alpha_1 & -1 & -1 & 0 & & \vdots & \vdots & 0 \\
0 & \kappa_1 & -\alpha_1\mu_1 & -\kappa_2 & \mu_2 & 0 & & \vdots & \vdots & 0 \\
\cdots & \cdots & \cdots & \cdots & \cdots & \cdots & \cdots & \vdots & \vdots & \vdots \\
0 & 0 & 0 & 0 & 0 & \vdots & 1 & \alpha_{n-1} & -1 & -1 \\
0 & 0 & 0 & 0 & 0 & \vdots & \kappa_{n-1} & -\alpha_{n-1}\mu_{n-1} & -\kappa_n & \mu_n \\
0 & 0 & 0 & 0 & 0 & \cdots & \cdots & 0 & \kappa_n & -\alpha_n\mu_n
\end{bmatrix}
\begin{bmatrix}
C_0 \\ C_1 \\ C_2/r_0^2 \\ \vdots \\ \vdots \\ \vdots \\ C_{2n-1} \\ C_{2n}/r_{n-1}^2
\end{bmatrix} = 0 \qquad (3.3)$$

where $\alpha_k = \frac{r_{k-1}^2}{r_k^2},\ k = 1,\ldots,n.$ (3.4)

Denoting D_{2n+1} as the determinant of the matrix of coefficients in (3.3), a nontrivial solution exists only if $D_{2n+1} = 0.$

For a general inhomogeneity satisfying (3.1), the matrix of coefficients in (3.3) is tetra-diagonal and it is quite difficult to evaluate its determinant – that is to say, the determinant form can of course be written out, but it cannot be simplified to the point that it is useable. If the bulk modulus or the shear modulus in the heterogeneous coating is constant, the matrix of coefficients in (3.3) is reduced to tri-diagonal, permitting simplification of its determinant to a useable form. Let us therefore analyze the special case in which the pointwise bulk modulus does not change; in Appendix B, we analyze the constant shear modulus case. Constant bulk modulus in the coating means of course

$$\kappa_1 = \ldots = \kappa_k = \ldots = \kappa_n = \overline{\kappa}\,. \tag{3.5}$$

With (3.5), the determinant D_{2n+1} simplifies to

$$D_{2n+1}=\begin{vmatrix}
\kappa_0+\mu_1 & -(\bar{\kappa}+\mu_1) & 0 & 0 & 0 & 0 & & \vdots & \vdots & 0 \\
\kappa_0 & -\bar{\kappa} & \mu_1 & 0 & 0 & 0 & & \vdots & \vdots & 0 \\
0 & (\bar{\kappa}+\mu_2) & \alpha_1(\mu_2-\mu_1) & -(\bar{\kappa}+\mu_2) & 0 & 0 & & \vdots & \vdots & 0 \\
0 & 0 & \alpha_1(\bar{\kappa}+\mu_1) & 0 & -(\bar{\kappa}+\mu_2) & 0 & & \vdots & \vdots & 0 \\
\cdots & \cdots & \cdots & \cdots & \cdots & \cdots & \cdots & \vdots & \vdots & \vdots \\
0 & 0 & 0 & 0 & 0 & \vdots & (\bar{\kappa}+\mu_n) & \alpha_{n-1}(\mu_n-\mu_{n-1}) & -(\bar{\kappa}+\mu_n) & 0 \\
0 & 0 & 0 & 0 & 0 & \vdots & 0 & \alpha_{n-1}(\bar{\kappa}+\mu_{n-1}) & 0 & -(\bar{\kappa}+\mu_n) \\
0 & 0 & 0 & 0 & 0 & \cdots & \cdots & 0 & \bar{\kappa} & -\alpha_n\mu_n
\end{vmatrix}.$$

Following Cahill (2002), by cofactor expansion on the last column and then the last row of the above determinant, we have the following recurrence relations:

$$\begin{cases}
D_{2n+1}=-\alpha_n\mu_n D_{2n}+\bar{\kappa}(\bar{\kappa}+\mu_n)D_{2n-1} \\
D_{2n}=\alpha_{n-1}(\bar{\kappa}+\mu_{n-1})(\bar{\kappa}+\mu_n)D_{2n-2}=\ldots=\dfrac{D_2}{\alpha_n(\bar{\kappa}+\mu_n)(\bar{\kappa}+\mu_1)}\prod_{i=1}^{n}\left[\alpha_i(\bar{\kappa}+\mu_i)^2\right] \\
D_{2n-1}=\alpha_{n-1}(\mu_n-\mu_{n-1})D_{2n-2}+(\bar{\kappa}+\mu_{n-1})(\bar{\kappa}+\mu_n)D_{2n-3}
\end{cases} \tag{3.6}$$

where $D_2=\kappa_0(\bar{\kappa}+\mu_1)-\bar{\kappa}(\kappa_0+\mu_1)=\mu_1(\kappa_0-\bar{\kappa}),\quad D_1=(\kappa_0+\mu_1).$ (3.7)

From (3.6) one arrives at the final result

$$\begin{aligned}
D_{2n+1}=\frac{D_2\prod_{i=1}^{n}\left[\alpha_i(\bar{\kappa}+\mu_i)^2\right]}{(\bar{\kappa}+\mu_1)}\Bigg\{&-\frac{\mu_n}{(\bar{\kappa}+\mu_n)}+\frac{\bar{\kappa}(\mu_n-\mu_{n-1})}{\alpha_n(\bar{\kappa}+\mu_n)(\bar{\kappa}+\mu_{n-1})}+\frac{\bar{\kappa}(\mu_{n-1}-\mu_{n-2})}{\alpha_n\alpha_{n-1}(\bar{\kappa}+\mu_{n-1})(\bar{\kappa}+\mu_{n-2})} \\
&+\ldots+\frac{\bar{\kappa}(\mu_2-\mu_1)}{\alpha_n\alpha_{n-1}\ldots\alpha_2(\bar{\kappa}+\mu_2)(\bar{\kappa}+\mu_1)}-\frac{D_1\bar{\kappa}\mu_1}{D_2(\bar{\kappa}+\mu_1)\prod_{i=1}^{n}\alpha_i}\Bigg\}.
\end{aligned} \tag{3.8}$$

Hence a nontrivial solution exists if

$$-\frac{\mu_n}{(\bar{\kappa}+\mu_n)}+\frac{\bar{\kappa}(\mu_n-\mu_{n-1})}{\alpha_n(\bar{\kappa}+\mu_n)(\bar{\kappa}+\mu_{n-1})}+\frac{\bar{\kappa}(\mu_{n-1}-\mu_{n-2})}{\alpha_n\alpha_{n-1}(\bar{\kappa}+\mu_{n-1})(\bar{\kappa}+\mu_{n-2})}+\ldots+\frac{\bar{\kappa}(\mu_2-\mu_1)}{\alpha_n\alpha_{n-1}\ldots\alpha_2(\bar{\kappa}+\mu_2)(\bar{\kappa}+\mu_1)}-\frac{D_1\bar{\kappa}\mu_1}{D_2(\bar{\kappa}+\mu_1)\prod_{i=1}^{n}[\alpha_i]}=0.$$

Definition (3.4) transforms the above expression into

$$-\frac{1}{b^2}+\frac{\bar{\kappa}}{a^2(\bar{\kappa}+\mu_1)}+\sum_{k=1}^{n}\frac{\bar{\kappa}}{\bar{\kappa}+\mu_k}\left(\frac{1}{r_k^2}-\frac{1}{r_{k-1}^2}\right)-\frac{D_1\bar{\kappa}\mu_1}{a^2D_2(\bar{\kappa}+\mu_1)}=0. \tag{3.9}$$

We employ the following approximation (which becomes exact when we then take the $n\to\infty$ limit)

$$\frac{1}{r_k^2}-\frac{1}{r_{k-1}^2}=-\frac{r_k^2-r_{k-1}^2}{r_k^2r_{k-1}^2}=-\frac{(r_k-r_{k-1})(r_k+r_{k-1})}{r_k^2r_{k-1}^2}\approx-\frac{2r_k\Delta r}{r_k^2r_{k-1}^2}\approx-\frac{2\Delta r}{r_k^3} \tag{3.10}$$

to convert the summation in (3.9) into an integration. Finally substituting (3.7) into the converted (3.9) gives the stability-instability boundary:

$$\kappa_0=\bar{\kappa}-\frac{\bar{\kappa}}{2a^2\bar{\kappa}H+\alpha}, \tag{3.11}$$

where $H=\int_a^b\frac{dr}{\left(\bar{\kappa}+\mu(r)\right)r^3}$ and $\alpha=\prod_{i=1}^{n}[\alpha_i]=\alpha_n\alpha_{n-1}\ldots\alpha_1=\frac{a^2}{b^2}$ is the volume ratio of the inclusion.

3.2.1.2. Determination of composite stability domain – continuum approach

Next we show an alternative, continuum derivation of (3.11). As we seek the axisymmetric $m = 0$ mode solution, we begin with the axisymmetric version of the equilibrium equation:

$$\sigma_{rr,r} + \frac{\sigma_{rr} - \sigma_{\theta\theta}}{r} = 0. \tag{3.12}$$

Employing Hooke's law

$$\sigma_{rr} = \lambda(\varepsilon_{rr} + \varepsilon_{\theta\theta}) + 2\mu\varepsilon_{rr}, \qquad \sigma_{\theta\theta} = \lambda(\varepsilon_{rr} + \varepsilon_{\theta\theta}) + 2\mu\varepsilon_{\theta\theta} \tag{3.13}$$

and the axisymmetric forms of the strain-displacement relations

$$\varepsilon_{rr} = u_{r,r}, \quad \varepsilon_{\theta\theta} = \frac{u_{\theta,\theta} + u_r}{r} = \frac{u_r}{r} \tag{3.14}$$

(3.12) becomes

$$\frac{d}{dr}\left[(\lambda + 2\mu)\left(u_{r,r} + \frac{u_r}{r}\right)\right] - 2\frac{d}{dr}\left[\mu\frac{u_r}{r}\right] + 2\mu\left(\frac{u_{r,r}}{r} - \frac{u_r}{r^2}\right) = 0. \tag{3.15}$$

Since we consider the special case of constant bulk modulus

$$\kappa(r) = \lambda(r) + \mu(r) = \overline{\kappa}\left(= \overline{\lambda} + \overline{\mu}\right) = \text{constant}. \tag{3.16}$$

For this case, the second-order ordinary differential equation (3.15) has by inspection one solution $u_r = r$; from this, using variation of parameters, its general solution is

$$u_r = r\big(C_1 + C_2 h(r)\big), \tag{3.17}$$

where

$$h(r) = \int_0^r \frac{dr}{\big(\lambda(r) + 2\mu(r)\big) r^3} = \int_0^r \frac{dr}{\big(\bar{\kappa} + \mu(r)\big) r^3}. \tag{3.18}$$

We now employ these results to seek nontrivial axisymmetric equilibrium solutions. The displacement field in each region is:

In the inclusion $0 \le r \le a$: (choosing as before $C_2 = 0$ to avoid a singularity at $r = 0$)

$$u_r^I = C_0 r,\ \sigma_{rr}^I = (\lambda_0 + 2\mu_0)\varepsilon_{rr}^I + \lambda_0 \varepsilon_{\theta\theta}^I = (\lambda_0 + 2\mu_0) u_{r,r}^I + \lambda_1 \frac{u_r^I}{r} = 2(\lambda_0 + \mu_0) C_0 = 2\kappa_0 C_0. \tag{3.19}$$

And in the coating $a \le r \le b$:

$$u_r^{II} = r\big(C_1 + C_2 h(r)\big), \quad \sigma_r^{II} = \lambda(\varepsilon_{rr}^{II} + \varepsilon_{\theta\theta}^{II}) + 2\mu\varepsilon_{rr}^{II} = 2\bar{\kappa}\big(C_1 + C_2 h(r)\big) + \frac{C_2}{r^2}. \tag{3.20}$$

Applying the conditions of continuous displacement and traction vectors across the interface $r = a$ and the zero traction boundary condition on the outside surface $r = b$, we obtain the following system for the three unknowns $C_0,\ C_1,\ C_2$:

$$\begin{bmatrix} 1 & -1 & -h(a) \\ \kappa_0 & -\bar{\kappa} & -\bar{\kappa}h(a)-\dfrac{1}{2a^2} \\ 0 & \bar{\kappa} & \bar{\kappa}h(b)+\dfrac{1}{2b^2} \end{bmatrix} \begin{Bmatrix} C_0 \\ C_1 \\ C_2 \end{Bmatrix} = \begin{Bmatrix} 0 \\ 0 \\ 0 \end{Bmatrix}. \tag{3.21}$$

A nontrivial equilibrium solution exists if the determinant of the above matrix of coefficients is zero. This gives:

$$\kappa_0 = \bar{\kappa} - \frac{\bar{\kappa}}{2a^2\bar{\kappa}H + \alpha}, \tag{3.22}$$

where

$$H = h(b) - h(a) = \int_a^b \frac{dr}{\left(\bar{\kappa} + 2\mu(r)\right) r^3}. \tag{3.23}$$

Clearly (3.22) is identical to (3.11).

Let us perform one simple check of (3.22) with (3.23) by applying it to the homogeneous coating case; then

$$\mu(r) = \bar{\mu} \text{ and } H = \int_a^b \frac{dr}{\left(\bar{\kappa} + \mu(r)\right) r^3} = \frac{1}{2\left(\bar{\kappa} + \bar{\mu}\right)}\left(\frac{1}{a^2} - \frac{1}{b^2}\right) \rightarrow \kappa_0 = -\frac{(1-\alpha)\bar{\kappa}\bar{\mu}}{\bar{\kappa} + \alpha\bar{\mu}}$$

which is the known stability boundary (See Eq. (2.20) in Chapter 2).

3.2.2. Determination of optimal composite with smoothly-varying coating shear modulus

We now seek the optimal coating heterogeneity (meaning, within our assumption of constant coating bulk modulus, the optimal coating shear modulus variation with radius) such that the inclusion has the most negative stiffness possible with the entire composite remaining stable. From (3.22),

$$\frac{d\kappa_0}{dH} = \frac{2a^2\bar{\kappa}^2}{\left(2a^2\bar{\kappa}H + \alpha\right)^2} > 0. \tag{3.24}$$

This shows that the stability domain is largest if H is minimum. To determine a lower bound on H, we apply the Cauchy–Bunyakovsky–Schwarz inequality for integration,

$$\left(\int_a^b u(x)v(x)dx\right)^2 \le \int_a^b u^2(x)dx \int_a^b v^2(x)dx, \text{ with equality holding when } u(x) = \text{Const } v(x)$$

to the following integral

$$\left(\ln b - \ln a\right)^2 = \left(\int_a^b \frac{dr}{r}\right)^2 = \left(\int_a^b \frac{1}{\sqrt{r^3(\lambda+2\mu)}}\sqrt{r(\lambda+2\mu)}dr\right)^2 \le \int_a^b \frac{dr}{r^3(\lambda+2\mu)} \int_a^b (\lambda+2\mu)\, r\, dr. \tag{3.25}$$

Conditions (3.1) give:

$$\int_a^b (\lambda+2\mu)\, r\, dr = \frac{b^2-a^2}{2}(\bar{\kappa}+\bar{\mu}). \tag{3.26}$$

Substituting this into (3.25), it shows that

$$H = \int_a^b \frac{dr}{(\lambda+2\mu)r^3} \geq \frac{2(\ln b - \ln a)^2}{\left(b^2-a^2\right)(\bar{\kappa}+\bar{\mu})}, \tag{3.27}$$

and substituting this with the equality chosen into (3.22) therefore gives

$$\kappa_0^{\min} = \bar{\kappa} - \frac{\bar{\kappa}}{\dfrac{4a^2\bar{\kappa}(\ln b - \ln a)^2}{\left(b^2-a^2\right)(\bar{\kappa}+\bar{\mu})} + \alpha}. \tag{3.28}$$

For H to be a minimum, the inequality in (3.25) must be an equality, which (3.25) shows to require

$$\int_a^b \frac{dr}{r^3(\lambda+2\mu)} \int_a^b (\lambda+2\mu)\, r\, dr = \left(\int_a^b \frac{dr}{r}\right)^2 \tag{3.29}$$

This is true if and only if

$$\lambda+2\mu = \frac{C}{r^2}, \tag{3.30}$$

where C is a constant. Combining (3.30) with (3.16) gives the relations

$$\mu(r)=\frac{C}{r^2}-\bar{\kappa},\quad \lambda(r)=\bar{\kappa}-\mu(r) \tag{3.31}$$

where C is determined by substitution of (3.30) into (3.26):

$$C=\frac{\left(b^2-a^2\right)\left(\bar{\kappa}+\bar{\mu}\right)}{2\left(\ln b-\ln a\right)}>0. \tag{3.32}$$

To ensure that (3.31) satisfies pointwise stability, we require

$$\mu(r)>0 \quad \forall r\in[a,b] \;\rightarrow\; \bar{\mu}>\left[\frac{2\left(\ln b-\ln a\right)b^2}{b^2-a^2}-1\right]\bar{\kappa}. \tag{3.33}$$

Thus, among all radially inhomogeneous isotropic materials satisfying (3.1), (3.16) and (3.33), which include homogeneous ones as subsets, the inhomogeneous material of type (3.31) with (3.32) gives the largest stability domain. Recall that this conclusion is only valid if the critical mode is the $m = 0$ one; that it is will be confirmed in the next section.

Remark 1:

It is interesting to note that if we mentally divide the optimal, continuously varying heterogeneous coating (3.31) [with (3.32)] into a two-layer one by an "optimal" cylindrical cut $r=r^*$ determined from formula (2.47) in Chapter 2, the volume averages of elastic moduli of each layer of the divided coating are the same as those of the optimal 2-layer piecewise

homogeneous coating whose bulk modulus is constant, determined in Section 2.4.2.2 in Chapter 2. Indeed, applying definition (2.35) in Chapter 2 to the divided coating,

$$\alpha^* = \frac{a^2}{r^{*2}},\quad t = \frac{a^2}{b^2},\quad z = \frac{\overline{\kappa}}{\overline{\mu}},$$

the optimal distance $r = r^*$ of the common interface of the optimal two-layer coating is found from:

$$\alpha^* = \sqrt{t} \to r = r^* = \sqrt{ab}\,.$$

So the volume averages of elastic moduli in each layer of the divided coating are:

- For the inside layer $a \le r \le r^*$, using (3.31) and (3.32) one obtains

$$\overline{\mu}_{in} = \frac{2}{r^{*2} - a^2}\int_a^{r^*} \mu(r)\, r\, dr = \frac{2}{a(b-a)}\int_a^{\sqrt{ab}} \left(\frac{C}{r^2} - \overline{\kappa}\right) r\, dr = \frac{a+b}{2a}\left(\overline{\kappa} + \overline{\mu}\right) - \overline{\kappa}.$$

Hence, (see definition (2.35) in chapter 2)

$$v^* = \frac{\overline{\mu}_{in}}{\overline{\mu}} = \frac{1 + 1/\sqrt{t}}{2}(z+1) - z = \frac{(1-z) + (1+z)/\sqrt{t}}{2} \tag{3.34}$$

- For the outside layer $r^* \le r \le b$, similarly one gets

$$\bar{\mu}_{out}=\frac{2}{b^2-r^{*2}}\int_{r^*}^{b}\mu(r)\,r\,dr=\frac{2}{b(b-a)}\int_{\sqrt{ab}}^{b}\left(\frac{C}{r^2}-\bar{\kappa}\right)r\,dr=\frac{a+b}{2b}(\bar{\kappa}+\bar{\mu})-\bar{\kappa},$$

and (see definition (2.35) in chapter 2)

$$u^*=\frac{\bar{\mu}_{out}}{\bar{\mu}}=\frac{1+\sqrt{t}}{2}(z+1)-z=\frac{(1-z)+(1+z)\sqrt{t}}{2}. \tag{3.35}$$

Expressions (3.34) and (3.35) are identical to those of the optimal two-layer coating whose shear modulus is piecewise-varying as determined in Chapter 2 (see the first equation of (2.47) in chapter 2).

Remark 2:

Among all composites whose coating materials are radially inhomogeneous isotropic materials satisfying (3.1), (3.16) and (3.33), the optimal one – whose coating is made of inhomogeneous material (3.31), (3.32) – has the largest effective composite bulk modulus. Specifically, the effective composite bulk modulus for the case of continuously varying shear modulus is (Lakes & Drugan, 2002)

$$\kappa_{eff}=\bar{\kappa}+\frac{a^2(\kappa_0-\bar{\kappa})}{b^2+2a^2b^2(\kappa_0-\bar{\kappa})H}\rightarrow\ \frac{\mathrm{d}\kappa_{eff}}{\mathrm{d}H}=-\frac{2a^4b^2(\kappa_0-\bar{\kappa})^2}{\left[b^2+2a^2b^2(\kappa_0-\bar{\kappa})H\right]^2}<0$$

So $H=H_{\min}$ implies $\kappa_{eff}=\kappa_{eff}^{\max}$.

3.2.3. Confirmation of $m = 0$ mode criticality for optimal composite with smoothly-varying coating shear modulus

To confirm that the $m = 0$ mode is the critical one, we must examine stability-instability boundary curves for all modes m and all possible choices of parameters. Throughout Chapters 2 and 3, the criticality of mode $m = 0$ for all cases is proved with the same sets of parameters, in order to provide a direct comparison of the distributions of modes for the two cases (thin and thick coatings) in different models: homogeneous coating, piecewise heterogeneous coating, inhomogeneous coating. Of course, we did confirm numerically the criticality of mode $m = 0$ for the full range of parameters in the optimal composites. The curve for mode $m = 0$ is already determined in Eq. (3.28), while the $m = 1$ mode does not exist, similarly to the two-layer coating composites in Chapter 2. The remaining curves for modes $m \geq 2$ are determined using the general strategy we use throughout the paper. First, one writes the displacement fields for the inclusion (containing two constants, i.e. see Eq. (3.19) above) and for the coating (containing 4 constants, see Appendix A). From these, one determines the stress fields with the help of Hooke's law. Next, one applies four continuity conditions of displacement and traction vectors across the inclusion-coating interface and two zero-traction boundary conditions on the outside of the coating to provide a homogeneous algebraic system for the 6 constants. Last, requiring the determinant of the system's coefficient matrix to be zero to permit nontrivial solutions gives the instability conditions. The $m = 1$ mode is not shown since it does not exist if rigid-body motion

is removed from all phases; if rigid-body motion is only removed from the outer phase, the m = 1 mode will exist, but it will always lie between the m = 0 and m = 2 curves.

Let us first analyze the case where the optimal composite has a very thin coating to confirm our analysis above. When the coating is very thin, the effects of heterogeneity become negligible, meaning that the results for the cases of homogeneous and heterogeneous coatings should converge. Our numerical results below demonstrate this, i.e. Fig. 2.2(a), Fig. 2.5(a) in Chapter 2 and Fig. 3.2(a) here are exactly the same. Note that although we only plot results through m = 8, we have confirmed that all curves for higher m values lie to the left of the curves plotted.

For a thicker heterogeneous coating, the stability map indeed confirms the critical property of mode m = 0 as shown in Fig. 3.2(b). This has been drawn for the same parameter values as that for the homogeneous coating shown in Fig. 2.2(b) and Fig. 2.5(b) in chapter 2. Comparing all three figures, we observe that all stability curves for the optimal smoothly varying shear modulus coating composite lie to the left of those for the piecewise varying shear modulus coating one, which in turn all lie to the left of those for the homogeneous coating one. This means that among these coatings, the overall stability regime for the continuously varying heterogeneous-coating composite is the largest.

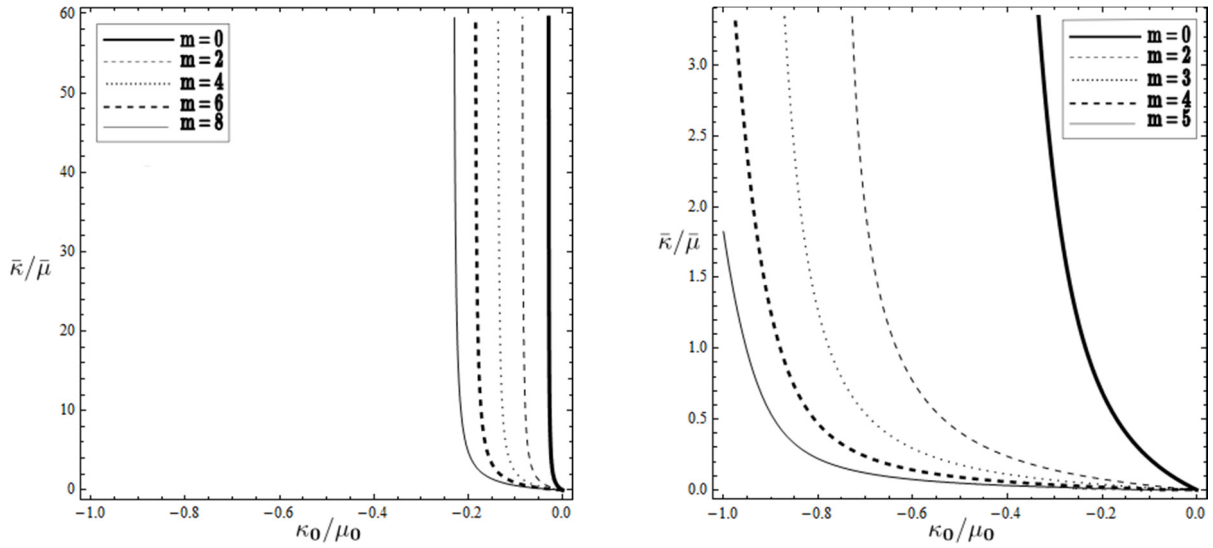

b) $\mu/\mu_0 = 1.5,\ a/b = 0.99$ b) $\mu/\mu_0 = 0.85,\ a/b = 0.76$

Figure 3.2. Restrictions on the elastic moduli in the plane $\kappa_0/\mu_0 - \kappa/\mu$ for the optimal composite with a smoothly-varying shear modulus in the coating with (a) thin and (b) thick coatings.

3.3. Determination of the optimal composite with both moduli varying in the coating

Although analytical treatment of the case in which both moduli are permitted arbitrary radial variation does not appear possible, we here provide and justify the optimal solution for this case, obtained by use of the case of both moduli having arbitrary piecewise variation in the two-layer coating from Chapter 2, together with the heuristic and mathematical reasoning presented below.

The optimal solution for a composite with both moduli permitted arbitrary radial variation in the coating is either: both moduli exhibit Dirac-delta variations with *r* if both moduli are

permitted to be infinite; or both moduli exhibit Heaviside step function variations with r if, as would be the case practically, both moduli have upper limits on their attainable values. The former solution means both moduli are zero everywhere except at the inclusion-coating interface where they are infinite (this is our conclusion in Section 2.4.2.3, Chapter 2). Meanwhile, the latter solution means both moduli have their maximum permitted values throughout a homogeneous layer just adjacent to the inclusion, whose thickness is determined by the coating effective moduli requirements, and then jump to zero outside this layer. In other words, for the Heaviside step function solution:

$$(r)=\begin{cases}\mu_{\max} \text{ for } a \le r \le b^* \\ 0 \text{ for } b^* \le r \le b\end{cases}, \ \kappa(r)=\begin{cases}\kappa_{\max} \text{ for } a \le r \le b^* \\ 0 \text{ for } b^* \le r \le b\end{cases} \tag{3.36}$$

where b^* is determined from Eq. (3.1).

Heuristically, it is clear that (3.36) is the optimal solution for the case when both moduli are permitted arbitrary radial variation in the coating but have upper limits on their attainable values; to see this, one asks how their radial variations could be modified from (3.36) to increase the stability regime. Their values cannot be *increased* in the layer near the boundary with the inclusion, since they are already at their maximum values throughout this layer; thus, any variation with radius in this layer would involve having the moduli *decrease* over some radial range, which would make the coating layer thicker in order that its effective moduli satisfy (3.1). This type of modification would go against everything learned in Chapter 2 about optimizing the

coating. Additional confirmation is provided by the following simplified analysis, in which we prove that permitting the homogeneous layer adjacent to the inclusion, $a \le r \le b^*$ in (3.36), to be piecewise heterogeneous does not improve the stability domain. To do this, we divide this homogeneous layer into two homogeneous layers by an arbitrary cylindrical cut $r = r^* \left(a \le r^* \le b^* \right)$

$$\mu(r) = \begin{cases} \mu_2 & \forall a \le r \le r^* \\ \mu_3 & \forall r^* \le r \le b^* \end{cases}, \quad \kappa(r) = \begin{cases} \kappa_2 & \forall a \le r \le r^* \\ \kappa_3 & \forall r^* \le r \le b^* \end{cases} \tag{3.37}$$

where

$$0 < \mu_2, \ \mu_3 \le \mu_{\max}, \ 0 < \kappa_2, \ \kappa_3 \le \kappa_{\max} \tag{3.38}$$

and the requirements of the same moduli require (similar to Eq. (2.34) in Chapter 2)

$$\left(b^{*2} - r^{*2} \right) \mu_3 + \left(r^{*2} - a^2 \right) \mu_2 = \left(b^{*2} - a^2 \right) \mu_{\max} \tag{3.39a}$$

$$\left(b^{*2} - r^{*2} \right) \kappa_3 + \left(r^{*2} - a^2 \right) \kappa_2 = \left(b^{*2} - a^2 \right) \kappa_{\max} . \tag{3.39b}$$

The optimization solution of the 2-layer coating composite in Chapter 2 reveals that to have the most negative inclusion stiffness possible while maintaining overall composite stability, both moduli in the homogeneous layer just adjacent to the inclusion must have their maximum

permitted values. Applying this to the case here, we see that $\mu_2 = \mu_{\max}$, $\kappa_2 = \kappa_{\max}$ (see Eq. (3.38)) and hence $\mu_3 = \mu_2 = \mu_{\max}$, $\kappa_3 = \kappa_2 = \kappa_{\max}$ (see Eq. (3.39)).

Thus, in the case of both finite moduli in the coating, a homogeneous coating whose moduli have their maximum permitted values and thickness is determined by the coating effective moduli requirements stabilizes the negative stiffness inclusion most while maintaining overall composite stability.

Let us explain clearly why the results of this section differ from those of Section 3.2, as the reader may wonder why they do not coincide. In both Sections 3.2 and 3.3, the coating thickness was prescribed, and the radial variations of the moduli in this coating were determined to optimize the ability of the overall composite to stabilize the largest range of negative inclusion stiffness. In Section 3.2, the bulk modulus of the coating was prescribed to have a constant, nonzero value throughout the coating, and the optimal coating shear modulus variation was derived. In the present section, both bulk and shear moduli were permitted to have arbitrary radial variations throughout the coating, which were determined to be Heaviside step functions of radius for the practically-significant bounded-moduli case. This solution in effect says that the optimal coating is homogeneous, *but of a smaller thickness than that prescribed*, this thickness being determined by enforcement of the coating effective modulus constraints (3.1) on a coating with constant maximum moduli values. Thus, if the coating thickness is prescribed and the moduli values are required to be nonzero throughout the coating (as geometrical requirements in practice could well dictate), if the coating bulk modulus is constant throughout the coating, the

shear modulus distribution of Section 2 [(3.31), (3.32)] is optimal; if however the moduli values *are* permitted to vanish at arbitrary locations in the coating, the optimal solution is that of the present section, and this is the best possible coating under the coating effective moduli constraints (3.1).

To illustrate the improved stability regime produced by our optimal heterogeneous coating, i.e. how much more negative the inclusion bulk modulus can be while maintaining overall composite stability, we compare composite solids having an optimal homogenous coating of a smaller thickness than that prescribed to one having optimal heterogeneous coatings of the prescribed thickness, whose bulk modulus is unchanged and shear modulus is piecewise or continuously varying; and to one having a homogeneous coating of the prescribed thickness, with all composites having the same volume averages of moduli in the coating.

Figure 3.3 displays the stability-instability boundaries for the overall composite for these four cases. Note that the stability-instability boundary (which is always the $m = 0$ mode for all the cases we compare) for the composite having the optimal heterogeneous coating determined in this section can be sensibly compared to that having the constant bulk modulus optimal coating determined in Section 2 when the upper limit of shear modulus $\mu_{\max}$ in Eq. (3.36) is greater than or equal to the maximum of $\mu(r)$ in Eqs. (3.31), (3.32). Indeed, to sensibly compare the composite having the present section's optimal heterogeneous coating to all other cases, we must simply have $\mu_{\max}$ in Eq. (3.36) $\geq \max \mu(r)$ of the other coatings; whenever this is true, the present section's optimal coating composite stability boundary, drawn as heavy solid curves in

Fig. 3.3, is seen always to lie to the left of all other curves. Observe that the amount of stability regime enhancement is small for very thin coatings or for large matrix/inclusion shear ratios, but it is quite substantial for thicker coatings and/or for small to moderate shear ratios. Also observe, interestingly, that if the coating thickness is prescribed and the coating bulk modulus is constant throughout the coating, although the continuously-varying shear modulus coating provides the largest stability regime enhancement, the piecewise-varying shear modulus coating is nearly as good and presumably much simpler to fabricate.

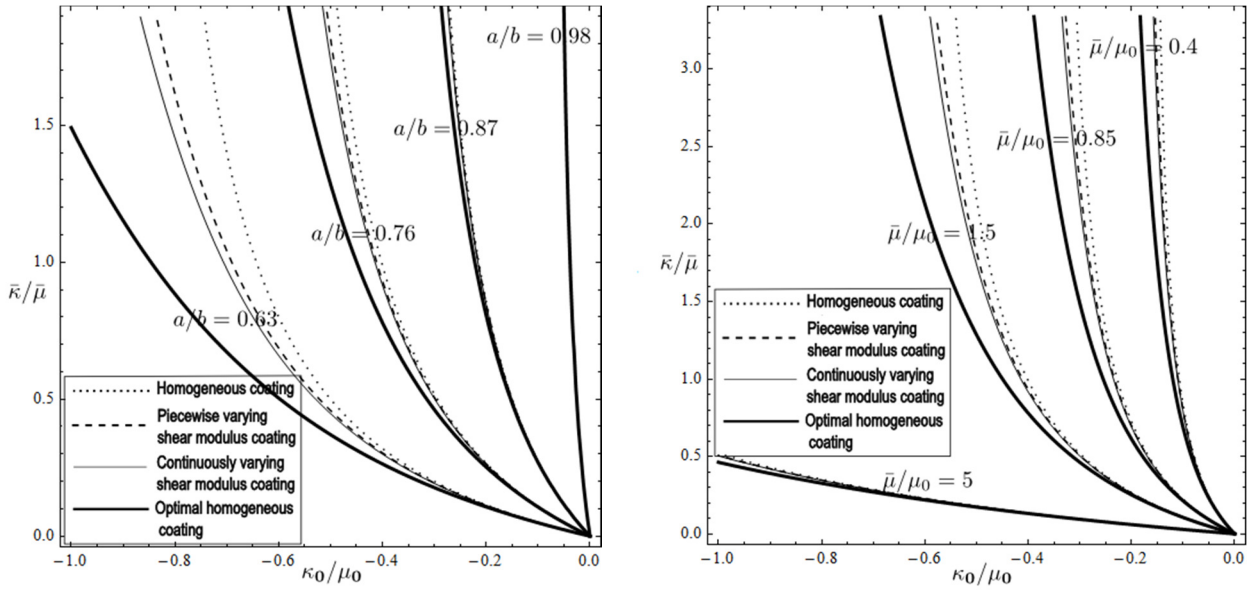

a) $\bar{\mu}/\mu_0 = 1.5$ b) $a/b = 0.76$

Figure 3.3. Composite stability regimes (above and to the right of the curves) in the plane $\kappa_0/\mu_0 - \bar{\kappa}/\bar{\mu}$ for (a) a fixed shear ratio and (b) a fixed volume ratio.

3.4. Conclusions

We have employed a static stability analysis for a composite solid comprised of a negative-stiffness homogeneous circular cylinder with a heterogeneous positive-definite concentric coating for arbitrary volume ratios. We have analyzed three special classes of arbitrary radial heterogeneity in the coating: bulk modulus constant with varying shear modulus, shear modulus constant with varying bulk modulus, and both moduli varying. We have solved in all three cases for the optimal heterogeneity in the coating permitting the most negative inclusion stiffness while maintaining overall composite stability. The results show a substantial increase in the permissible inclusion negative stiffness range to be provided by the heterogeneous coatings as compared to a homogeneous coating, while maintaining overall composite stability.

Chapter 4. Viscoelastic composite solids

4.1. Introduction

After carefully analyzing the elastic composite solids in Chapters 2 and 3, we here expand results obtained for those solids to viscoelastic composite solids in which both phases are comprised of linear, isotropic, viscoelastic materials, by employing the correspondence principle. In this chapter, we investigate the effective linear viscoelastic response of the composite solids and explore the effects of heterogeneous materials on the overall damping. We show that the specific heterogeneity of the positive-definite phase that was shown in Chapter 3 to permit the largest inclusion negative stiffness while maintaining overall composite stability, can increase the effective loss tangent of the composites near the stability boundary and decrease the lowest exciting frequency at which the infinite dynamic effective composite bulk modulus is achieved. The chapter is organized as follows: Section 4.2 introduces the theoretical framework for viscoelastic models heavily relying on Kochmann (2013); Section 4.3 examines an illustrative spring-dashpot system to show via simpler mathematics the interesting phenomena which are analyzed in Section 4.4 in the two-phase viscoelastic composite solids comprised of a coated cylindrical inclusion with either a homogeneous or heterogeneous coating.

4.2. Linear viscoelastic solids

4.2.1. Constitutive model

For linear viscoelastic solids assuming infinitesimal stress and strain tensors, the constitutive relation employs the Boltzmann superposition integral:

$$\sigma_{ij} = \int_0^t C_{ijkl}(t-\tau)\frac{\partial \varepsilon_{kl}(\tau)}{\partial \tau} d\tau \tag{4.1}$$

where $\mathbf{C}(t)$ is the time-dependent fourth order viscoelastic modulus tensor, which can be approximated by a finite number N of relaxation responses with relaxation times τ

$$\mathrm{C}(t) = \sum_{\alpha=1}^{N} C_\alpha e^{-t/\tau_\alpha}. \tag{4.2}$$

The constitutive relation of linear viscoelastic solids alternatively can be given by the differential equations:

$$\left(\eta_0 + \sum_{\alpha=1}^{n} \eta_\alpha \frac{\partial^\alpha}{\partial t^\alpha}\right)\sigma_{ij}(t) = \left(C^0_{ijkl} + \sum_{\alpha=1}^{n} C^\alpha_{ijkl} \frac{\partial^\alpha}{\partial t^\alpha}\right)\varepsilon_{kl}(t). \tag{4.3}$$

If one denotes

$$D_\alpha = \frac{\partial^\alpha}{\partial t^\alpha} \quad \forall \alpha \geq 1, \qquad D_0 = 1, \;\; \alpha = 1, \ldots, n \tag{4.4}$$

(4.3) becomes

$$\sum_{\alpha=0}^{n} \eta_\alpha D_\alpha \sigma_{ij}(t) = \sum_{\alpha=0}^{n} C_{ijkl}^{\alpha} D_\alpha \varepsilon_{kl}(t) \tag{4.5}$$

where $\mathbf{C}^\alpha$ are constant fourth order tensors; assuming isotropy, they can be expressed as:

$$C_{ijkl}^{\alpha} = \lambda_\alpha \delta_{ij}\delta_{kl} + \mu_\alpha \left(\delta_{ik}\delta_{jl} + \delta_{il}\delta_{jk}\right) \tag{4.6}$$

where $\lambda_\alpha, \mu_\alpha$ are the Lamé moduli. Using (4.6), equation (4.5) is reduced to:

$$\sum_{\alpha=0}^{n} \eta_\alpha D_\alpha \sigma_{ij}(t) = \sum_{\alpha=0}^{n} \lambda_\alpha D_\alpha \varepsilon_{kk}(t)\delta_{ij} + 2\sum_{\alpha=0}^{n} \mu_\alpha D_\alpha \varepsilon_{ij}(t). \tag{4.7}$$

Thus, employing the constitutive relation (4.7) and the strain-displacement relation, the governing equation without body forces, $\rho \ddot{\mathbf{u}} = \nabla.\boldsymbol{\sigma},$ becomes

$$\rho \sum_{\alpha=0}^{n} \eta_\alpha D_\alpha \ddot{u}_i = \sum_{\alpha=0}^{n} (\lambda_\alpha + \mu_\alpha) D_\alpha u_{j,ji} + \sum_{\alpha=0}^{n} \mu_\alpha D_\alpha u_{i,jj}. \tag{4.8}$$

4.2.2. Harmonic viscoelastic response

To study the harmonic viscoelastic response when the system is driven at frequency Ω, one assumes

$$\mathbf{u}(\mathbf{x},t)=\hat{\mathbf{u}}(\mathbf{x})\exp(i\Omega t),\ \boldsymbol{\varepsilon}(\mathbf{x},t)=\hat{\boldsymbol{\varepsilon}}(\mathbf{x})\exp(i\Omega t),\ \boldsymbol{\sigma}(\mathbf{x},t)=\hat{\boldsymbol{\sigma}}(\mathbf{x})\exp(i\Omega t) \tag{4.9}$$

where $\hat{\mathbf{u}}(\mathbf{x}),\hat{\boldsymbol{\varepsilon}}(\mathbf{x}),\hat{\boldsymbol{\sigma}}(\mathbf{x})$ are complex amplitudes.

Substituting (4.9) into (4.8), using definition (4.4), one obtains:

$$\rho\sum_{\alpha=0}^{n}\eta_\alpha(i\Omega)^{\alpha+2}\hat{u}_i=\sum_{\alpha=0}^{n}(\lambda_\alpha+\mu_\alpha)(i\Omega)^\alpha\hat{u}_{j,ji}+\sum_{\alpha=0}^{n}\mu_\alpha(i\Omega)^\alpha\hat{u}_{i,jj}\,. \tag{4.10}$$

Let us define the frequency-dependent parameters

$$\rho^*=\rho\sum_{\alpha=0}^{n}\eta_\alpha(i\Omega)^\alpha,\quad \lambda^*=\sum_{\alpha=0}^{n}\lambda_\alpha(i\Omega)^\alpha,\qquad \mu^*=\sum_{\alpha=0}^{n}\mu_\alpha(i\Omega)^\alpha \tag{4.11}$$

to arrive at the dynamic Navier equation

$$-\rho^*\Omega^2\hat{u}_i=(\lambda^*+\mu^*)\hat{u}_{j,ji}+\mu^*\hat{u}_{i,jj}\,. \tag{4.12}$$

From (4.12), one concludes that for this particular model of linear viscoelastic solids, $\hat{\mathbf{u}}(\mathbf{x})$ can be determined from the linear elastodynamic equations, with the help of the correspondence principle, simply by making the replacements $(\rho,\lambda,\mu)\to(\rho^*,\lambda^*,\mu^*)$.

4.3. Spring-dashpot system

Newton's law gives the governing equations for the spring-dashpot system illustrated in Figure 4.1 as:

$$\begin{cases} k_2(x_2 - x_1) - k_1 x_1 + c_2(\dot{x}_2 - \dot{x}_1) - c_1 \dot{x}_1 + F_1 = m_1 \ddot{x}_1 \\ -k_2(x_2 - x_1) - k_3 x_2 - c_2(\dot{x}_2 - \dot{x}_1) - c_3 \dot{x}_2 + F_2 = m_2 \ddot{x}_2 . \end{cases} \tag{4.13}$$

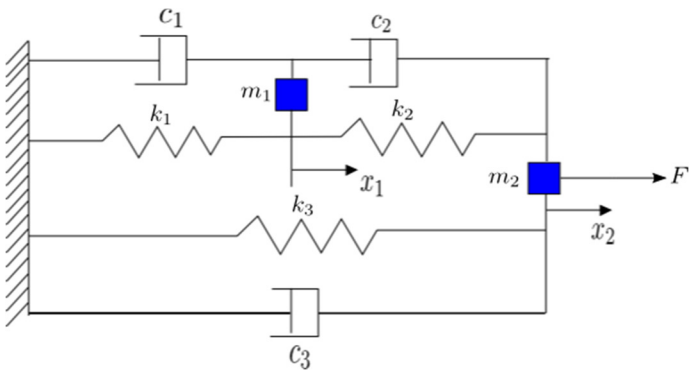

Figure 4.1. Spring-dashpot system, with masses.

Applying harmonic external forces $\mathbf{F}(t) = \begin{pmatrix} \hat{F}_1 & \hat{F}_2 \end{pmatrix}^T \exp(i\Omega t) = \begin{pmatrix} 0 & \hat{F} \end{pmatrix}^T \exp(i\Omega t)$ to the two nodes results in displacements $\mathbf{x}(t) = \begin{pmatrix} \hat{x}_1 & \hat{x}_2 \end{pmatrix}^T \exp(i\Omega t)$. Substituting these expressions into (4.13) gives

$$\begin{bmatrix} k_1 + ic_1\Omega + k_2 + ic_2\Omega - m_1\Omega^2 & -k_2 - ic_2\Omega \\ -k_2 - ic_2\Omega & k_2 + ic_2\Omega + k_3 + ic_3\Omega - m_2\Omega^2 \end{bmatrix} \begin{pmatrix} \hat{x}_1 \\ \hat{x}_2 \end{pmatrix} = \begin{pmatrix} 0 \\ \hat{F} \end{pmatrix}. \tag{4.14}$$

A system's effective viscoelastic stiffness is by definition $k_{eff}^* = \hat{F} / \hat{x}_2$, so from (4.14) for the discrete system it is

$$k_{eff}^{*} = k_2 + ic_2\Omega + k_3 + ic_3\Omega - m_2\Omega^2 - \frac{(k_2 + ic_2\Omega)^2}{k_1 + ic_1\Omega + k_2 + ic_2\Omega - m_1\Omega^2}. \tag{4.15}$$

If there are no viscous elements, the above effective viscoelastic stiffness correctly reduces to the effective elastic stiffness

$$k_{eff} = k_2 + k_3 - m_2\Omega^2 - \frac{k_2^2}{k_1 + k_2 - m_1\Omega^2}. \tag{4.16}$$

The stability condition for the system can be determined by using either the energy, dynamic or static approach. The static approach proceeds by first setting $m_1 = m_2 = 0$, $\hat{F} = 0$ and $c_1 = c_2 = c_3 = 0$ (adding viscosity does not change the stability domain) in (4.14) to obtain

$$\begin{bmatrix} k_1 + k_2 & -k_2 \\ -k_2 & k_2 + k_3 \end{bmatrix} \begin{pmatrix} \hat{x}_1 \\ \hat{x}_2 \end{pmatrix} = \begin{pmatrix} 0 \\ 0 \end{pmatrix}. \tag{4.17}$$

The trivial equilibrium solution $\hat{x}_1 = \hat{x}_2 = 0$ always satisfies (4.17). Instability arises if a nontrivial equilibrium solutions exists, which will occur if

$$Det\begin{bmatrix} k_1 + k_2 & -k_2 \\ -k_2 & k_2 + k_3 \end{bmatrix} = 0 \qquad \text{or} \qquad k_1 = -\frac{k_2 k_3}{k_2 + k_3}.$$

In conclusion, for the trivial equilibrium solution to be stable, one must satisfy

$$k_1 > -\frac{k_2 k_3}{k_2 + k_3}. \tag{4.18}$$

Alternatively one can set $m_1 = m_2 = 0$ in (4.16) and require the positivity of the system effective elastic stiffness to arrive at the same stability condition (4.18).

The loss tangent is by definition found from (4.15)

$$\tan\delta = \frac{\Im\left(k_{eff}^*\right)}{\Re\left(k_{eff}^*\right)} \tag{4.19}$$

where $\Im$ and $\Re$ denote imaginary and real parts, respectively.

4.3.1. Inertia effects neglected

Setting $m_1 = m_2 = 0$ in (4.15), the effective viscoelastic stiffness now becomes

$$k_{eff}^* = k_2 + ic_2\Omega + k_3 + ic_3\Omega - \frac{\left(k_2 + ic_2\Omega\right)^2}{k_1 + ic_1\Omega + k_2 + ic_2\Omega}. \tag{4.20}$$

Applying (4.19) to (4.20) gives the loss tangent

$$\tan\delta = \frac{\Omega\left[c_2 k_1^2 + c_1 k_2^2 + c_3\left(k_1 + k_2\right)^2 + \left(c_1 + c_2\right)\left(c_1 c_3 + c_2 c_3 + c_1 c_2\right)\Omega^2\right]}{\left(k_1 + k_2\right)\left(k_1 k_3 + k_2 k_3 + k_1 k_2\right) + \left[c_2^2 k_1 + c_1^2 k_2 + \left(c_1 + c_2\right)^2 k_3\right]\Omega^2}. \tag{4.21}$$

Let us define the nondimensional parameters

$$x=\frac{k_1}{k_3},\ \ y=\frac{k_2}{k_3}>0,\ \ u=\frac{c_1}{c_3}>0,\ \ v=\frac{c_2}{c_3}>0,\ \ \overline{\Omega}=\Omega\frac{c_3}{k_3}>0 \tag{4.22}$$

in terms of which (4.21) becomes

$$\tan\delta=\frac{\overline{\Omega}\left[v\,x^2+u\,y^2+(x+y)^2+(u+v)(u+v+u\,v)\overline{\Omega}^2\right]}{(x+y)(x+y+xy)+\left[x\,v^2+y\,u^2+(u+v)^2\right]\overline{\Omega}^2}. \tag{4.23}$$

The stability condition (4.18) is then

$$x>-\frac{y}{y+1}. \tag{4.24}$$

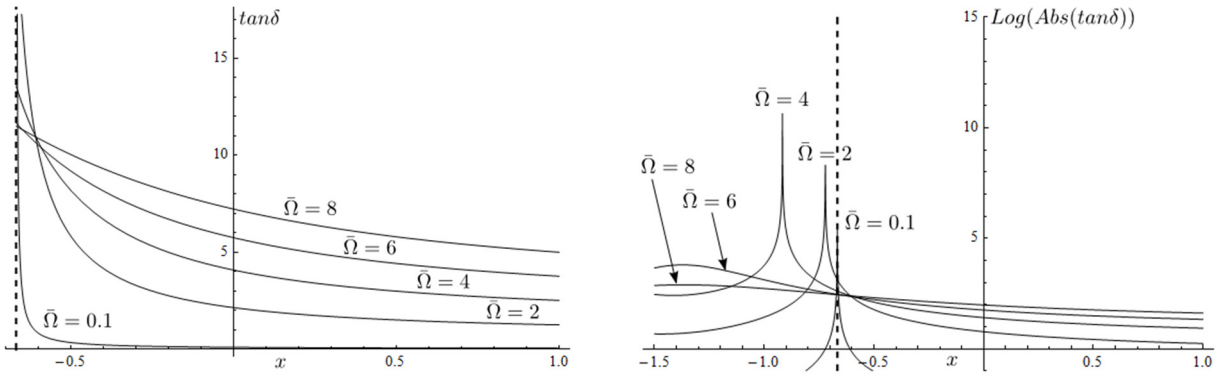

Figure 4.2. The effective damping of the spring-dashpot system of negligible masses versus $x>-2/3$ for different frequencies $\overline{\Omega}$ with parameters $y=2,\ u=v=0.1$.

From (4.22), (4.23) and (4.24), it is not difficult to see that the loss tangent in the case of negligible inertia is always positive in the stable regime as in Fig. 4.2 (left). Although all the peaks of the loss tangent (which are infinite theoretically) are in the unstable regime,

nevertheless the loss tangent right at the stable/unstable boundary is infinite for $\overline{\Omega}=0$ and very large for small exciting frequencies, as illustrated in Fig. 4.2 (right):

$$\tan\delta\big|_{x=-y/(y+1)}=\frac{y^2\left[v+y^2+u(1+y)^2\right]+(u+v)(u+v+uv)(1+y)^2\overline{\Omega}^2}{(1+y)(u+v+uy)^2\overline{\Omega}}. \tag{4.25}$$

4.3.2. Inertia effects retained

Here we assume $m_1=0,\ m_2=m\neq 0$ to remove the effects of local resonance (internal effects). The effective viscoelastic stiffness is, from (4.15)

$$k_{eff}^{*}=k_2+ic_2\Omega+k_3+ic_3\Omega-m\Omega^2-\frac{(k_2+ic_2\Omega)^2}{k_1+ic_1\Omega+k_2+ic_2\Omega} \tag{4.26}$$

and hence the loss tangent is by definition (4.19), which gives

$$\tan\delta=\frac{\Omega\left[c_2k_1^2+c_1k_2^2+c_3(k_1+k_2)^2+(c_1+c_2)(c_1c_3+c_2c_3+c_1c_2)\Omega^2\right]}{(k_1+k_2)(k_1k_3+k_2k_3+k_1k_2)+\left[c_2^2k_1+c_1^2k_2+(c_1+c_2)^2k_3-(k_1+k_2)^2m\right]\Omega^2-(c_1+c_2)^2m\Omega^4}. \tag{4.27}$$

In contrast to the case of negligible masses (see Eqn. (4.21)), Eqn. (4.27) contains two negative terms in the denominator, which makes the loss tangent negative for some frequencies even in the stable regime. To see this, let us choose $m=c_3^2/k_3$ and use (4.22) to rewrite (4.27) as

$$\tan\delta=\frac{\overline{\Omega}\left[v\,x^2+u\,y^2+(x+y)^2+(u+v)(u+v+u\,v)\overline{\Omega}^2\right]}{(x+y)(x+y+xy)+\left[x\,v^2+y\,u^2+(u+v)^2-(x+y)^2\right]\overline{\Omega}^2-(u+v)^2\overline{\Omega}^4}. \tag{4.28}$$

The loss tangent right at the stable/unstable boundary is infinite for $\overline{\Omega}=0$ and very large for small exciting frequencies as for the case of negligible masses:

$$\tan\delta\big|_{x=-y/(y+1)}=\frac{y^2\left[v+y^2+u(1+y)^2\right]+(u+v)(u+v+uv)(1+y)^2\overline{\Omega}^2}{\left[(1+y)(u+v+uy)^2-y^4\right]\overline{\Omega}-(1+y)^2(u+v)^2\overline{\Omega}^3}. \tag{4.29}$$

Figure 4.3 plots the loss tangent for different frequencies. In the stable regime, for some frequencies, these curves consist of two branches, one with positive values and the other with negative ones.

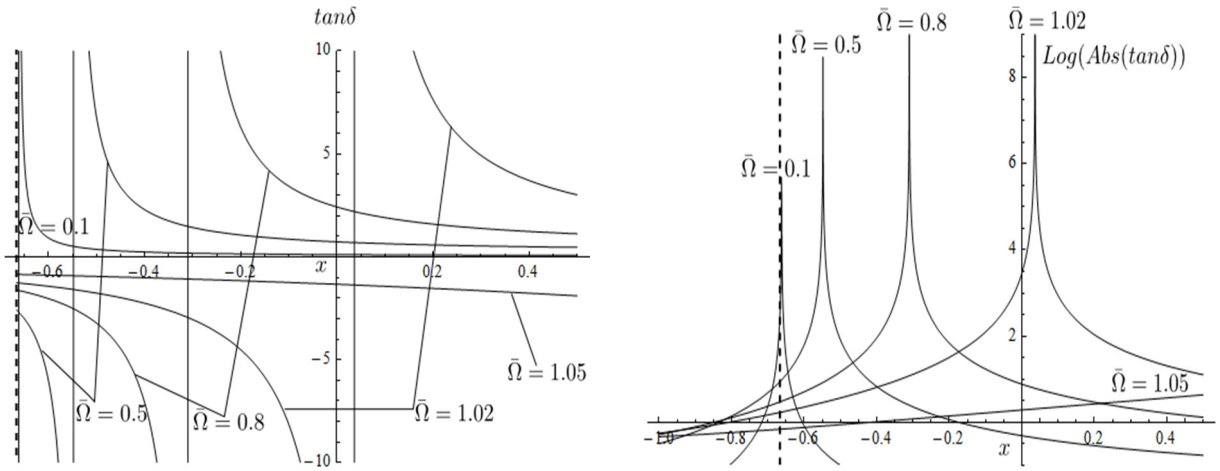

Figure 4.3. The effective damping of the spring-dashpot system versus $x>-2/3$ for different frequencies $\overline{\Omega}$ with masses included and parameters $y=2,\ u=v=0.1$.

Let us now investigate the case of resonance. For this case the exciting frequency satisfies

$$\Omega=\sqrt{k_{static}/m}=\sqrt{\left(\frac{k_1k_2}{k_1+k_2}+k_3\right)\Big/m}\ ,$$

where k_{static} is the effective elastic stiffness of the system (i.e. setting $m_1 = m_2 = 0$ in (4.16)). As before, choosing $m = c_3^2/k_3$ and substituting these relations into (4.27) with relations (4.22) gives the loss tangent:

$$\tan\delta = \frac{v x^2(x+y)+v^2(x+y+xy)+(x+y)^3+u^2(1+v)(x+y+xy)+u\left[v(v+2)(x+y+xy)+y^2(x+y)\right]}{(vx-uy)^2\sqrt{\dfrac{x+y+xy}{x+y}}}. \tag{4.30}$$

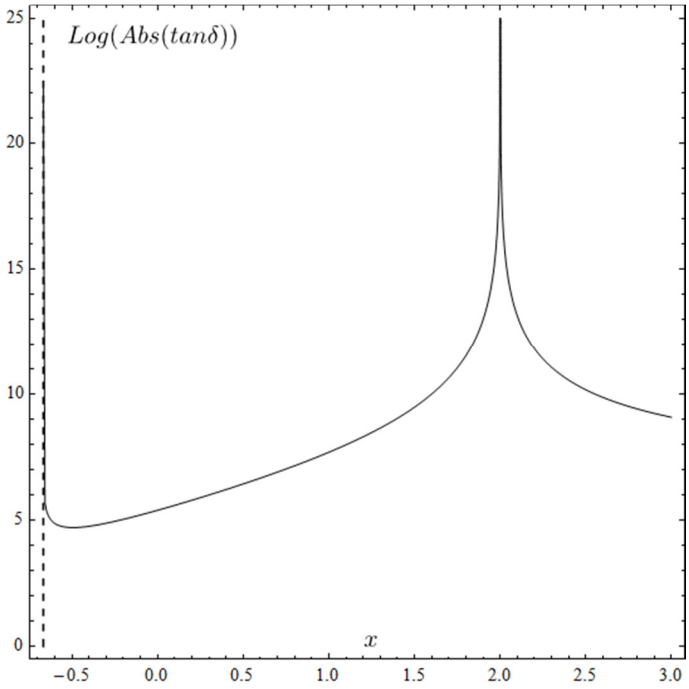

Figure 4.4. The effective damping of the spring-dashpot system near resonance versus $x > -2/3$ with parameters $y = 2,\ u = v = 0.1$.

Eq. (4.30) shows that the loss tangent is always positive in the stable regime near resonance and near the stability boundary (4.24) $x + y + xy \to 0$, it has a peak. Moreover, it has another peak inside the stable regime at $x = uy/v > 0$. Figure 4.4 illustrates this.

4.4. Viscoelastic composite solids

In this section, we will first determine the effective loss tangent of a circular cylindrical composite solid consisting of an inclusion of radius a, Lamé moduli λ_1, μ_1, bulk modulus $\kappa_1 = \lambda_1 + \mu_1$ and a coating of outer radius b, Lamé moduli λ_2, μ_2, bulk modulus $\kappa_2 = \lambda_2 + \mu_2$, as illustrated in Fig. 4.5; both phases are homogeneous, isotropic, viscoelastic material. We next consider the more general case where the coating is heterogeneous, isotropic, viscoelastic material.

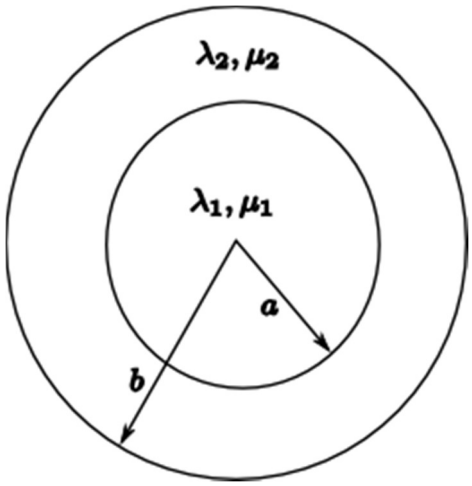

Figure 4.5. The coated-cylinder composite.

To find the effective loss tangent of the composite solid, we assume frequencies of interest are small (in the subresonant domain) and hence one can neglect inertial effects. Also we consider the simplest viscoelastic model where $n=1$ in (4.11), so that

$$\mu^* = \mu_0 + \mu_1(i\Omega) \equiv \mu(1+i\Omega\tan\delta),\ \kappa^* = (\lambda^* + \mu^*) = \kappa_0 + \kappa_1(i\Omega) \equiv \kappa(1+i\Omega\tan\delta). \tag{4.31}$$

4.4.1. Viscoelastic composite solids with a homogeneous coating.

4.4.1.1. Inertial effects neglected

The static effective elastic bulk modulus of a composite solid consisting of the elastic inclusion and coating when neglecting inertial effects is

$$\kappa_{eff} = \frac{\kappa_2(\kappa_1+\mu_2)+\alpha(\kappa_1-\kappa_2)\mu_2}{\kappa_1+\mu_2-\alpha(\kappa_1-\kappa_2)}. \tag{4.32}$$

The stability regime of the elastic composite solid is

$$\kappa_1 > -\frac{(1-\alpha)\kappa_2\mu_2}{\kappa_2+\alpha\mu_2}. \tag{4.33}$$

For the viscoelastic solid with both phases comprised of viscoelastic material, from (4.31), one has

$$\kappa_1^* = \kappa_1(1+i\Omega t_1),\ \mu_1^* = \mu_1(1+i\Omega t_1),\ \kappa_2^* = \kappa_2(1+i\Omega t_2),\ \mu_2^* = \mu_2(1+i\Omega t_2) \tag{4.34}$$

where t_1, t_2 are the loss tangent of the inclusion and the coating respectively. Using the correspondence principle, from (4.32), one gets the static effective viscoelastic bulk modulus of the composite when neglecting inertial effects

$$\kappa_{eff}^{*} = \frac{\kappa_2^{*}\left(\kappa_1^{*}+\mu_2^{*}\right)+\alpha\left(\kappa_1^{*}-\kappa_2^{*}\right)\mu_2^{*}}{\kappa_1^{*}+\mu_2^{*}-\alpha\left(\kappa_1^{*}-\kappa_2^{*}\right)}. \tag{4.35}$$

Extracting the real and imaginary parts of the static effective viscoelastic bulk modulus (4.35) and substituting them into (4.19) gives the static effective loss tangent of the viscoelastic composite. Although this effective loss tangent can be determined symbolically, its expression is complicated and we will evaluate it numerically.

We observe that the static effective loss tangent in the stable regime is positive if $t_1 < t_2$ and negative if $t_1 > t_2$ as in Fig. 4.6a and 4.6b. Also, all the peaks are in the unstable regime as illustrated in Fig. 4.6c. Denoting nondimensional parameters

$$x = \kappa_1/\mu_1,\ y = \kappa_2/\mu_2 > 0,\ s = \mu_2/\mu_1 > 0,\ 0 < \alpha = a^2/b^2 < 1 \tag{4.36}$$

the stability domain of the viscoelastic solid is the same as that of the elastic solid and hence from (4.33) it is

$$x > -\frac{(1-\alpha)sy}{y+\alpha} \equiv x_{\min}. \tag{4.37}$$

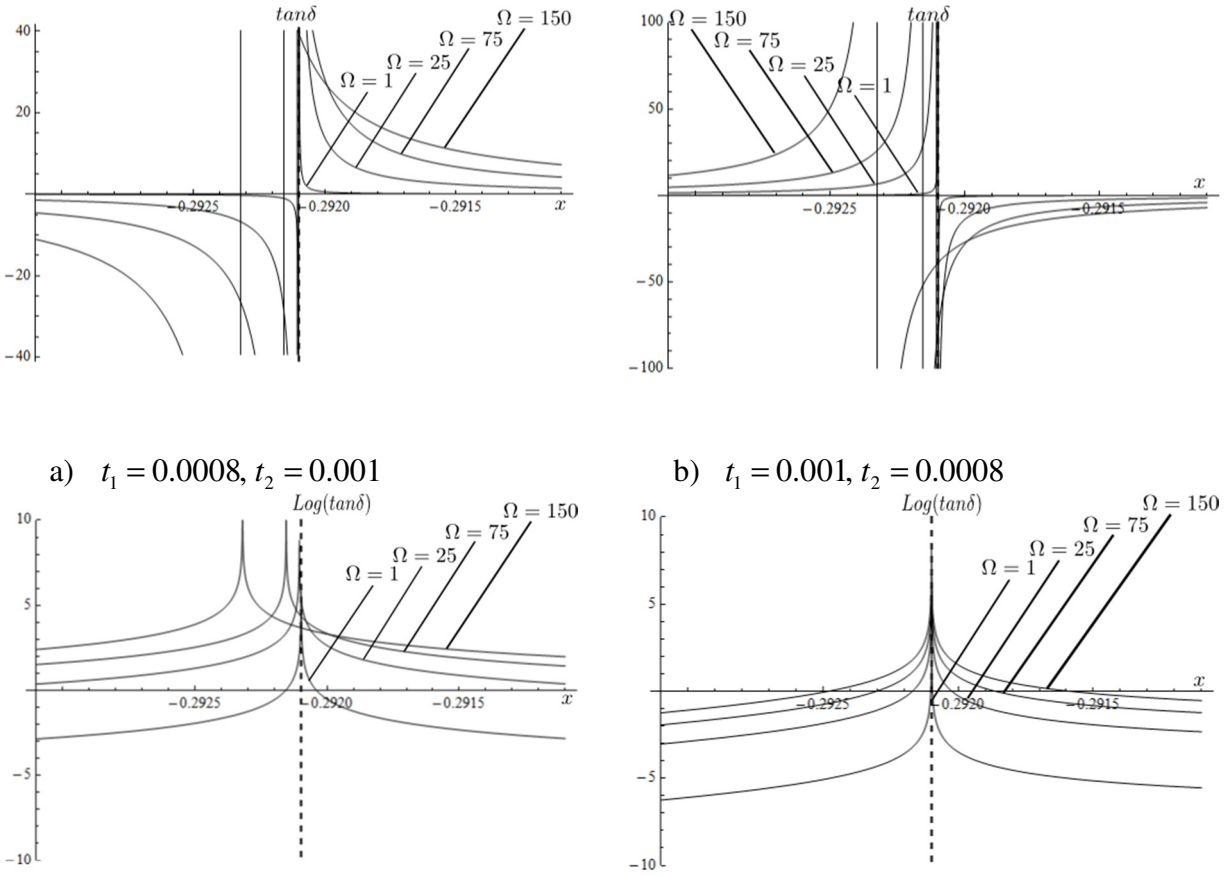

a) $t_1 = 0.0008,\ t_2 = 0.001$

b) $t_1 = 0.001,\ t_2 = 0.0008$

c) $t_1 = 0.0008,\ t_2 = 0.001$

d) $t_1 = 0.00099,\ t_2 = 0.001$

Figure 4.6. The static effective loss tangent of the viscoelastic composite for different frequencies versus the normalized inclusion bulk modulus $x = \kappa_1/\mu_1$ with parameter values $y = 7/26,\ s = 26/50 > 0,\ \alpha = 0.142.$

The static effective loss tangent of the viscoelastic composite right at the stability

boundary is

$$\tan\delta_{eff}\Big|_{x=x_{\min}} = -\frac{(1+y)^2\alpha + t_2\left[t_2(y+\alpha)(1+y\alpha) - t_1 y(1-\alpha)^2\right]\Omega^2}{(t_1-t_2)(1-\alpha)^2\, y\,\Omega}. \tag{4.38}$$

From (4.38), one sees that the static effective loss tangent can be theoretically infinite for all exciting frequencies right at the stability boundary if the loss tangents of each phase are close to one another, $t_1 \approx t_2$. Fig. 4.6d illustrates this.

4.4.1.2. Inertial effects retained

When inertial effects are included, the dynamic effective composite bulk modulus is sought by applying time-harmonic tensile hydrostatic pressure $\mathbf{t}(t) = \hat{p}e^{i\Omega t}\mathbf{e}_r$ on the outside surface to result in only nonzero radial displacement $\mathbf{u}(r,t) = \hat{u}_r(r)e^{i\Omega t}\mathbf{e}_r$ (Wojnar and Kochmann, 2014); here $\mathbf{e}_r$ is the radial unit vector. The governing equation without body forces reads

$$\operatorname{div}\boldsymbol{\sigma} = \rho\ddot{\mathbf{u}} \tag{4.39}$$

where $\boldsymbol{\sigma}, \rho$ are the stress tensor and mass density respectively.

Using Hooke's law for homogeneous isotropic linear elastic materials and the strain-displacement relation transforms (4.39) into the dynamic Navier equation, which in terms of our

assumed radial-only displacement field becomes:

$$r^2\hat{u}_r^{''} + r\hat{u}_r^{'} + \left(\frac{\rho\Omega^2 r^2}{\lambda+2\mu} - 1\right)\hat{u}_r = 0. \tag{4.40}$$

The general solution of (4.40) is

$$\hat{u}_r(r) = C_1 J_1(\chi r) + C_2 Y_1(\chi r) \tag{4.41}$$

where $\chi = \sqrt{\rho\Omega^2/(\lambda+2\mu)}$ and $J_1(z), Y_1(z)$ are the first order Bessel functions of the first and second kind respectively.

The radial stress field from Hooke's law is $\sigma_{rr}(r,t) = \hat{\sigma}_{rr}(r)e^{i\Omega t}$ with amplitude

$$\hat{\sigma}_{rr}(r) = \chi(\lambda+2\mu)\left[C_1 J_1^{'}(\chi r) + C_2 Y_1^{'}(\chi r)\right] + \frac{\lambda}{r}\left[C_1 J_1(\chi r) + C_2 Y_1(\chi r)\right].$$

The dynamic effective composite bulk modulus is (Wojnar and Kochmann, 2014)

$$\kappa_{eff} = \frac{b}{2\hat{u}_r(b)}\left(\hat{p} + \frac{\Omega^2}{b^2}\int_0^b \rho\hat{u}_r(r)r^2 dr\right). \tag{4.42}$$

Using the two conditions of continuous traction and displacement across the common interface $r = a$, namely $[[\hat{\sigma}_{rr}(a)]] = 0, [[\hat{u}_r(a)]] = 0$ where $[[(\ )]]$ denotes the jump of $(\ )$ and the boundary condition at the outside interface $r = b$, $\hat{\sigma}_{rr}(b) = \hat{p}$ yields the displacement field. The

resulting displacement field is substituted to (4.42) to give the dynamic effective composite bulk modulus.

Since the analytical expression of (4.42) is fairly long, we do not write it and the dynamic effective composite loss tangent, from definition (4.19), will be treated numerically. Before analyzing the composite loss tangent, we mention one interesting point about the dynamic effective composite bulk modulus, Wojnar and Kochmann (2014); they showed that the stably infinite static effective composite bulk modulus cannot be obtained for any combinations of composite material and geometry parameters while the stably infinite dynamic one can be for exciting frequency $\Omega \geq \Omega_{\min}$.

To see this, one sees that the static effective composite bulk modulus (4.32) becomes infinite if $\kappa_1 + \mu_2 - \alpha(\kappa_1 - \kappa_2) = 0$ or in terms of nondimensional parameters (4.36) it is

$$f(x, y) \equiv (1-\alpha)x + s(1+\alpha y) = 0. \tag{4.43}$$

The dynamic effective composite bulk modulus from (4.42) becomes infinite if $\hat{u}_r(b) = 0$ or

$$\begin{aligned} g(x, y) \equiv{}& (1+x)\alpha\xi_1 J_1'(\alpha\xi_1)[J_1(\alpha\xi_2)Y_1(\xi_2) - Y_1(\alpha\xi_2)J_1(\xi_2)] - s(1+y)\alpha\xi_2 J_1(\alpha\xi_1)[J_1'[\alpha\xi_2]Y_1(\xi_2) \\ & - Y_1'[\alpha\xi_2]J_1(\xi_2)] + (x-1+s-sy)J_1(\alpha\xi_1)[J_1(\alpha\xi_2)Y_1(\xi_2) - Y_1(\alpha\xi_2)J_1(\xi_2)] \end{aligned} \tag{4.44}$$

where $\xi_1 = \sqrt{\rho_1 \Omega^2 b^2 / (\lambda_1 + 2\mu_1)}$, $\xi_2 = \sqrt{\rho_2 \Omega^2 b^2 / (\lambda_2 + 2\mu_2)}$.

In Fig. 4.7, the shaded region is the unstable domain and the thick, bold curve is the stability boundary (4.37), $h(x, y) \equiv x + \dfrac{(1-\alpha)sy}{y+\alpha} = 0$.

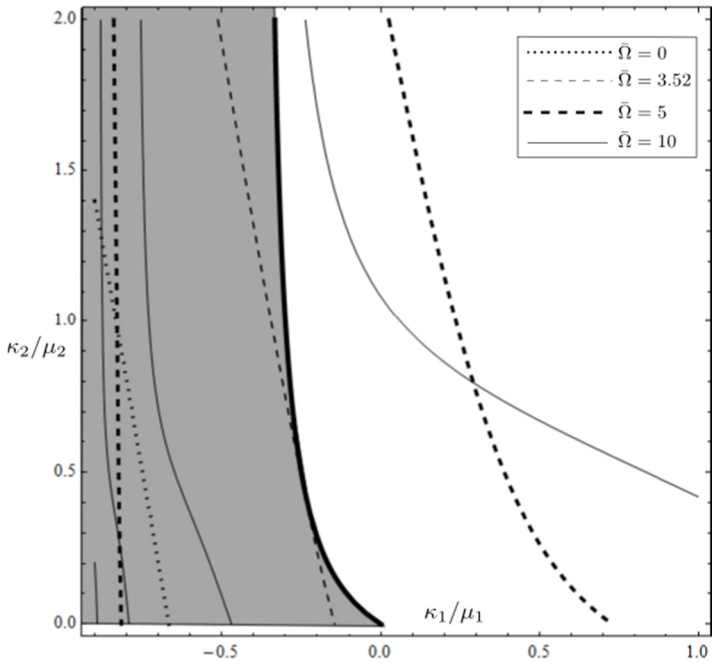

Figure. 4.7. Moduli combinations leading to infinite static and infinite dynamic effective composite bulk modulus for $a/b = 0.5$, $\mu_2/\mu_1 = 0.5$, $\rho_1 = \rho_2 = \rho$, $\Omega = \bar{\Omega}\sqrt{\mu_2/(\rho b^2)}$.

The infinite static effective composite bulk modulus corresponding to Eq. (4.43) [or Eq. (4.44) when $\Omega = 0$] is the dotted line which always lies in the unstable domain; the infinite dynamic effective composite bulk modulus curve corresponding to Eq. (4.44) for nonzero

exciting frequencies can lie in the stable domain if $\Omega \geq \Omega_{\min}$ where $\Omega_{\min}$ is sought from the condition that the curve (4.44) is tangent to the stability boundary, namely

$$\begin{cases} g(x,y)=0 \\ h(x,y)=0 \\ \dfrac{\partial g/\partial x}{\partial g/\partial y}=\dfrac{\partial h/\partial x}{\partial h/\partial y} \end{cases} \quad \rightarrow \quad \overline{\Omega}=\overline{\Omega}_{\min}.$$

From the data in Fig. 4.7, $\overline{\Omega}_{\min} \approx 3.52$. Note that Wojnar and Kochmann (2014) did not show how to find the $\overline{\Omega}=\overline{\Omega}_{\min}$.

4.4.2. Composite solids with a heterogeneous coating.

Let us now consider the composite solid with a heterogeneous coating whose bulk modulus is constant and shear modulus varies continuously in the specific manner found in Chapter 3 that permits maximum inclusion negative bulk modulus while maintaining overall composite stability:

$$\kappa(r)=\kappa_2, \quad \mu(r)=\frac{(b^2-a^2)(\kappa_2+\mu_2)}{2(\ln b-\ln a)}\frac{1}{r^2}-\kappa_2, \quad \frac{2}{b^2-a^2}\int_a^b \mu(r)rdr=\mu_2. \tag{4.45}$$

4.4.2.1. Inertial effects neglected

The static effective elastic bulk modulus of a composite solid consisting of the elastic homogeneous inclusion and heterogeneous coating is

$$\kappa_{eff} = \kappa_2 + \frac{\alpha(\kappa_1 - \kappa_2)}{1 + \frac{\alpha(\ln\alpha)^2}{1-\alpha}\frac{(\kappa_1 - \kappa_2)}{(\kappa_2 + \mu_2)}}. \tag{4.46}$$

The stability regime of the elastic composite solid is

$$\kappa_1 > \kappa_2 - \frac{\kappa_2}{\frac{\alpha(\ln\alpha)^2}{1-\alpha}\frac{\kappa_2}{\kappa_2 + \mu_2} + \alpha}\ , \tag{4.47}$$

or in the form of nondimensional parameters (4.36)

$$x > sy\left(1 - \frac{1}{\frac{\alpha(\ln\alpha)^2}{1-\alpha}\frac{y}{y+1} + \alpha}\right) \equiv x_{\min}. \tag{4.48}$$

By repeating exactly the same steps carried out in Section 4.4.1.1, i.e. using the correspondence principle, one can determine the static effective loss tangent of the viscoelastic composite with a heterogeneous coating. And one can learn the same lesson as that for a viscoelastic composite with a homogeneous coating. Specifically, the static effective loss tangent can be positive (or negative) for all frequencies in the stable regime if the coating is more (or less) viscous than the inclusion; all the peaks of the static loss tangent are in the unstable regime and one can shift these peaks to the stability boundary by making the loss tangents of each phase close to one another. So what is the advantage of using a heterogeneous coating?

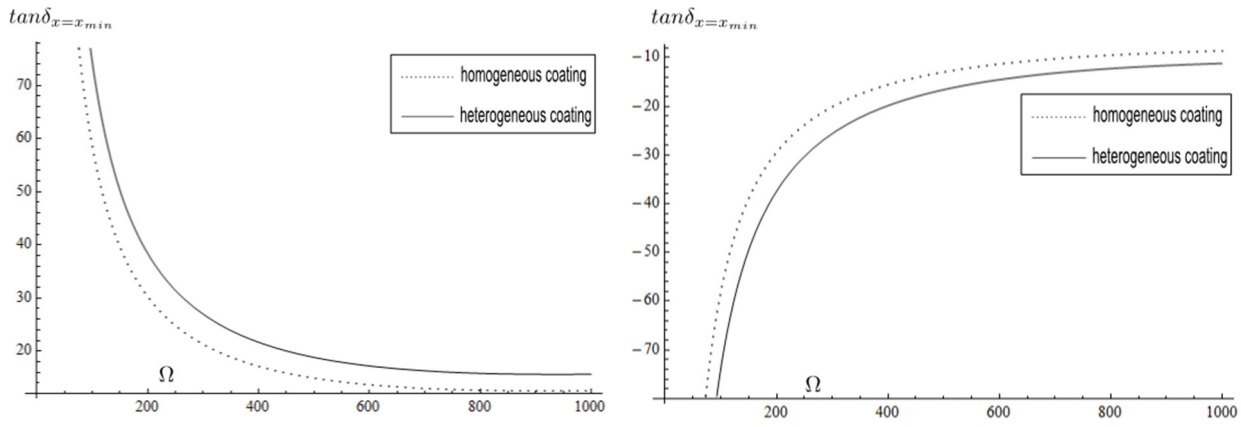

a) $t_1 = 0.0008,\ t_2 = 0.001$ b) $t_1 = 0.001,\ t_2 = 0.0008$

Figure 4.8. The static effective loss tangent at the stability boundary of the viscoelastic composite for homogeneous and heterogeneous coatings versus exciting frequency for parameter values $y = 7/26,\ s = 26/50 > 0,\ \alpha = 0.142.$

The answer is that the absolute value of static effective loss tangent of a composite with a heterogeneous coating at its stability boundary (4.48) for all frequencies,

$$\tan\delta_{eff}\Big|_{x=x_{\min}} = t_2\Omega + \frac{(1-\alpha)^2(1+y)^2\left(1+t_2^2\Omega^2\right)}{(t_1-t_2)(\ln\alpha)^2\left[\alpha(\ln\alpha)^2 y-(1-\alpha)^2(1+y)\right]y\,\Omega}, \tag{4.49}$$

is higher than that of a composite with a homogeneous coating at its stability boundary (4.38) as illustrated in Fig. 4.8.

4.4.2.2. Inertial effects retained

To determine the dynamic bulk modulus (4.42) one first applies time-harmonic tensile hydrostatic pressure $\mathbf{t}(t) = \hat{p}e^{i\Omega t}\mathbf{e}_r$ on the outside surface to result in only nonzero radial

displacement $\mathbf{u}(r,t) = \hat{u}_r(r)e^{i\Omega t}\mathbf{e}_r$ (Wojnar & Kochmann, 2014) as before. Then one needs to seek the displacement field in the homogeneous inclusion and the heterogeneous coating. The former is Eq. (4.41) with the second term removed to avoid a singularity at the origin $r = 0$. The latter is found from the governing equation (4.39) and the strain-displacement relation with Hooke's law for heterogeneous material (4.45) to arrive at the dynamic Navier equation:

$$r^2\hat{u}_r'' - r\hat{u}_r' + (\xi^2 r^4 + 1)\hat{u}_r = 0. \tag{4.50}$$

The general solution of (4.50) is

$$\hat{u}_r(r) = r\left(C_1 J_0\left(\frac{\xi r^2}{2}\right) + C_2 Y_0\left(\frac{\xi r^2}{2}\right)\right) \tag{4.51}$$

where $\xi = \sqrt{\frac{2(\ln b - \ln a)\rho_2 \Omega^2}{(b^2 - a^2)(\kappa_2 + \mu_2)}}$ and $J_0(z), Y_0(z)$ are the zero order Bessel functions of the first and second kind respectively.

Now repeating the same procedure to find the extreme static and extreme dynamic effective composite bulk modulus as before by setting the denominator of Eq. (4.46) to equal zero and $\hat{u}_r(b) = 0$ in Eq. (4.51). With those two equations along with the stability regime (4.47), one can produce the Fig. 4.9 similar to Fig. 4.7.

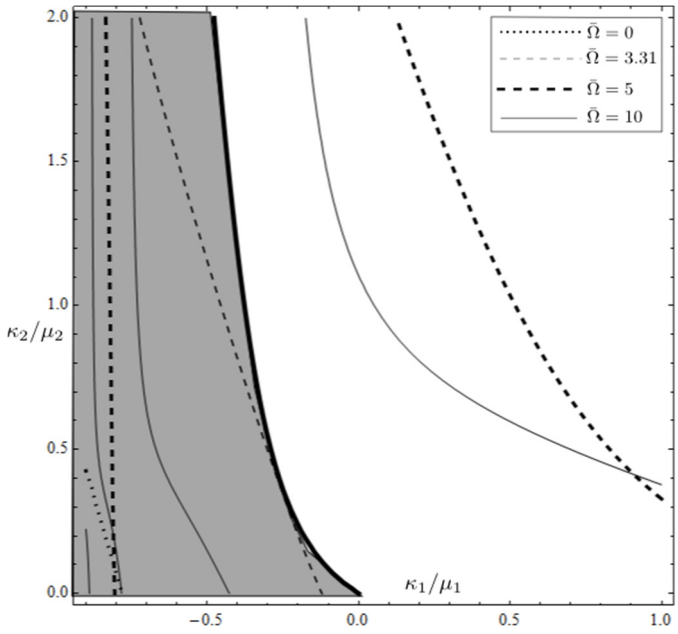

Figure. 4.9. Moduli combinations leading to infinite static and infinite dynamic effective composite bulk modulus for $a/b = 0.5$, $\mu_2 \big/ \mu_1 = 0.5$, $\rho_1 = \rho_2 = \rho$, $\Omega = \overline{\Omega}\sqrt{\mu_2 / \left(\rho b^2\right)}$.

One sees that the infinite static effective composite bulk modulus curve, i.e. the dotted line, always lies in the unstable domain while the infinite dynamic effective composite bulk modulus curve lies in the stable domain if $\Omega \geq \Omega_{\min} \approx 3.31$. It is interesting to note that the critical exciting frequency to have the infinite dynamic effective composite bulk modulus for a homogeneous coating is higher than that for a heterogeneous one with the same volume averages of the elastic moduli in the coating. We expect that the critical exciting frequency in the heterogeneous coating case can be lowered further by optimizing the coating heterogeneity for this purpose.

4.5. Conclusions

We have applied the results obtained for elastic composite solids in Chapters 2 and 3 to analyze viscoelastic composite solids. We showed that by tuning heterogeneity of the materials in the coating appropriately, one (i) increases the effective composite loss tangent near the stability domain where the static effective composite bulk modulus becomes zero and (ii) decreases the critical exciting frequency at which the dynamic effective composite bulk modulus becomes infinite.

Chapter 5. Future work

For the buckling and post-buckling problem of a column, we modeled changes in its buckled patterns observed experimentally by employing a small deviation from end flatness. Experiments also revealed that high damping occurs in a flat-end column subjected to snap-through buckling, provided that the ends of the column undergo tilting from flat to edge contact. This end tilt buckling exhibits incremental negative stiffness and gives rise to large hysteresis that can be useful in structural damping and potentially catastrophic in the context of design of structural support columns. For example, this flat-end column is included in stable structures such as modules of clamped columns by a press-fit condition to provide greatly enhanced damping; this is very useful for vibration damping. Currently, I am continuing to develop the theoretical framework to understand this extreme high damping property occurring not only in columns but in other structures such as tubes as well.

For elastic composite solids, we showed that permitting heterogeneity of the positive-definite phase can substantially increase the range of constituent negative stiffness while maintaining overall composite stability. I however have not analyzed the case in which the inclusion material is also permitted to be heterogeneous. I anticipate this would permit a further enlargement of the composite stability regime. Work is underway to explore this. Moreover, those novel composite materials with negative stiffness inclusions have extremely high damping (Lakes, R.S, Lee, T.,

Bersie, A., Wang, Y.C., 2001) but they are not very stiff. Current research is seeking novel ways to achieve tunable static effective composite bulk modulus.

For viscoelastic composite solids, we demonstrated that the optimally specific heterogeneity of the positive-definite phase, which permits the inclusion to have the most negative stiffness while maintaining overall composite stability, can increase the effective loss tangent of the composites near the stability boundary. However, it is more appropriate to find optimally heterogeneous material in the coating that allows the effective loss tangent near the stability boundary of the composites the maximum value while maintaining overall composite stability. Ongoing research is being developed to discover this.

Appendix A. Structure of equilibrium solutions in the isotropic, circular domain for the optimal composite with a radially-varying coating shear modulus

In this section, we seek the displacement field in the circular domain for the optimal composite with a constant bulk modulus, whose coating material is heterogeneous of form (3.31). Similarly to the approach for homogeneous materials employed in Part I, application of Hooke's law for radially heterogeneous materials

$$\boldsymbol{\sigma} = \lambda(r)\,\mathrm{tr}\boldsymbol{\varepsilon}\,\mathbf{I} + 2\mu(r)\boldsymbol{\varepsilon}, \tag{A.1}$$

to the equilibrium equation

$$\nabla \bullet \boldsymbol{\sigma} = \mathbf{0}, \tag{A.2}$$

using the strain-displacement relations and assuming separable forms for the displacement field in polar coordinates

$$u_r = f(r)e^{im\theta}, \;\; u_\theta = g(r)e^{im\theta} \tag{A.3}$$

one obtains:

$$f'' + \left(\frac{\lambda' + 2\mu'}{\lambda + 2\mu} + \frac{1}{r}\right)f' + \left[\frac{\lambda'}{\lambda+2\mu}\frac{1}{r} - \left(1 + \frac{m^2\mu}{\lambda+2\mu}\right)\frac{1}{r^2}\right]f - \frac{im}{\lambda+2\mu}\left[(\lambda+3\mu)\frac{g}{r^2} - \lambda'\frac{g}{r} - (\lambda+\mu)\frac{g'}{r}\right] = 0 \tag{A.4a}$$

$$g''+\left(\frac{\mu'}{\mu}+\frac{1}{r}\right)g'-\left[\frac{\mu'}{\mu}\frac{1}{r}+\left(1+\frac{(\lambda+2\mu)m^2}{\mu}\right)\frac{1}{r^2}\right]g+\frac{im}{\mu}\left[(\lambda+3\mu)\frac{f}{r^2}+\mu'\frac{f}{r}+(\lambda+\mu)\frac{f'}{r}\right]=0 \qquad \text{(A.4b)}$$

where primes denote derivatives with respect to r.

For the optimal constant bulk modulus composite, we found the heterogeneity to have form (3.31). Substituting (3.31), system (A.4) becomes:

$$Cr^2f''-Crf'+\left[C\left(1-m^2\right)+\kappa m^2r^2\right]f+i\kappa mr^2\left(g+rg'\right)=0 \qquad \text{(A.5a)}$$

$$r^2\left(\kappa r^2-C\right)g''+r\left(C+\kappa r^2\right)g'-\left[C\left(1-m^2\right)+\kappa r^2\right]g+i\kappa mr^2\left(f-rf'\right)=0\,. \qquad \text{(A.5b)}$$

Making the change of variable

$$r\to\sqrt{Cz/\kappa} \qquad \text{(A.6)}$$

transforms (A.5) into

$$4z^2\ddot{f}+\left[\left(1-m^2\right)+m^2z\right]f+imz\left(g+2z\dot{g}\right)=0 \qquad \text{(A.7a)}$$

$$4z^2(z-1)\ddot{g}+4z^2\dot{g}-\left[\left(1-m^2\right)+z\right]g+imz\left(f-2z\dot{f}\right)=0, \qquad \text{(A.7b)}$$

where dots denote derivatives with respect to z.

The above system consists of two linear second-order ordinary differential equations, so its general solution will contain four arbitrary independent constants. We seek the general solution (i.e., four linearly independent solutions) of (A.7) in the Frobenius forms:

$$f(z)=z^s\sum_{k=0}^{\infty}a_k z^k,\quad g(z)=i\,z^s\sum_{k=0}^{\infty}b_k z^k\,. \tag{A.8}$$

Substituting (A.8) into (A.7) and requiring coefficients of equal power terms to vanish gives

- For the lowest term z^s

$$s=\frac{1\pm m}{2} \tag{A.9}$$

- For the general term z^k

$$a_k=\frac{m\left[ma_{k-1}+(1-2k-2s)b_{k-1}\right]}{(m+1-2k-2s)(m-1+2k+2s)},\quad b_k=\frac{(2k+2s-3)\left[ma_{k-1}+(1-2k-2s)b_{k-1}\right]}{(m+1-2k-2s)(m-1+2k+2s)}. \tag{A.10}$$

Now consider the following cases:

A.1. Case $s=s_1=\dfrac{1+m}{2}$

(A.10) becomes

$$a_k = \frac{m\left[-ma_{k-1} + (m+2k)b_{k-1}\right]}{4k(m+k)}, \quad b_k = \frac{(m+2k-2)\left[-ma_{k-1} + (m+2k)b_{k-1}\right]}{4k(m+k)}. \tag{A.11}$$

Solving the recursive system (A.11) gives:

$$\begin{aligned} a_k &= \frac{\Pi_{i=1}^{k-1}\left[i(i+m)-1\right]}{\Pi_{i=2}^{k}\left[i(i+m)\right]}a_1, \quad b_k = \left(\frac{m+2k-2}{m}\right)\frac{\Pi_{i=1}^{k-1}\left[i(i+m)-1\right]}{\Pi_{i=2}^{k}\left[i(i+m)\right]}a_1 \text{ for } k \geq 2 \\ a_1 &= b_1 = \frac{m\left[-ma_0 + (m+2)b_0\right]}{4(m+1)}. \end{aligned} \tag{A.12}$$

Substituting (A.11) into (A.8) one has

$$f(z) = z^{s_1}\sum_{k=0}^{\infty} a_k z^k = a_0 f_1(z) + b_0 f_2(z), \quad g(z) = i\,z^s \sum_{k=0}^{\infty} b_k z^k = i\left[a_0 g_1(z) + b_0 g_2(z)\right] \tag{A.13}$$

where

$$f_1(z) = \frac{1}{4}z^{s_1}\left\{4 - m^2 + m_2^2 F_1\left[\frac{1}{2}\left(m - \sqrt{4+m^2}\right), \frac{1}{2}\left(m + \sqrt{4+m^2}\right), 1+m, z\right]\right\}$$

$$g_1(z) = \frac{1}{4}z^{s_1}\left\{\begin{array}{l} 2m - m^2 - \left(2m - m^2\right)\,{}_2F_1(\alpha,\beta,\gamma,z)\left[\frac{1}{2}\left(m - \sqrt{4+m^2}\right), \frac{1}{2}\left(m + \sqrt{4+m^2}\right), 1+m, z\right] \\ -2mz\,{}_2F_1\left[\frac{1}{2}\left(2+m - \sqrt{4+m^2}\right), \frac{1}{2}\left(2+m + \sqrt{4+m^2}\right), 2+m, z\right] \end{array}\right\}$$

$$f_2(z)=\frac{1}{4}z^{s_1}\left(2m+m^2\right)\left\{1-{}_2F_1\left[\frac{1}{2}\left(m-\sqrt{4+m^2}\right),\frac{1}{2}\left(m+\sqrt{4+m^2}\right),1+m,z\right]\right\}$$

$$g_2(z)=\frac{1}{4}z^{s_1}\left\{\begin{matrix}m^2+\left(4-m^2\right){}_2F_1\left[\frac{1}{2}\left(m-\sqrt{4+m^2}\right),\frac{1}{2}\left(m+\sqrt{4+m^2}\right),1+m,z\right]\\+2(m+2)z\,{}_2F_1\left[\frac{1}{2}\left(2+m-\sqrt{4+m^2}\right),\frac{1}{2}\left(2+m+\sqrt{4+m^2}\right),2+m,z\right]\end{matrix}\right\}$$

and where $y(z)={}_2F_1(\alpha,\beta,\gamma,z)$ is the hypergeometric function, which satisfies the second-order ordinary differential equation:

$$z(z-1)\ddot{y}+\left[(\alpha+\beta+1)z-\gamma\right]\dot{y}+\alpha\beta y=0.$$

A.2. Case $s=s_2=\frac{1-m}{2}$

(A.10) becomes:

$$a_k=\frac{m\left[ma_{k-1}+(m-2k)b_{k-1}\right]}{4k(m-k)},\quad b_k=-\frac{(m-2k+2)\left[ma_{k-1}+(m-2k)b_{k-1}\right]}{4k(m-k)}. \qquad \text{(A.14)}$$

From (A.14), one observes that a_k,b_k are well-defined for $k\neq m$, so one considers 3 cases:

a) When $k<m$:

(A.14) has the solution:

$$a_k = \frac{\Pi_{i=1}^{k-1}\left[i(m-i)+1\right]}{\Pi_{i=2}^{k}\left[i(m-i)\right]}a_1, \quad b_k = -\left(\frac{m-2k+2}{m}\right)\frac{\Pi_{i=1}^{k-1}\left[i(m-i)+1\right]}{\Pi_{i=2}^{k}\left[i(m-i)\right]}a_1 \text{ for } 2 \le k \le m-1$$
$$a_1 = -b_1 = \frac{m\left[ma_0 + (m-2)b_0\right]}{4(m-1)}. \tag{A.15}$$

b) When $k = m$:

Denominators in (A.14) are zero, so a solution exists if numerators are zero also. This means:

$$ma_{k-1} + (m-2k)b_{k-1} = 0 \text{ at } k = m \text{ and } a_m, b_m \text{ are arbitrary constants.} \tag{A.16}$$

Application of (A.15) with $k = m-1$to (A.16) gives:

$$a_1 = 0 \quad \text{or} \quad ma_0 + (m-2)b_0 = 0. \tag{A.17}$$

With (A.17), from (A.15) one arrives at:

$$a_1 = a_2 = \cdots = a_{m-1} = 0, \quad b_1 = b_2 = \cdots = b_{m-1} = 0. \tag{A.18}$$

c) When $k > m$:

(A.14) is rewritten in the form

$$a_{m+k} = \frac{m\left[-ma_{m+k-1} + (m+2k)b_{m+k-1}\right]}{4k(m+k)}, \quad b_{m+k} = \frac{(m+2k-2)\left[-ma_{m+k-1} + (m+2k)b_{m+k-1}\right]}{4k(m+k)} \quad \forall k \ge 1. \tag{A.19}$$

Redefining $\tilde{a}_k \equiv a_{m+k}, \tilde{b}_k \equiv b_{m+k}$, (A.19) is rewritten as

$$\tilde{a}_k = \frac{m\left[-m\tilde{a}_{k-1} + (m+2k)\tilde{b}_{k-1}\right]}{4k(m+k)}, \quad \tilde{b}_k = \frac{(m+2k-2)\left[-m\tilde{a}_{k-1} + (m+2k)\tilde{b}_{k-1}\right]}{4k(m+k)}. \tag{A.20}$$

From (A.16), a_m, b_m are arbitrary constants, as are $\tilde{a}_0, \tilde{b}_0$. Combining all three cases (a), (b) and (c) above, we have:

$$\begin{aligned} f(z) &= z^{s_2}\sum_{k=0}^{\infty} a_k z^k = a_0 z^{s_2} + z^{s_2}\sum_{k=m}^{\infty} a_k z^k = a_0 z^{s_2} + z^{s_1}\sum_{k=0}^{\infty} a_{m+k} z^k = a_0 z^{s_2} + z^{s_1}\sum_{k=0}^{\infty} \tilde{a}_k z^k, \\ g(z) &= i z^{s}\sum_{k=0}^{\infty} b_k z^k = i\left[b_0 z^{s_2} + z^{s_2}\sum_{k=m}^{\infty} b_k z^k\right] = i\left[b_0 z^{s_2} + z^{s_1}\sum_{k=0}^{\infty} b_{m+k} z^k\right] = i\left[b_0 z^{s_2} + z^{s_1}\sum_{k=0}^{\infty} \tilde{b}_k z^k\right]. \end{aligned} \tag{A.21}$$

Comparing (A.21) with (A.11), we see that the second parts in (A.21) actually give rise to the first solution in the first case where $s = s_1$. As the system (A.7) is linear, one can remove that solution from (A.21) to obtain an independent solution:

$$f(z) = a_0 z^{s_2} = \frac{2-m}{m} b_0 z^{s_2} = b_0 f_3(z), \quad g(z) = i b_0 z^{s_2} = b_0 g_3(z) \tag{A.22}$$

where

$$f_3(z) = \frac{2-m}{m} z^{s_2}, \quad g_3(z) = i z^{s_2}.$$

A.3. Case $s_1 - s_2 = m =$ a positive interger

Following Hildebrand (1976), we seek the last independent solution in the form:

$$f(z)=u(z)\ln z+F(z),\quad g(z)=v(z)\ln z+G(z), \tag{A.23}$$

where $u(z)$, $v(z)$ are in the form of (A.13)

$$u(z)=z^{s_1}\sum_{k=0}^{\infty}a_k z^k,\quad v(z)=i\,z^{s_1}\sum_{k=0}^{\infty}b_k z^k \tag{A.24}$$

and a_k, b_k are in the form of (A.11). $F(z)$, $G(z)$, which are new unknown functions, are sought in Frobenius forms also:

$$F(z)=z^{s_2}\sum_{k=0}^{\infty}A_k z^k,\quad G(z)=i\,z^{s_2}\sum_{k=0}^{\infty}B_k z^k. \tag{A.25}$$

Plugging (A.25) into the system (A.7), using the fact that $u(z)$, $v(z)$ are also solutions of (A.7), the subsequent equations are simplified to:

$$4z^2\ddot{F}+\left[\left(1-m^2\right)+m^2 z\right]F+imz\left(G+2z\dot{G}\right)=4u(z)-8z\dot{u}(z)-2imzv(z) \tag{A.26a}$$

$$4z^2\left(z-1\right)\ddot{G}+4z^2\dot{G}-\left[\left(1-m^2\right)+z\right]G+imz\left(F-2z\dot{F}\right)=2imzu(z)-4v(z)+8z\left(1-z\right)\dot{v}(z). \tag{A.26b}$$

Using (A.24), the non-homogeneous parts of (A.26) in series form are:

$$z^{s_1}\sum_{k=0}^{\infty}c_k z^k=4u(z)-8z\dot{u}(z)-2imzv(z)\ \text{or}\ c_k=-4\left(m+2k\right)a_k+2mb_{k-1} \tag{A.27a}$$

$$iz^{s_1}\sum_{k=0}^{\infty} d_k z^k = 2imzu(z) - 4v(z) + 8z(1-z)\dot{v}(z) \text{ or } d_k = -2ma_{k-1} + 4(m+2k-1)b_{k-1} - 4(m+2k)b_k \quad \text{(A.27b)}$$

Putting (A.25) into (A.26) and matching terms in the left hand sides with ones having the same powers in the right hand sides, equating their coefficients gives:

a) When $k < m$:

$$A_k = \frac{m\left[mA_{k-1} + (m-2k)B_{k-1}\right]}{4k(m-k)}, \quad B_k = -\frac{(m-2k+2)\left[mA_{k-1} + (m-2k)B_{k-1}\right]}{4k(m-k)} \quad \text{for } k = 1,..,m-1 \quad \text{(A.28)}$$

(A.28) has the solution:

$$\begin{aligned} A_k &= \frac{\Pi_{i=1}^{k-1}\left[i(m-i)+1\right]}{\Pi_{i=2}^{k}\left[i(m-i)\right]}A_1, \quad B_k = -\left(\frac{m-2k+2}{m}\right)\frac{\Pi_{i=1}^{k-1}\left[i(m-i)+1\right]}{\Pi_{i=2}^{k}\left[i(m-i)\right]}A_1 \text{ for } 2 \le k \le m-1 \\ A_1 &= -B_1 = \frac{m\left[mA_0 + (m-2)B_0\right]}{4(m-1)} \end{aligned} \quad \text{(A.29)}$$

b) When $k = m$

$$m\left[mA_{k-1} + (m-2k)B_{k-1}\right] = c_0, \quad -(m-2k+2)\left[mA_{k-1} + (m-2k)B_{k-1}\right] = d_0 \quad \text{(A.30)}$$

for $k = m$ and A_m, B_m arbitrary.

Using (A.27), (A.30) becomes

$$m^2\left[A_{m-1}-B_{m-1}\right]=-4ma_0,\quad m(m-2)\left[A_{m-1}-B_{m-1}\right]=-4mb_0 \tag{A.31}$$

(A.31) has a solution for $A_{m-1},\ B_{m-1}$ if

$$b_0=\frac{m-2}{m}a_0 \tag{A.32}$$

and

$$A_{m-1}=-a_0,\ B_{m-1}=-\frac{m-4}{m}a_0\,. \tag{A.33}$$

Combining (A.29) with (A.33) gives:

$$A_1=-\frac{\Pi_{i=2}^{m-1}\left[i(m-i)\right]}{\Pi_{i=1}^{m-2}\left[i(m-i)+1\right]}a_0 \text{ and } A_0=\frac{4(m-1)}{m^2}A_1+\frac{2-m}{m}B_0 \tag{A.34}$$

The second part in the second equation of (A.34) gives rise to a solution (A.22) which is already known. So we omit it and conclude that:

$$\begin{aligned} &A_k=\frac{\Pi_{i=1}^{k-1}\left[i(m-i)+1\right]}{\Pi_{i=2}^{k}\left[i(m-i)\right]}A_1,\ \ B_k=-\left(\frac{m-2k+2}{m}\right)\frac{\Pi_{i=1}^{k-1}\left[i(m-i)+1\right]}{\Pi_{i=2}^{k}\left[i(m-i)\right]}A_1 \ \text{ for } 2\le k\le m-1\\ &A_1=-B_1=-\frac{\Pi_{i=2}^{m-1}\left[i(m-i)\right]}{\Pi_{i=1}^{m-2}\left[i(m-i)+1\right]}a_0,\ A_0=\frac{4(m-1)}{m^2}A_1,\ B_0=0 \end{aligned} \tag{A.35}$$

c) When $k>m$

Similar to the case 2c) above, we define $\tilde{A}_k = A_{m+k},\ \tilde{B}_k = B_{m+k}$ and:

$$\tilde{A}_k = \frac{m\left[-m\tilde{A}_{k-1} + (m+2k)\,\tilde{B}_{k-1}\right] + c_k}{4k(m+k)},\ \tilde{B}_k = \frac{(m+2k-2)\left[-m\tilde{A}_{k-1} + (m+2k)\,\tilde{B}_{k-1}\right] + d_k}{4k(m+k)}\ \ \forall k \geq 1 \quad \text{(A.36)}$$

where $\tilde{A}_0,\ \tilde{B}_0$ are arbitrary constants from (A.30). (A.36) has a solution as:

$$\tilde{A}_{k+1} = \begin{cases} R_0 \ \text{ for } k = 0 \\ R_k + \sum_{i=0}^{k-1} \left(\Pi_{j=i+1}^{j=k} p_j \right) R_i \ \ \forall k \geq 1 \end{cases},\ \tilde{B}_{k+1} = \begin{cases} S_0 \ \text{ for } k = 0 \\ S_k + \sum_{i=0}^{k-1} \left(\Pi_{j=i+1}^{j=k} q_j \right) S_i \ \ \forall k \geq 1 \end{cases} \quad \text{(A.37)}$$

where

$$p_k = \frac{k}{k+1} - \frac{1}{k+m+1},\quad q_k = \frac{(2k+m)\left[k(k+m)-1\right]}{(k+1)(k+m+1)(2k+m-2)}\ \ \forall k \geq 1$$

$$R_k = \begin{cases} \dfrac{c_1}{4(m+1)} \ \text{ for } k = 0 \\ \dfrac{c_{k+1}}{4(k+1)(k+m+1)} - \dfrac{(2k+m+2)\left[(2k+m-2)c_k - md_k\right]}{16k(k+1)(k+m)(k+m+1)} \ \text{ for } k \geq 1 \end{cases}$$

$$S_k = \begin{cases} \dfrac{d_1}{4(m+1)} \ \text{ for } k = 0 \\ \dfrac{d_{k+1}}{4(k+1)(k+m+1)} - \dfrac{m(2k+m)\left[(2k+m-2)c_k - md_k\right]}{16k(k+1)(k+m)(k+m+1)(2k+m-2)} \ \text{ for } k \geq 1 \end{cases}$$

Finally, (A.25) becomes:

$$F(z)=z^{s_2}\sum_{k=0}^{\infty}A_k z^k=z^{s_2}\sum_{k=0}^{m-1}A_k z^k+z^{s_1}\sum_{k=1}^{\infty}\tilde{A}_k z^k,$$
$$G(z)=i\,z^{s}\sum_{k=0}^{\infty}B_k z^k=i\left[z^{s_2}\sum_{k=0}^{m-1}B_k z^k+z^{s_1}\sum_{k=1}^{\infty}\tilde{B}_k z^k\right] \qquad \text{(A.38)}$$

It is obvious that the last independent solution (the fourth solution) (A.33) contains one arbitrary parameter a_0, which can be set to 1 to obtain $f_4(z),\ g_4(z)$. Although the infinite series in (A.38) all converge, the converging functions have not yet been determined. Thus, this fourth solution is evaluated numerically by retaining a sufficient number of terms.

Appendix B. The optimal composite with a smoothly-varying bulk modulus in the coating

In this appendix, we analyze the continuously radially-varying heterogeneous coating model whose shear modulus is unchanged. Similar to procedures presented above, one can do this both ways, i.e. by a generalization of the two-homogeneous-layer coating analysis to the limit of an infinite-homogeneous-layer coating or by a direct continuum analysis. For simplicity, only the latter approach is shown here.

As the axisymmetric $m=0$ mode is assumed to be critical (it will be so for the solution we find), we begin with the axisymmetric version of the equilibrium equation, which, written in terms of displacements takes the form (3.15), repeated here for convenience:

$$\frac{d}{dr}\left[(\lambda+2\mu)\left(u_{r,r}+\frac{u_r}{r}\right)\right]-2\frac{d}{dr}\left[\mu\frac{u_r}{r}\right]+2\mu\left(\frac{u_{r,r}}{r}-\frac{u_r}{r^2}\right)=0. \tag{B.1}$$

Constant shear modulus means:

$$\mu(r)=\bar{\mu}=\text{const.} \tag{B.2}$$

For this case, the second order ordinary differential equation (B.1) has by inspection one solution $u_r=1/r$; from this, using variation of parameters, its general solution is

$$u_r=\frac{C_1+C_2\tilde{h}(r)}{r}, \tag{B.3}$$

where

$$\tilde{h}(r)=\int_0^r\frac{rdr}{\lambda+2\mu}. \tag{B.4}$$

Following the same procedure for seeking nontrivial axisymmetric equilibrium solutions as presented for the case of constant bulk modulus in the coating above, one arrives at the instability condition:

$$\kappa_0=-\bar{\mu}+\bar{\mu}\frac{a^2}{b^2-2\bar{\mu}\tilde{H}}, \tag{B.5}$$

where

$$\tilde{H} = \tilde{h}(b) - \tilde{h}(a) = \int_a^b \frac{r dr}{\lambda + 2\mu}. \tag{B.6}$$

From (B.5),

$$\frac{d\kappa_0}{d\tilde{H}} = \frac{2\bar{\mu}^2 a^2}{\left(b^2 - 2\bar{\mu}\tilde{H}\right)^2} > 0. \tag{B.7}$$

meaning the stability domain is largest if $\tilde{H}$ is minimum. To determine a lower bound on $\tilde{H}$, we apply the Cauchy–Bunyakovsky–Schwarz inequality for integration to the following integral

$$\left(\frac{b^2 - a^2}{2}\right)^2 = \left(\int_a^b r\, dr\right)^2 = \left(\int_a^b \frac{\sqrt{r}}{\sqrt{(\lambda + 2\mu)}} \sqrt{r(\lambda + 2\mu)}\, dr\right)^2 \le \int_a^b \frac{r dr}{\lambda + 2\mu} \int_a^b (\lambda + 2\mu) r\, dr. \tag{B.8}$$

Conditions (3.1) give:

$$\int_a^b (\lambda + 2\mu) r\, dr = \frac{b^2 - a^2}{2}\left(\bar{\lambda} + 2\bar{\mu}\right). \tag{B.9}$$

Substituting (B.9) into (B.8), it shows that

$$\tilde{H} = \int_a^b \frac{r dr}{\lambda + 2\mu} \ge \frac{b^2 - a^2}{2\left(\bar{\lambda} + 2\bar{\mu}\right)}, \tag{B.10}$$

and hence

$$\kappa_0^{\min} = -\bar{\mu} + \bar{\mu}\frac{a^2}{b^2 - \frac{\bar{\mu}}{\bar{\lambda}+2\bar{\mu}}\left(b^2 - a^2\right)}. \tag{B.11}$$

For $\tilde{H}$ to be a minimum, the inequality in (B.8) must be an equality, which requires

$$\frac{\sqrt{r}}{\sqrt{(\lambda+2\mu)}} = \text{Const}\sqrt{r(\lambda+2\mu)} \leftrightarrow \lambda+2\mu = \text{Const} \tag{B.12}$$

Combining (B.12) with (B.2) gives the relations

$$\mu(r) = \bar{\mu}, \quad \lambda(r) = \bar{\lambda}. \tag{B.13}$$

Thus, among all radially heterogeneous isotropic materials whose shear modulus is constant, which include the homogeneous isotropic ones as subsets, the homogeneous one gives the largest stability domain. Recall that this conclusion is also obtained when one analyzes the piecewise homogeneous two-layer coating model in the chapter 2.

References

Bolotin, V., 1964, *The Dynamic Stability of Elastic Systems*, Holden-Day.

Budiansky, B., 1974, Theory of Buckling and Post-Buckling Behavior of Elastic Structures, *Advances in Applied Mechanics* **14**, 1-65.

Cahill, Nathan D., 2002. Fibonacci Determinants, *College mathematics journal*, 33, 221.

Dong, L., Lakes, R. S., 2012, Advanced damper with negative structural stiffness elements, *Smart Materials and Structures*, **21**, 075026.

Dong, L. and Lakes, R. S., 2013, Advanced damper with high stiffness and high hysteresis damping based on negative structural stiffness, *Int. J. Solids Struct.,* **50**, 2413-2423.

Drugan, W.J., 2007. Elastic composite materials having a negative stiffness phase can be stable. *Phys. Rev. Lett.* 98 (5) article no. 055502.

Hildebrand, F.B., 1962. *Advanced calculus for applications*, Prentice-Hall, Inc.

Hill, R., 1957. On uniqueness and stability in the theory of finite elastic strain. *J. Mech. Phys. Solids* 5, 229–241.

Hoang, T. M., Drugan, W. J., 2014. Tailored Heterogeneity Increases Overall Stability Regime of Composites Having a Negative-Stiffness Inclusion, *J. Mech. Phys. Solids,* Accepted.

Jaglinski, T., Stone, D. S., Lakes, R. S., 2005, Internal friction study of a composite with a negative stiffness constituent, *Journal of Materials Research*, **20**(9), 2523-2533.

Kalathur, H., Lakes, R. S., 2013. Column dampers with negative stiffness: high damping at small amplitude, *Smart Materials and Structures,* **22,** 084013, 2013.

Kalathur, H., Hoang, T. M., Lakes, R. S., Drugan, W. J., 2013. Buckling Mode Jump at Very Close Load Values in Unattached Flat-End Columns: Theory and Experiment, *J. Appl. Mech.* 81(4), 041010.

Kelvin, Lord, 1888. (W. Thomson) Philos. Mag. **26**, 414-425

Kochmann, D.M., 2013. Stable extreme damping in viscoelastic two-phase composites with non-positive-definite phases close to the loss of stability, *Mechanics Research Communications*, In Press.

Kochmann, D.M., Drugan, W. J., 2009. Dynamic stability analysis of an elastic composite material having a negative-stiffness phase, *J. Mech. Phys. Solids* 57, 1122-1138.

Kochmann, D.M., Drugan, W. J., 2011. Infinitely-stiff composite via a rotation-stabilized negative-stiffness phase, *Appl. Phys. Lett.* 99, 011909.

Kochmann, D.M., Drugan, W. J., 2012. Analytical stability conditions for elastic composite materials with a non-positive-definite phase, *Proc. R. Soc. A* 468, 2230-2254.

Lakes, R. S., 2001, Extreme damping in compliant composites with a negative stiffness phase, *Philosophical Magazine Letters*, **81**(2), 95-100.

Lakes, R.S., Drugan, W.J., 2002. Dramatically stiffer elastic composite materials due to a negative stiffness phase?, *J. Mech. Phys. Solids* 50, 979–1009.

Lakes, R.S., Lee, T., Bersie, A., Wang, Y.C., 2001. Extreme damping in composite materials with negative stiffness inclusions, *Nature* 410, 565–567.

Lekhnitskii, S.G., 1962. Radial distribution of stresses in a wedge and in a half-plane with variable modulus of elasticity, *PMM* Vol.26, No.1, 146-151.

Pearson, C.E., 1956. General theory of elastic stability. *Q. Appl. Math.* 14, 133–144.

Plevako, V.P., 1971. On the theory of elasticity of inhomogeneous media, *PMM* Vol. 35, No.5, 853-860.

Simitses, G., 2005. *Fundamentals of structural stability*, Butterworth-Heinemann.

Farshad, Mehdi (1994), *Stability of structures*, Elsevier science Ltd.

Ter-Mkrtich'ian, L.N., 1961. Some problems in the theory of elasticity of nonhomogeneous elastic media, *PMM* Vol.25, No.6, 1120-1125.

Timoshenko, S. and Gere, J. M., 1963, *Theory of Elastic Stability*, McGraw-Hill.

Vinogradov, A. M., 1987, Buckling of Viscoelastic Beam Columns, *AIAA journal*, **26**(3), 479-483.

Wojnar, C. S., Kochmann, D.M., 2014. Stability of extreme static and dynamic bulk moduli of an elastic two-phase composite due to a non-positive-definite phase, *Phys. Status Solidi B* 251, 397-405.